

Introduction to Reservoir Geomechanics

1 Introduction

Definitions and some challenges of reservoir geomechanics.
Modeling of coupled phenomena.

2 Constitutive Laws: Behavior of Rocks

Fundamentals of Pore-Mechanics.

3 Constitutive Laws: Behavior of Fractures

Geomechanics of Fractured Media.

4 Reservoir Geomechanics

Elements of a geomechanical model and applications.

5 Unconventional Reservoirs

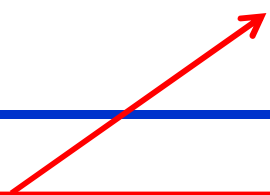
Naturally fractured reservoirs, hydraulic fracture, proppant and fracture closure model, validation (microseismicity).

6 Advanced Topics

Injection of reactive fluids and rock integrity.



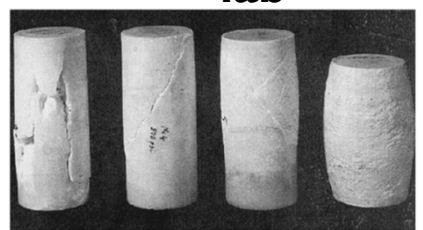
Constitutive Laws



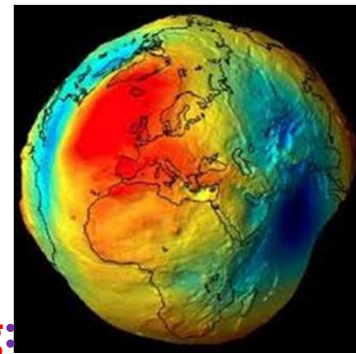
micro



lab

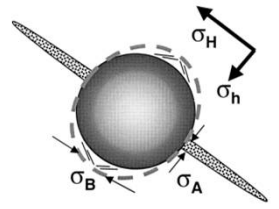
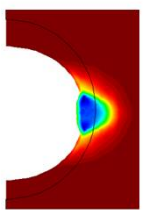
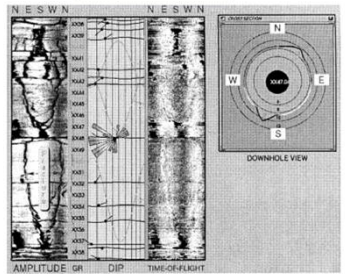
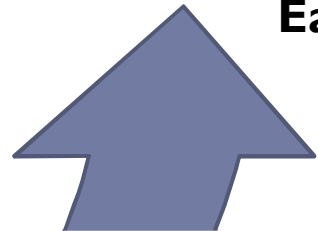


Earth Sciences and Engineering:

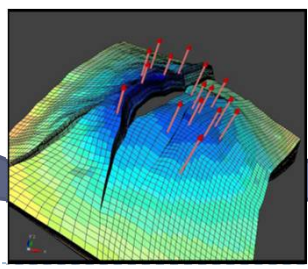


Earth

Problems Scales



wellbore



reservoir



basin





Introduction



Literature Review





Summary



Classical Models.

Basic concepts of joints, paper review and tests for obtaining parameters of Barton's model.

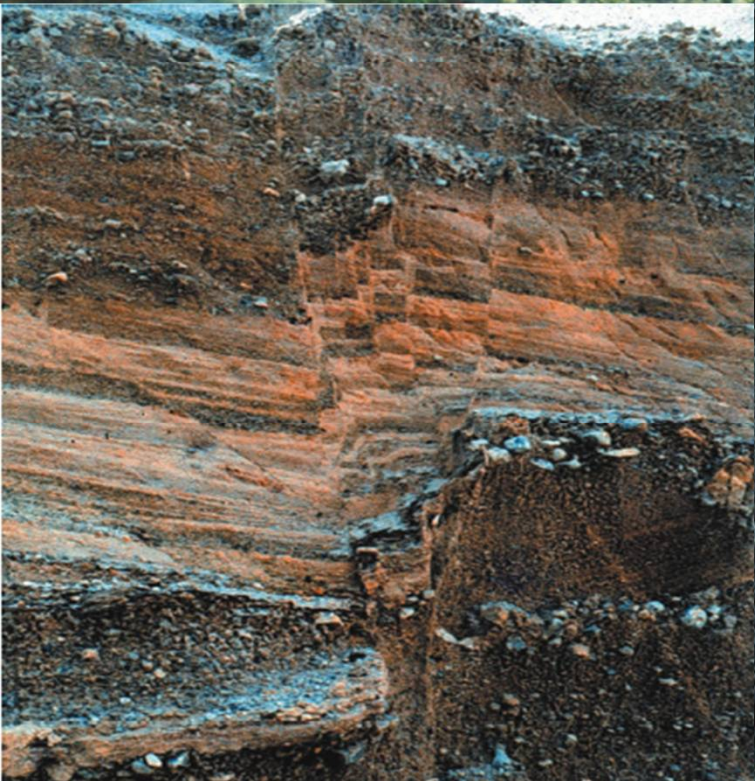
Recent Models

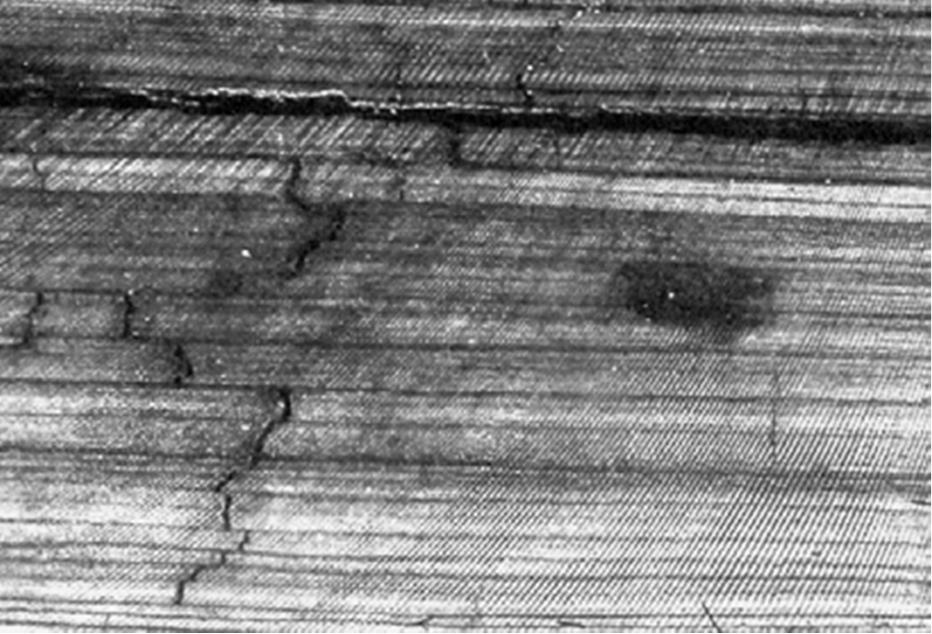
Experimental Procedures

Softwares

CMG Package: STARS and GEM

▶ ABAQUS







Shear Strength of Joints



- ❑ There are many parameters that affect the peak shear strength of a rock joint:
 - ▶ Type of rock;
 - ▶ Surface roughness;
 - ▶ Normal stress;
 - ▶ Uni-axial compressive strength of the joint wall surface.





Shear Strength of Joints



- ❑ There are many methods designed to available shear strength failure criteria that estimate the peak shear strength:
 - ▶ Some more empirically;
 - ▶ Others more theoretically.
- ❑ Basic shear mechanisms of rock joints unfilled will be explained considering friction and surface roughness.





Shear Strength of Joints



- ❑ Unfilled joints have been found to have the following characteristics:
 1. Tension cannot be carried in the normal direction.
 2. Shear strength is a function of normal stress and material properties parameters.
 3. Elastic behavior is exhibited within the yield envelope.





Shear Strength of Joints



- ▶ **Basic shear mechanisms of rock joints**
 - *Friction*: when two surfaces in contact move relative to each other, a sliding resistance is induced.
- ▶ **Fundamental laws of friction have been introduced by Amontons and Coulomb:**
 - ✓ **Amontons' First Law**: The force of friction is directly proportional to the applied load;
 - ✓ **Amontons' Second Law**: The force of friction is independent of the apparent area of contact;
 - ✓ **Coulomb's Law of Friction**: Kinetic friction is independent of the sliding velocity.

▶ The friction process is explained by the adhesion theory. It was first stated by Terzaghi (1925) and later approved by Bowden and Tabor (1950 and 1964).



Shear Strength of Joints



- Basic shear mechanisms of rock joints

- Friction:

Area \longrightarrow $A_c = \frac{N}{q_u}$

N ← normal force
 q_u ← the stress required to obtain plastic flow at the contact points.

The shear resistance is provided by these adhesive bonds and is given by:

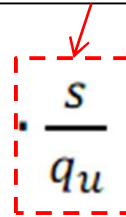
$$T = s \cdot A_c$$

sum of the adhesive strengths of the bonds



$$T = N \cdot \frac{s}{q_u}$$

coefficient of friction (μ)



$$T = N \tan \phi$$





Shear Strength of Joints

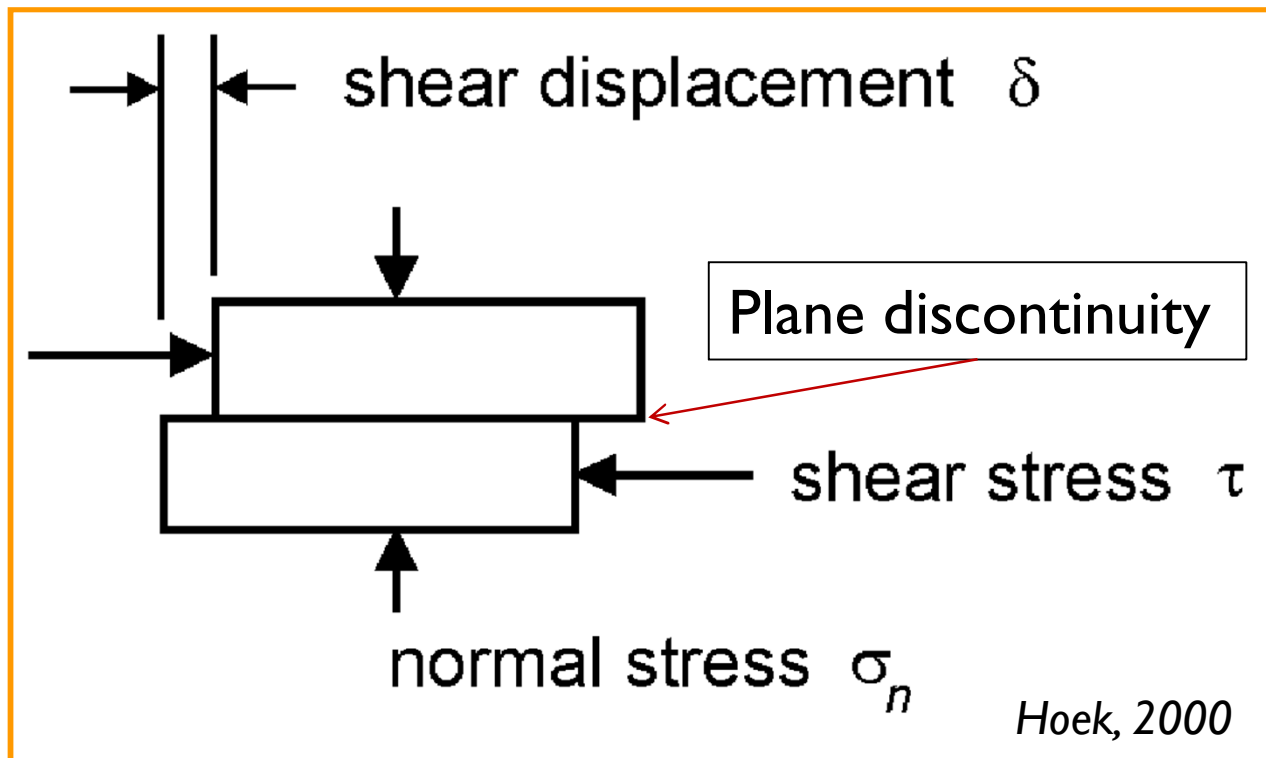


- ▶ Basic shear mechanisms of rock joints
- *Surface roughness*: property of the texture of a surface, it is quantified by the vertical deviations of the surface from the original smooth one. This property is very difficult to measure.
- The most common parameter to quantifying the roughness was proposed by Barton (1973) when he introduced the JRC (joint roughness coefficient).



- Coulomb Model adapted

$$\tau_p = c + \sigma_n \tan \phi$$





Shear Strength of Joints



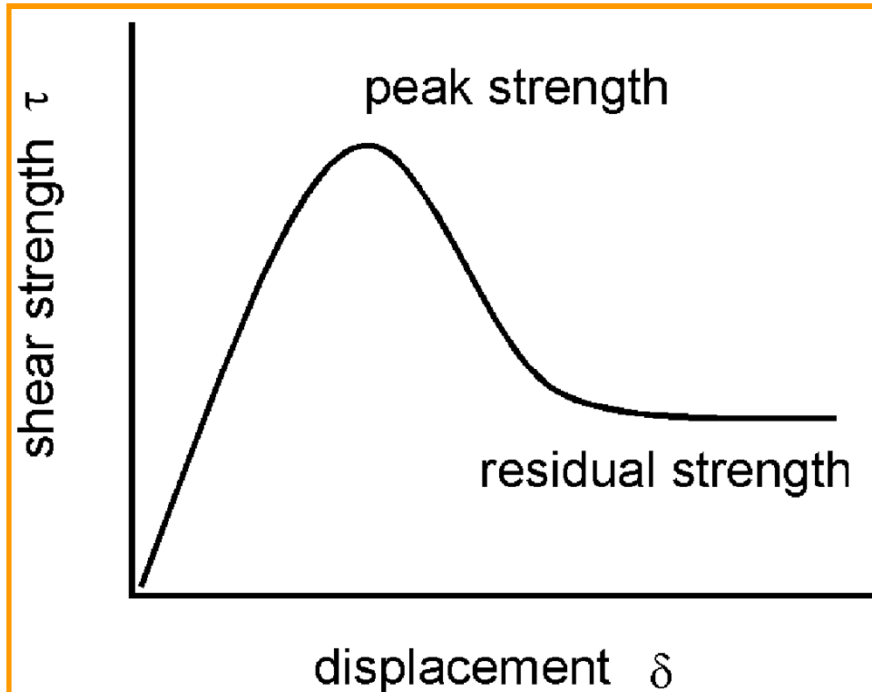
- Coulomb Model adapted

$$\tau = \mu \cdot \sigma_n$$

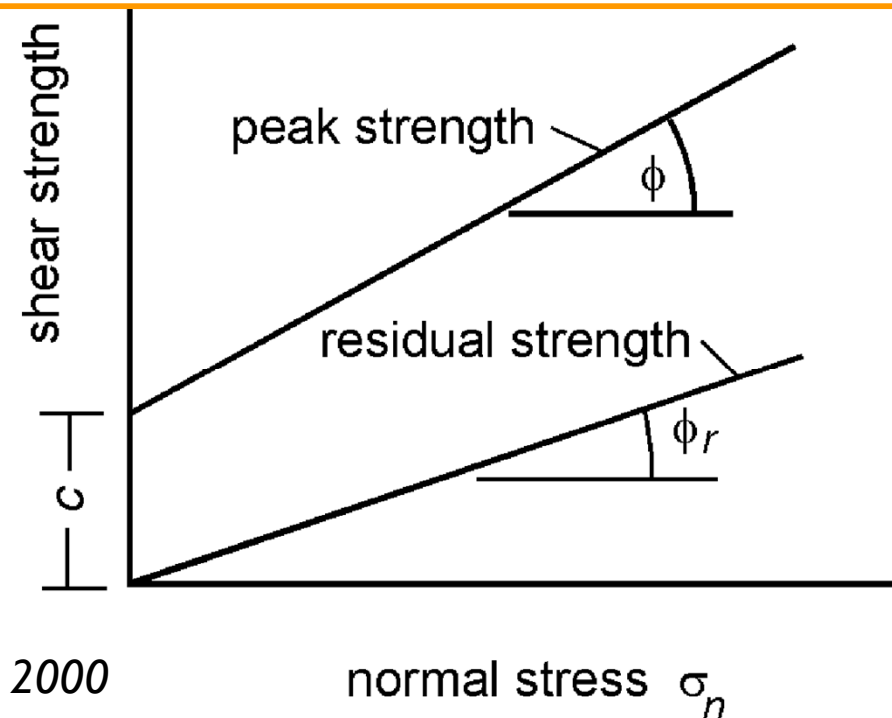


$$\tau_r = \sigma_n \tan \phi_b$$

basic friction angle of the failure plane.



Hoek, 2000





Shear Strength of Joints

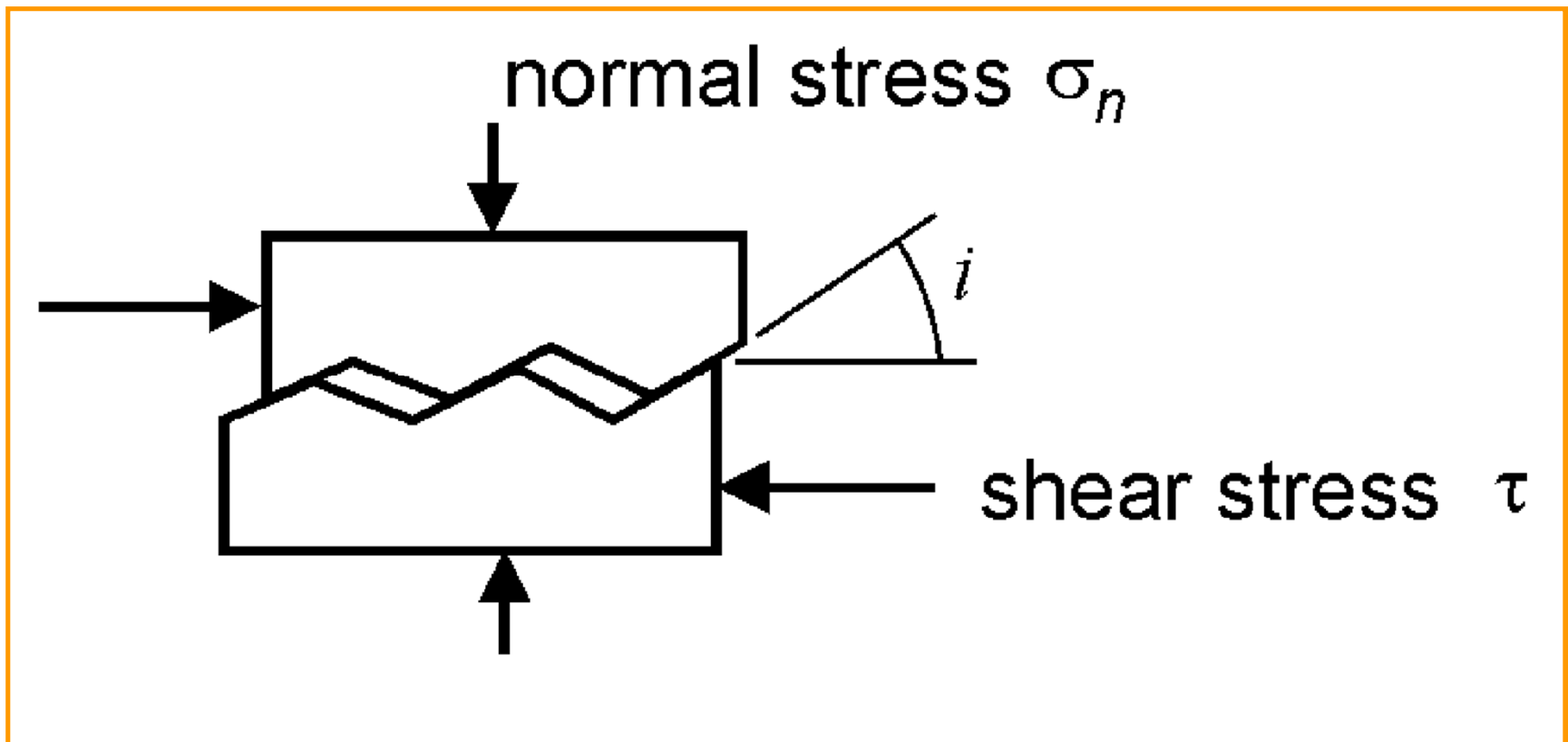


- Patton's Law
- ▶ Patton (1966) conceived the first successful model for the shear strength of a joint.

- ▶ Conclude that:
 - a) failure envelope for rough joints are curved;
 - b) changes in the slope of the failure envelope reflect changes in the mode of failure;
 - c) changes in the mode of failure are related to physical properties of the irregularities along the failure surface.



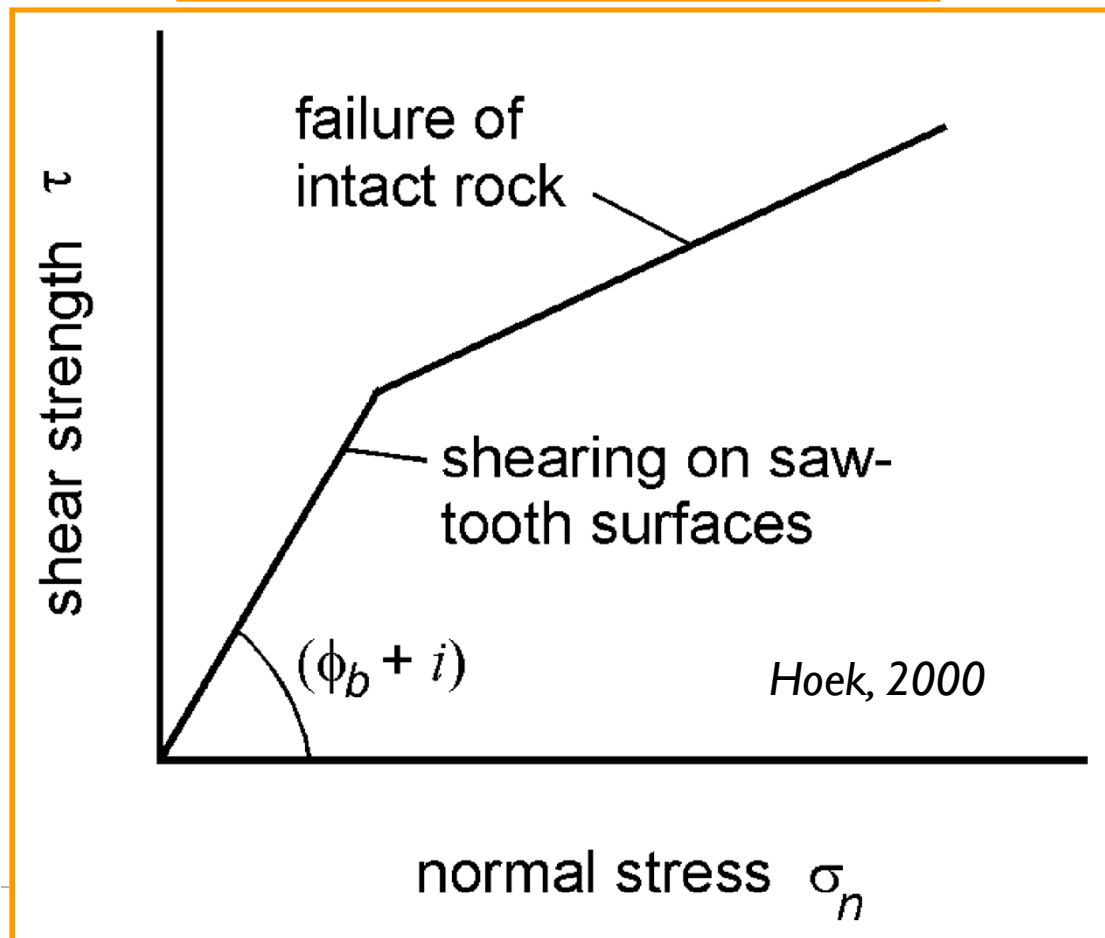
□ Patton's Law (1966)



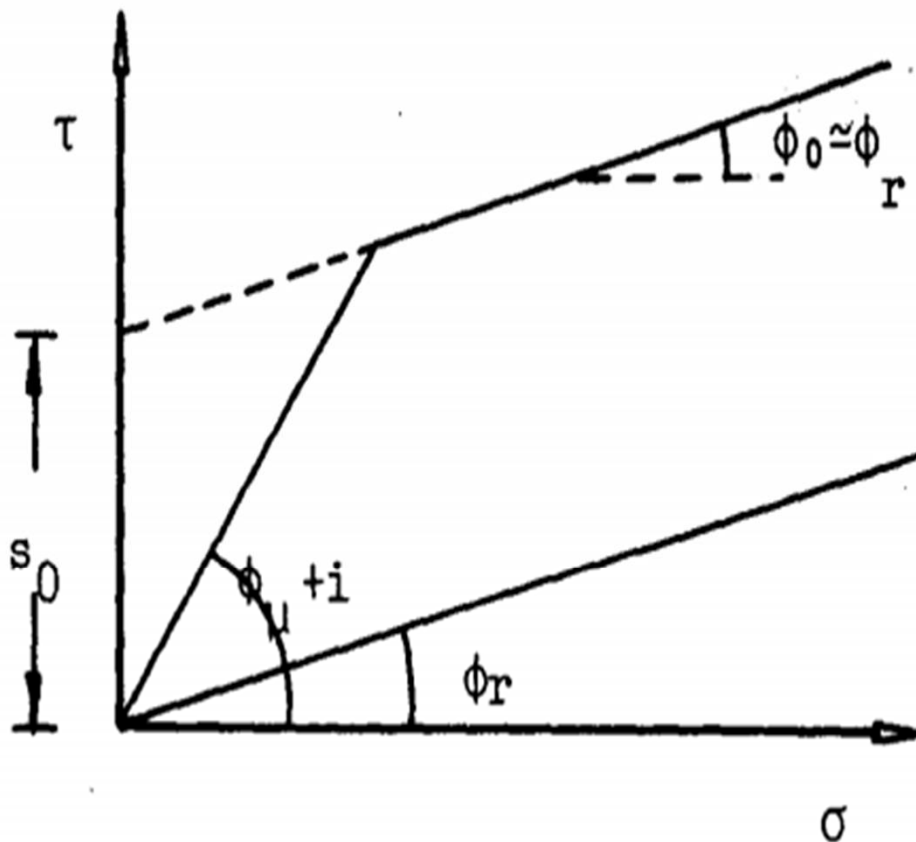


Shear Strength of Joints

$$\tau = \sigma_n \tan(\phi_b + i)$$



Patton's Law (1966)



$$\tau = \sigma_n \tan(\phi_b + i)$$

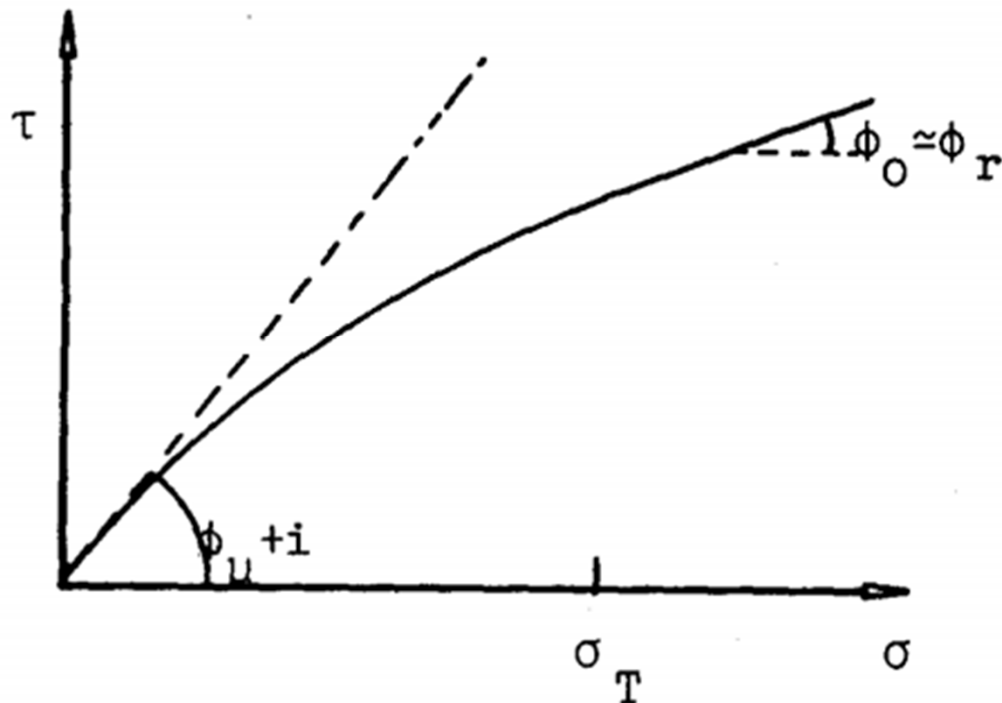
Low stress $\tau_p = \sigma \tan(\phi_\mu + i)$
 high stress $\tau_p = S_0 + \sigma \tan(\phi_0)$



Shear Strength of Joints



Patton's Law (1966) (with varying 'i')



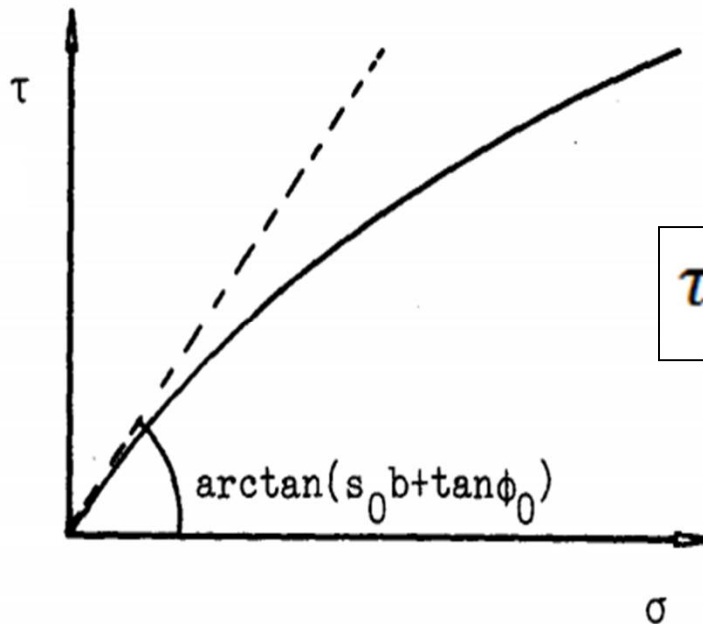
$$|\sigma| < |\sigma_T|$$

$$\tau_p = \sigma \tan(\phi_\mu + i)$$

$$\tan(i) = \left(1 - \left(\frac{\sigma}{\sigma_T}\right)^{0.25}\right) \tan(i_0)$$

$$i_0 \approx 33^\circ$$

- ▶ Jaeger's Law (1960) (varying cohesion)
- ▶ Case of discontinuous anisotropy, rock isotropic in strength, cut by a continuous joint set – plane as a weakness theory.



$$\tau_p = S_0(1 - e^{-b\sigma}) + \tan(\phi_0)$$



Shear Strength of Joints



- ▶ Generally, the surface roughness increases the shear strength of the surface, and this strength increasing is extremely important in terms of the rock stability.

The shear strength of Patton's saw-tooth specimens can be represented by:

$$\tau = \sigma_n \tan(\phi_b + i)$$

where ϕ_b is the basic friction angle of the surface and i is the angle of the saw-tooth face.

This equation is valid at low normal stresses where shear displacement is due to sliding along the inclined surfaces





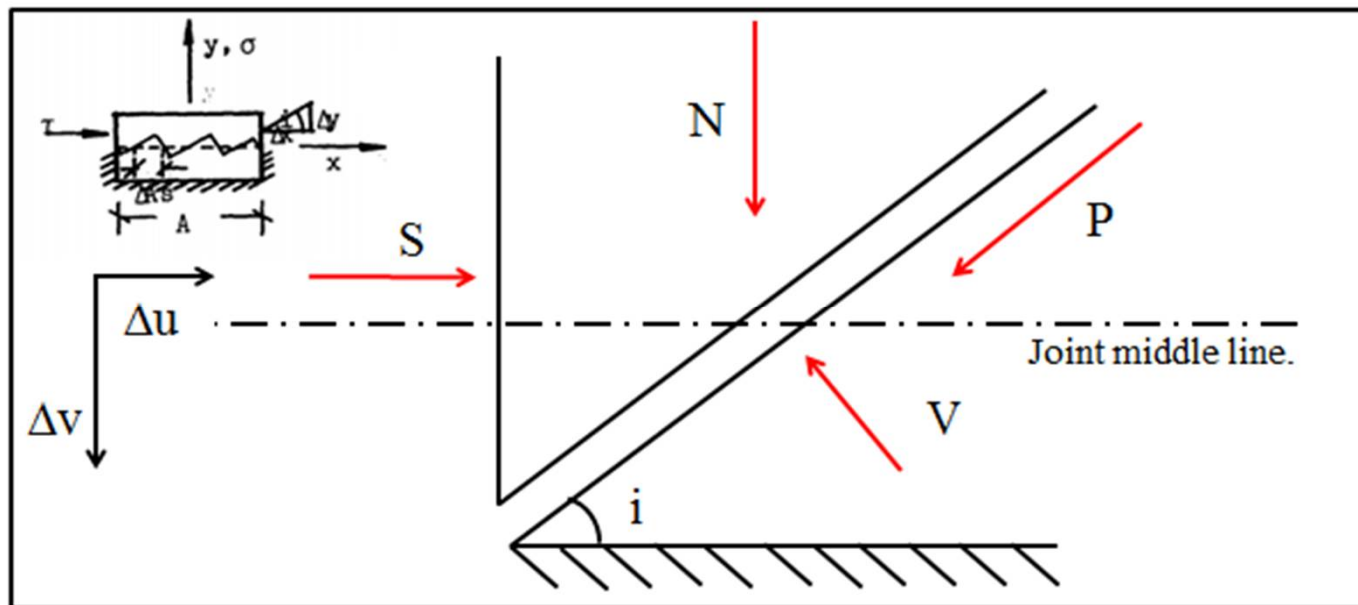
Shear Strength of Joints



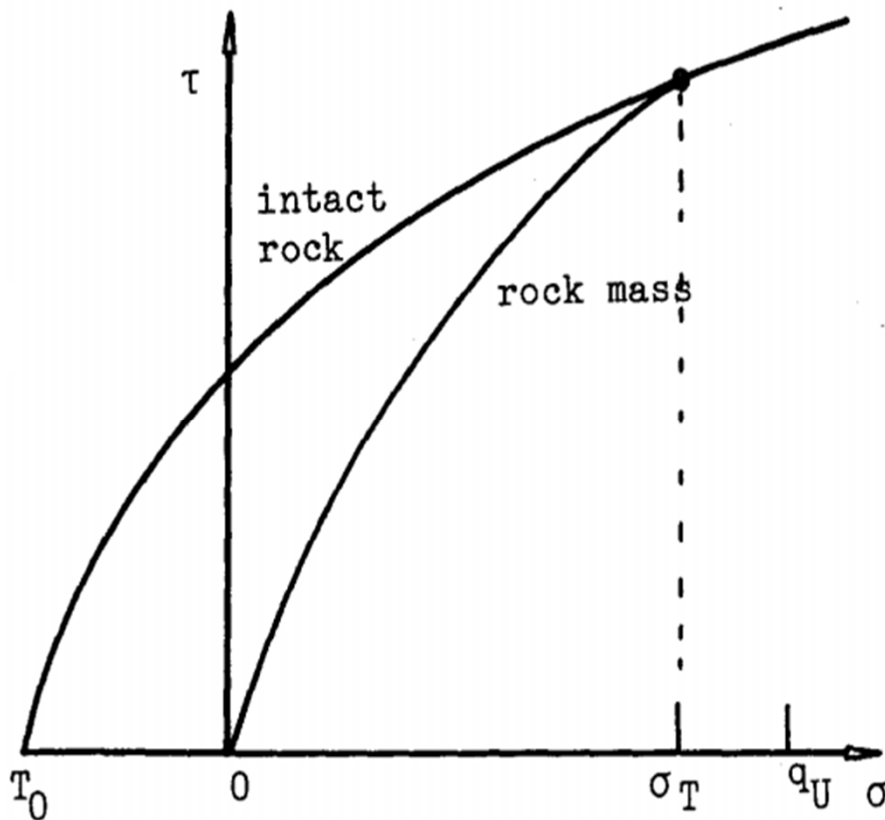
- ▶ **Ladanyi & Archambault (1970)**
- ▶ Proposed a curved failure envelope for the peak strength.
- ▶ The shear strength of the joint is assumed to be the sum of four separate strength components, S_1 , S_2 , S_3 , S_4 .
- ▶ The three first components assume no shearing occurs.



- **Ladanyi and Archambault (1970)**
- ▶ From static and limit equilibrium we have:
- ▶ $N \cdot \cos(i) + S \cdot \sin(i) = V$
- ▶ $(P / \cos(i)) = (N + S \cdot \tan(i)) \cdot \tan(\phi)$



■ Ladanyi and Archambault (1970)



$$\tau = \frac{\sigma_n \cdot (1 - a_s) \cdot (\tan \theta_p + \tan \phi_b) + a_s \cdot \tau_{rock}}{1 - (1 - a_s) \cdot \tan \theta_p \cdot \tan \phi_b}$$

Where:

τ : Peak shear strength of joint

σ_n : Effective normal stress

a_s : Area of the asperities that has been sheared

τ_{rock} : Shear strength of intact rock

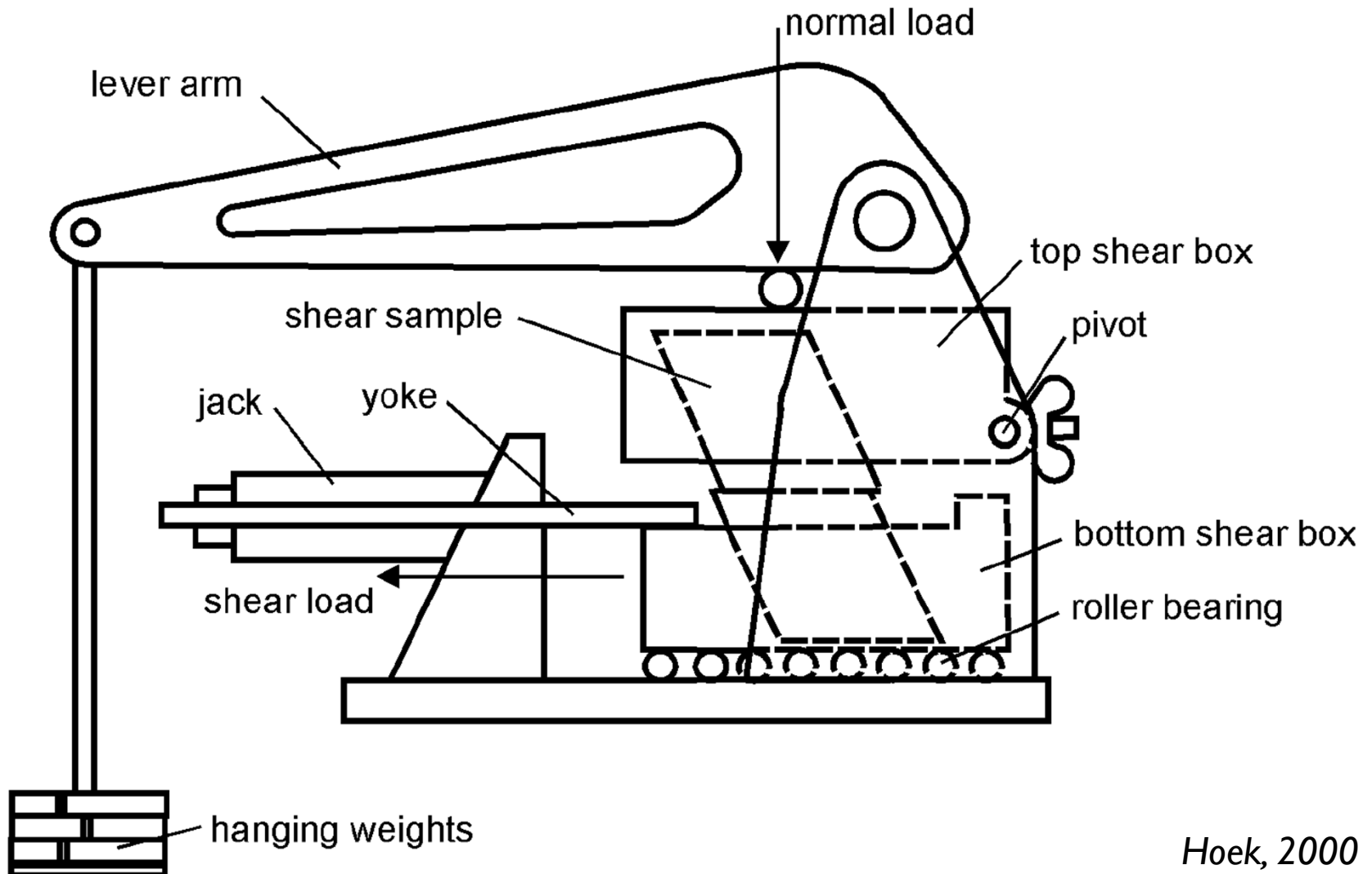
ϕ_b : Basic friction angle

θ_p : Dilatancy angle at the peak and $\theta_p = \arctan (v_p / u_p)$

Where v_p and u_p is the vertical and horizontal displacement of the average joint plane at the peak respectively with respect to the shear direction.



Shear Test

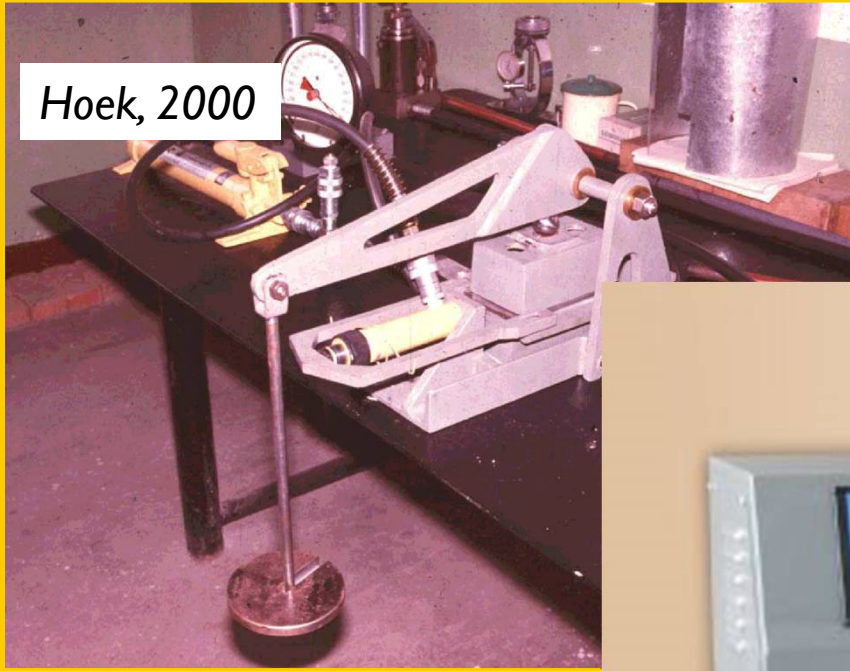




Shear Test



Hoek, 2000





CLASSICAL MODELS:

**Review of a New Shear-strength Criterion for Rock Joints
(Barton, 1973)**

**The Shear Strength of Rock Joints in Theory and Practice
(Barton & Choubey, 1977)**

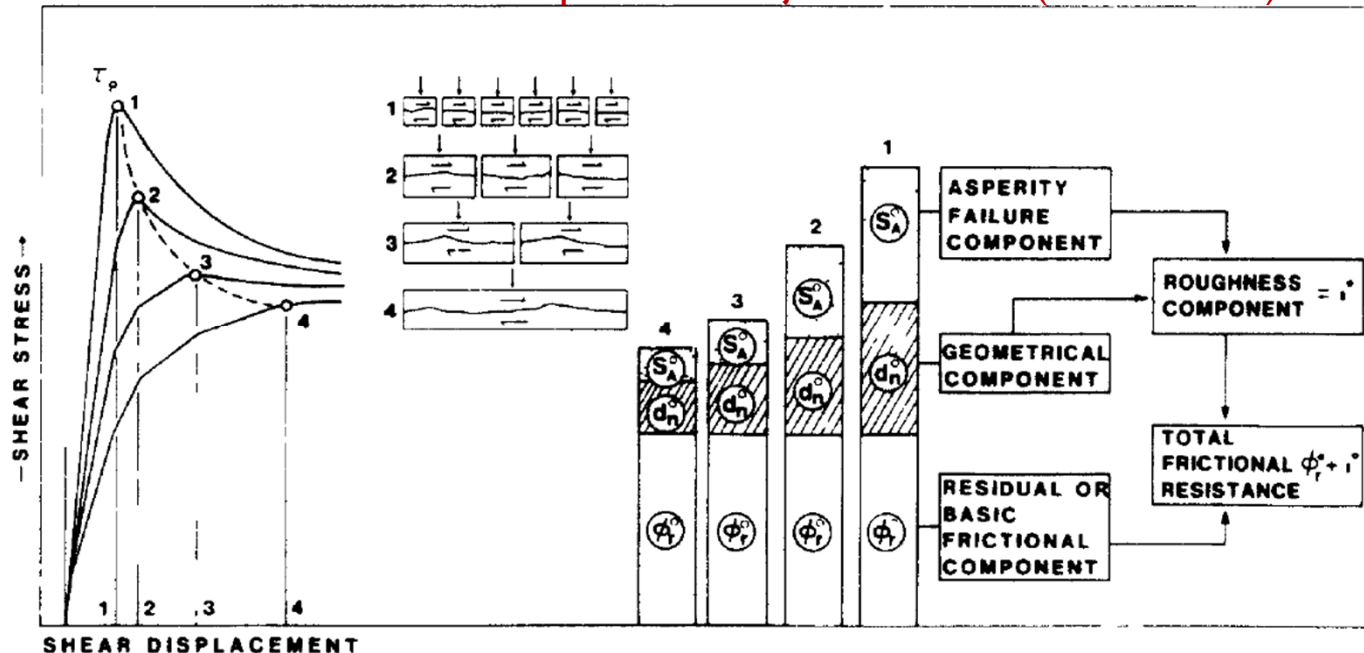
**Fundamentals of Rock Joint Deformation (Bandis et al.,
1983)**

**Strength, Deformation and Conductivity Coupling of Rock
Joints (Barton *et al.*, 1985)**



- The shear strength and deformability of rock joints are size-dependent parameters.
- The size dependence and general behavior are governed by surface characteristics, such as roughness and wall strength.

Illustration of the size dependence of joint behavior (Barton 1985)





Barton's estimate of shear strength



- ▶ While Patton's approach has the merit of being very simple, it does not reflect the reality that changes in shear strength with increasing normal stress are gradual rather than abrupt. Barton (1973) studied the behavior of natural rock joints and proposed that shear strength equation could be written as:

$$\tau = \sigma_n \tan \left(\phi_b + JRC \log_{10} \left(\frac{JCS}{\sigma_n} \right) \right)$$

basic friction angle

analysis of joint strength data reported in the literature

where JRC is the joint roughness coefficient and JCS is the joint wall compressive strength





Barton-Bandis criterion for rock joint strength and deformability



- ▶ Barton's estimate of shear strength

$$\tau = \sigma_n \tan \left(\phi_r + JRC \log_{10} \left(\frac{JCS}{\sigma_n} \right) \right)$$

Where ϕ_r is the residual friction angle

on the basis of their direct shear test results for 130 samples of variably weathered rock joints

- ▶ Barton and Choubey (1977) suggest that ϕ_r can be estimated from:

$$\phi_r = (\phi_b - 20) + 20(r / R)$$

Schmidt rebound number wet and weathered fracture surfaces

Schmidt rebound number on dry unweathered sawn surfaces





Barton's estimate of shear strength



	<u>FRESH TO SLIGHTLY WEATHERED</u>		<u>MODERATELY WEATHERED</u>		<u>WEATHERED</u>	
	JRC range	(ϕ_r°)	JRC range	(ϕ_r°)	JRC range	(ϕ_r°)
Slate ($\phi_b=31^\circ$)	4.0-5.0	(31°)	5.3	(31°)	6.0-6.8	(25°*)
Dolerite ($\phi_b=34^\circ$)	7.1-8.8	(34°)	-		6.0-7.7	(27°*)
Limestone ($\phi_b=33^\circ$)	5.6-11.4	(33°)	5.8-16.9	(30°*)	5.0-15.0	(22°*)
Siltstone ($\phi_b=28^\circ$)	8.8-11.8	(28°)	7.0-7.5	(25°*)	6.1-6.7	(21°*)
Sandstone ($\phi_b=24^\circ-30^\circ$)	5.4-10.7	(30°)	5.1-14.1	(26°*)	4.8-6.1	(24°)

Bandis (1980)



Joint Surface Characterization



- It is possible to predict shear strength-deformation behavior and normal stress-closure behavior with acceptable accuracy, using some very simple index tests.
- The parameters required for complete joint characterization can be defined as:
 - JRC - Joint roughness coefficient
 - JCS - Joint wall compression strength
 - σ_c - unconfined compression strength (rock adjacent to joint wall)
 - ϕ_r - residual friction angle
 - e - conducting aperture
 - E - mechanical aperture



□ The **Schmidt hammer** test is used to estimate the joint wall compression strength (JCS)

□ The Joint roughness coefficient (JRC) and the residual friction angle (ϕ_r) can be obtained **indirectly** from simple **tilt tests** using pieces of intact and jointed core.

□ JRC, JCS and ϕ_r are all that are needed to develop shear strength, displacement, dilatation and normal stress-closure curves for any given joint.

□ However, coupling conductivity with these processes requires additional information concerning initial joint aperture, since closure or dilatation resulting from stress changes are superimposed on these initial apertures

Schmidt hammer



Tilt test

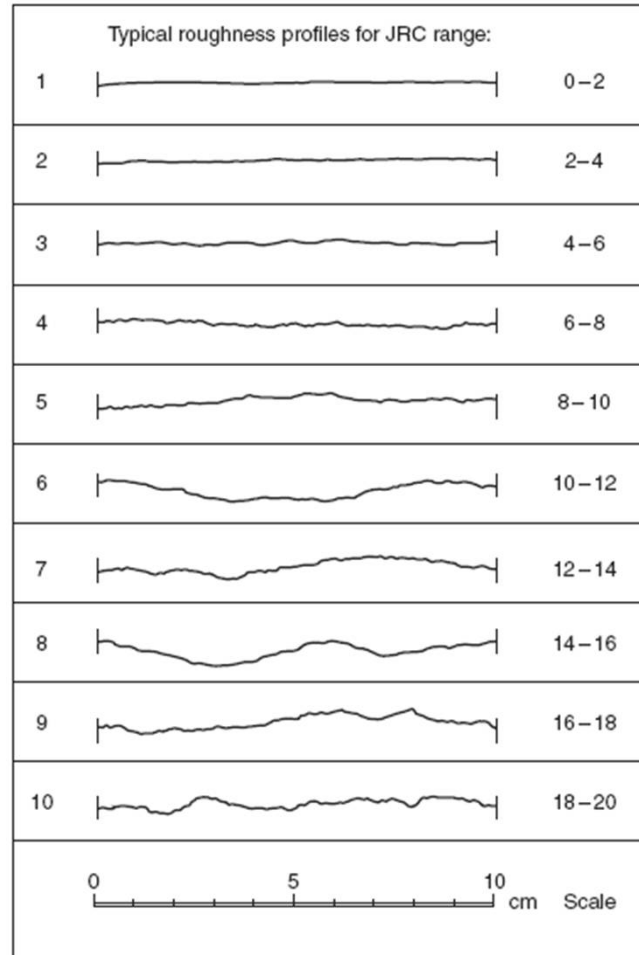




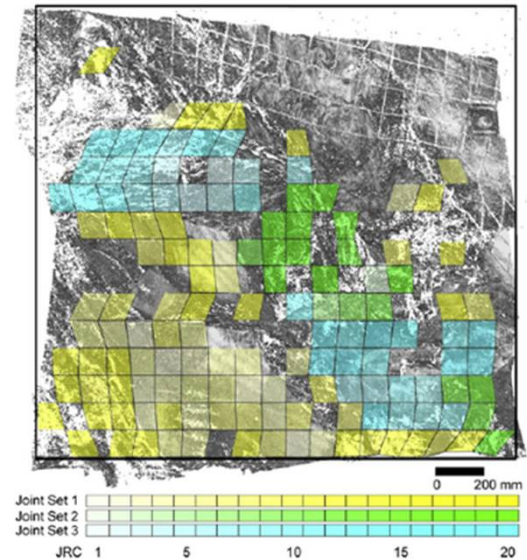
Obtaining the Joint roughness coefficient JRC



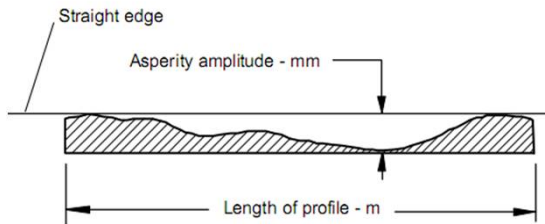
Profilometer



3D laser imaging for surface roughness analysis (McKinnon & Thibodeau, 2013)



- ▶ An alternative method for estimating JRC is presented by Barton (1982):



Lamaro,
(2000)

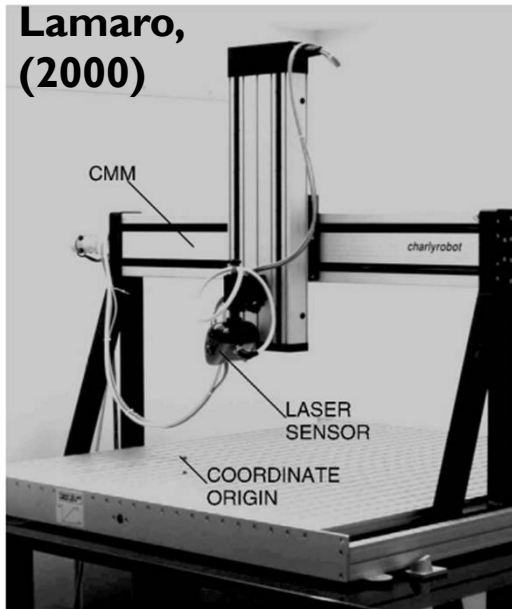


Fig. Overview of the 3-D-laser-scanning equipment.

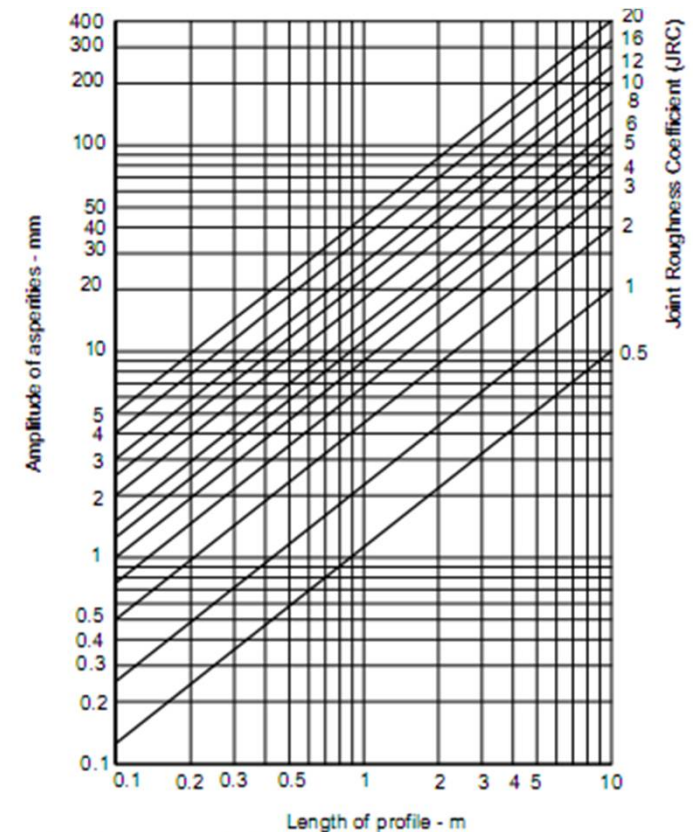
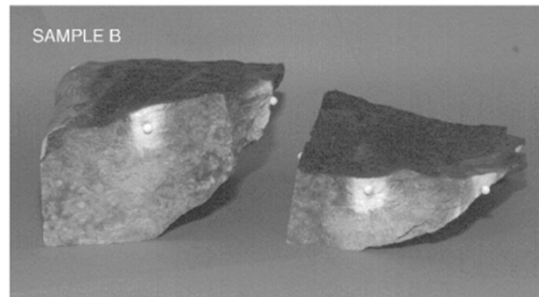
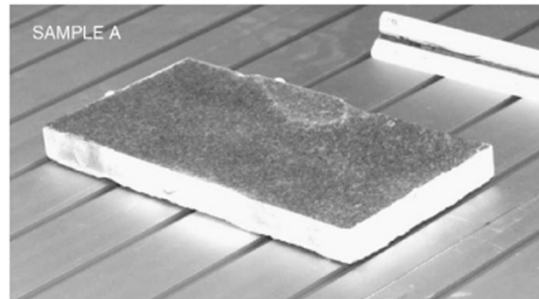


Figure 6: Alternative method for estimating *JRC* from measurements of surface roughness amplitude from a straight edge (Barton 1982).



Field estimates of JCS



- ❑ Suggested methods for estimating the joint wall compressive strength were published by the ISRM (1978).
- ❑ The use of the Schmidt rebound hammer for estimating joint wall compressive strength was proposed by Deere and Miller (1966)

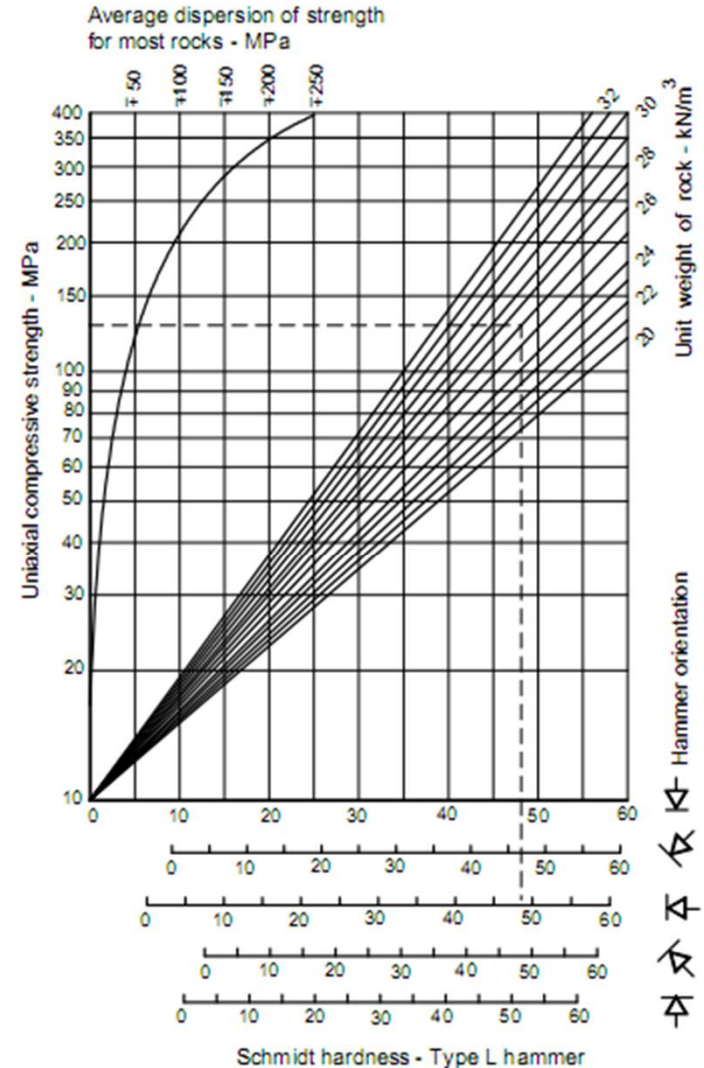


Figure 7: Estimate of joint wall compressive strength from Schmidt hardness.



Field estimates of JCS



$$\text{Log}_{10} \text{JCS} = 0.00088 * \text{gamma} * R + 1.01$$

Mean unit weight of joint wall material

Mean rebound number from Schmidt hammer

The various samples are described as fresh (F), slightly weathered (SW), moderately weathered (MW) and weathered (W)

Weathering State:

F to SW: $\text{Sig}_c / \text{JCS} \leq 1.2$

MW: $1.2 < \text{Sig}_c / \text{JCS} \leq 2$

W: $\text{Sig}_c / \text{JCS} > 2$



Influence of scale on JRC and JCS



- On the basis of extensive testing of joints, joint replicas, and a review of literature, Barton and Bandis (1982) proposed the scale corrections for JRC defined by the following relationship:

$$JRC_n = JRC_o \left(\frac{L_n}{L_o} \right)^{-0.02JRC_o}$$

where JRC_o , and L_o (length) refer to 100 mm laboratory scale samples and JRC_n , and L_n refer to in situ block sizes.





Influence of scale on JRC and JCS



- ▶ Because of the greater possibility of weaknesses in a large surface, it is likely that the average joint wall compressive strength (JCS) decreases with increasing scale. Barton and Bandis (1982) proposed the scale corrections for JCS defined by the following relationship:

$$JCS_n = JCS_o \left(\frac{L_n}{L_o} \right)^{-0.03JRC_o}$$

where JCS_o and L_o (length) refer to 100 mm laboratory scale samples and JCS_n and L_n refer to in situ block sizes.





Joint Aperture Characterization



□ It is possible to estimate the initial mechanical aperture based on the values of JRC and JCS:

$$E_0 \approx \frac{JRC}{5} \left(0,2 \frac{\sigma_c}{JCS} - 0,1 \right) \quad [\text{mm}]$$

note that, when a joint is unaltered or unweathered (i.e. $JCS = \sigma_c$), the initial aperture may be a function only of surface roughness





Cubic Flow Law



- ❑ The simplest model of flow through a rock fracture is the parallel plate model.
- ❑ This is the only fracture model for which an exact calculation of the hydraulic conductivity is possible; this calculation yields the well-known cubic law.
- ❑ The derivation of the cubic law begins by assuming that the fracture walls can be represented by two smooth, parallel plates, separated by an aperture e .
- ❑ The flow space remains bounded by impermeable and rigid fracture walls (*no-slip* boundary conditions) .
- ❑ This system creates a uniform pressure gradient which lies entirely in the plane of the fracture, resulting in a unidirectional flow through the system.





Modified Cubic Flow Law



- An approach for estimating aperture consists of indirect measurement using borehole pumping tests, aperture is given by:

$$e = (12k)^{0.5}$$

where k is the conductivity in units of length squared



Permeability

- The cubic law, relating flow rate to aperture cubed is valid for joints and fractures varying from $4\mu\text{m}$ to $250\mu\text{m}$ (Witherspoon *et al*, 1979).
- The real mechanical aperture was nearly the same as the conducting aperture. The reduction in flow rate is attributed to roughness effects.



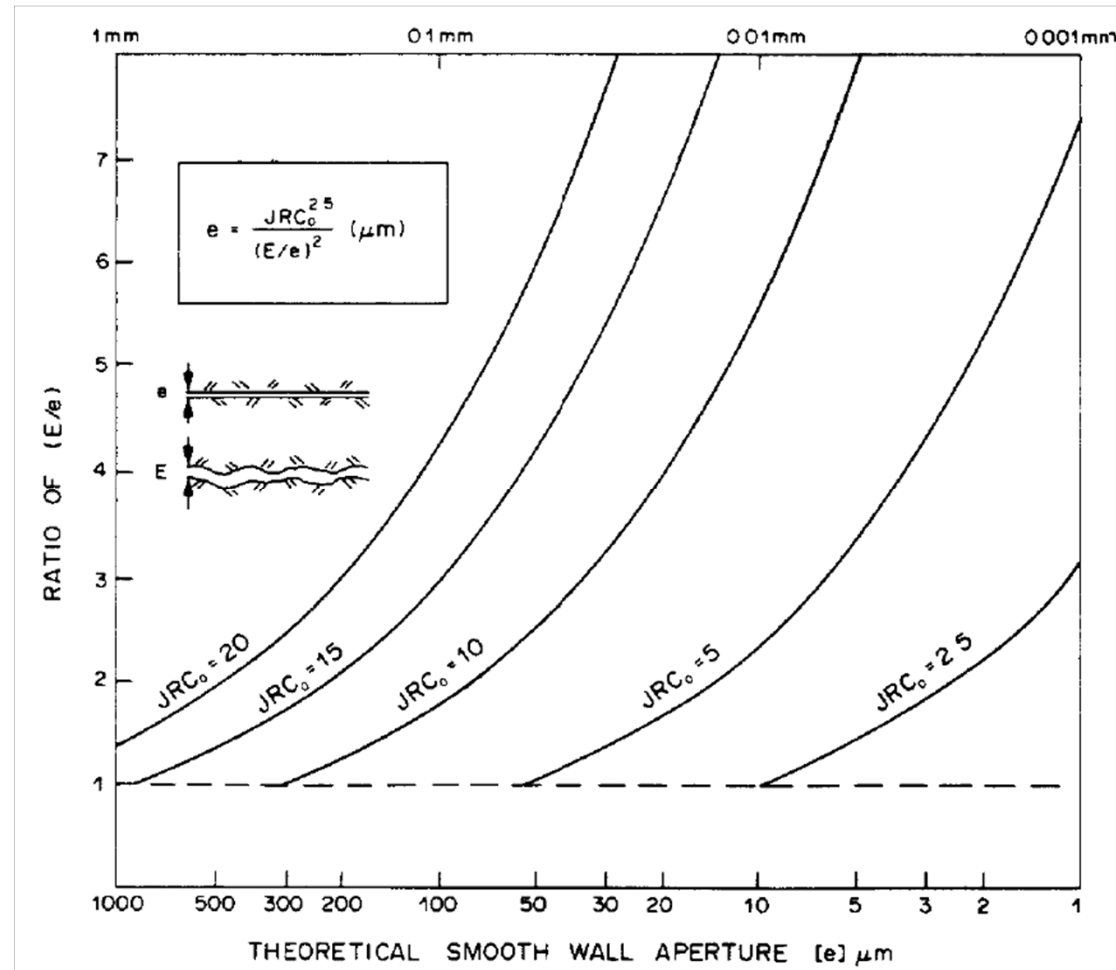


Modified Cubic Flow Law



□ An empirical relation incorporating JRC and aperture which satisfies the trends exhibited by available flow test data:

$$e = \frac{E^2}{JRC^{2,5}} \quad [\mu m]$$





Modified Cubic Flow Law



The permeability of the fracture can be identified as

$$k = \frac{e^2}{12}$$

The product of the permeability and area, also known as *transmissivity*, is equal to:

$$T \equiv kA = \frac{We^3}{12} \rightarrow \text{Fracture Frequency}$$

The dependence of T on e^3 is the essence of the well-known cubic law.





Normal Closure Behavior

Normal Closure Modeling



□ It is possible to predict shear strength-deformation behavior and normal stress-closure behavior with acceptable accuracy, using some very simple index tests.

Net deformation of the joints

$$\Delta V_j = \underbrace{\Delta V_t}_{\text{Total deformation across the jointed samples}} - \underbrace{\Delta V_r}_{\text{Deformation across the intact samples}}$$

Total deformation across the jointed samples

Deformation across the intact samples

$$\sigma_n = \frac{\Delta V_j}{a - b\Delta V_j}$$

$$\frac{\Delta V_j}{\sigma_n} = a - b\Delta V_j$$

$$\sigma_n \rightarrow \infty \Rightarrow \frac{a}{b} = V_m$$

$$\sigma_n \rightarrow 0 \Rightarrow \Delta V_j \rightarrow 0 \Rightarrow K_n = \frac{1}{a} = K_{ni}$$

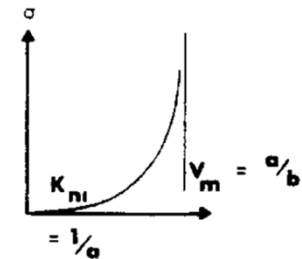
$$\sigma_n = \frac{K_{ni}V_m\Delta V_j}{V_m - \Delta V_j}$$

$$K_n = \frac{\partial \sigma_n}{\partial \Delta V_j} = \frac{1}{\left(1 - \frac{\Delta V_j}{V_m}\right)^2} = \frac{K_{ni}}{\left[1 - \frac{\sigma_n}{(K_{ni}V_m + \sigma_n)}\right]^2}$$

NORMAL CLOSURE OF JOINTS

(HYPERBOLIC FUNCTION)

$$\frac{\Delta V_j}{\sigma_n} = a - b\Delta V_j$$





Normal Closure Behavior

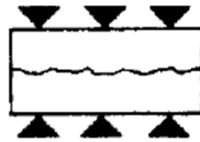
Normal Closure Modeling



NORMAL STIFFNESS OF JOINTS

(derivative of hyperbolic function)

$$K_n = K_{ni} \left[1 - \frac{\sigma_n}{v_m K_{ni} + \sigma_n} \right]^{-2}$$

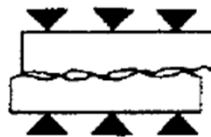


I. INTERLOCKING JOINTS

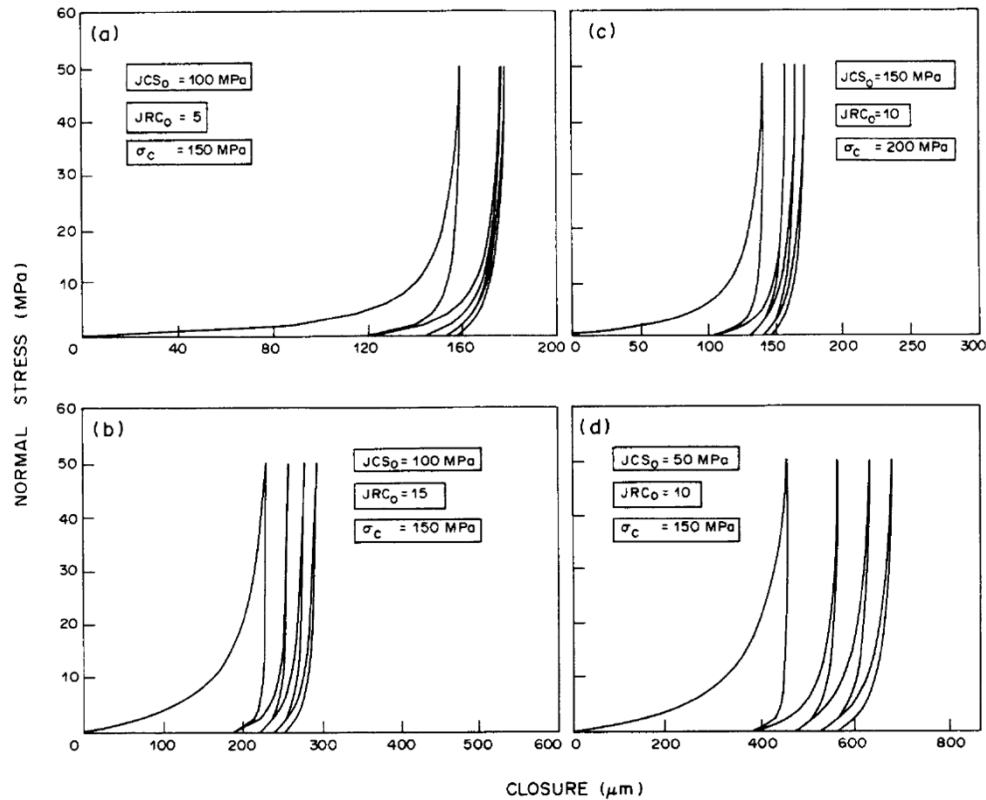
i.e. K_n is not proportional to σ_n

II. MISMATCHED JOINTS

K_n is proportional to σ_n



Stress closure modeling, showing the influence of roughness (Barton & Bakhtar, 1983)





Closure – Conductivity Coupling

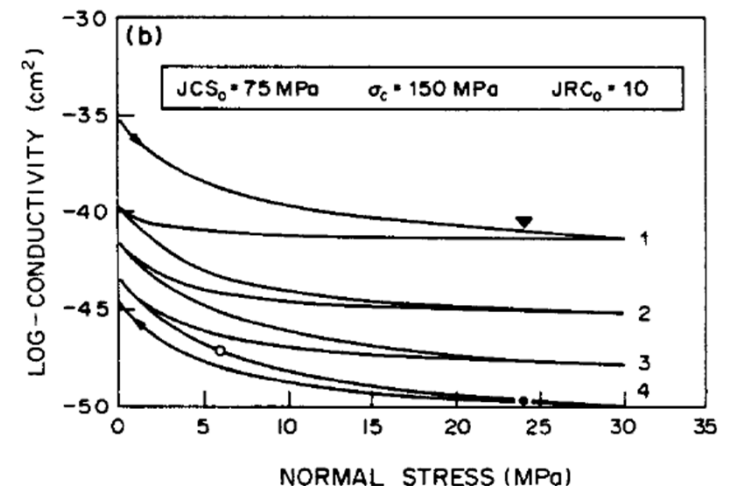
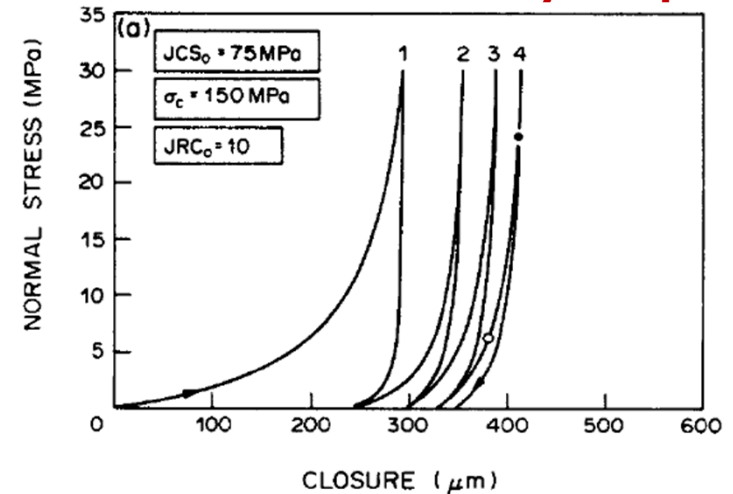


□ The above model describing changes of mechanical aperture (ΔE) with normal stress, provides simultaneous data concerning the residual mechanical aperture (E) by subtraction from the initial aperture E_0

$$E = E_0 - \Delta E$$

□ The joint conductivity can be estimated from the residual mechanical aperture (E) to the residual conducting apertures (e), the conductivity being proportional to e^2

Stress-closure-conductivity coupling





Conclusions



- ❑ Tilt tests and Schmidt rebound tests conducted on jointed core or on exposed jointed blocks are all that are required to obtain estimates of the roughness (JRC), the wall strength (JCS), the residual friction ($\phi_{b,r}$) and the conductivity aperture (e). Borehole pumping tests can be utilized if available.

- ❑ An important aspect of the coupling between joint deformation and conductivity, is the mismatch of the mechanical aperture (E) and the theoretical smooth wall conducting aperture (e) used in the cubic law for flow rate. Areas of asperity contact, tortuous flow, and wall roughness account for these differences, which can now be quantified, based on a constitutive model relating, E, e and JRC.

- ❑ In general, smooth joints and weak rocks close most readily under normal stress, and display low shear strength and weak coupling between shearing and conductivity.

- ❑ Rough joints and strong rocks close least under normal stress, and display high shear strength and strong coupling between shearing and conductivity.





RECENT MODELS:

Maksimovic (1992, 1996)

Kulatilake (1995)

Grasselli (2001)





Maksimovic (1992 and 1996)



- ▶ Proposed a hyperbolic function to deduce the angle of shearing resistance of rock joints.

$$\tau = \sigma_n \cdot \tan \left(\phi_b + \frac{\Delta_\phi}{1 + \frac{\sigma_n}{p_n}} \right)$$

Where τ is the peak shear strength of joint, σ_n is the effective normal stress and ϕ_b is the basic friction angle. The coefficient Δ_ϕ is the joint roughness angle which is the angle of maximum dilatancy. p_n is the median angle pressure which is equal to the normal stress when the contribution is equal to one half of Δ_ϕ





Kulatilake (1995)



- ▶ Proposed another equation to estimate the shear strength of rock joints based on fractal theory:

$$\tau = \sigma_n (\phi_b + a(SRP)^c \left(\log_{10} \left(\frac{\sigma_j}{\sigma} \right) \right)^d + I)$$

Where I is the average inclination of the asperities, σ_j the compressive strength of the joint surface. “ a ”, “ c ” and “ d ” are empirical constants which are determined by regression analysis of data from shear tests.

SRP is the stationary roughness parameter and is based on fractal parameters for quantification of surface roughness.





Grasselli (2001)



- ▶ In this case it was considered the anisotropy of the shear strength in the shear failure criterion.
- ▶ He used detailed surface measurements of joints by taking optical measurements (ATM - Advanced Topometric System).





Grasselli (2001)



The equation proposed is based on experimental results:

$$\tau = \sigma_n \cdot \tan(\phi'_r) \cdot (1 + g)$$

Where:

$$\phi'_r = \phi_b + \beta$$



(residual friction angle)

$$\beta = (C \cdot A_o^{1.5} \cdot \theta_{max}^* \cdot \left(1 - A_o^{\frac{1}{C}}\right))^{\cos \alpha}$$



(effect of roughness on the friction angle)

α is the angle of schistosity planes in the rock with respect to the normal of the joint





Grasselli (2001)



The equation proposed is based on experimental results:

$$\tau = \sigma_n \cdot \tan(\phi'_r) \cdot (1 + g)$$

Term taking into account the effect of the surface morphology on the peak shear strength.

$$g = e^{-\frac{\theta_{max}^* \cdot \sigma_n}{9 \cdot A_0 \cdot C \cdot \sigma_t}}$$

Where σ_t is the tensile strength of the intact rock





**OTHER RECENT MODELS:
HYDRO-MECANICAL MODELS FOR PREDICTING
CLOSURE BEHAVIOR OF ROCK JOINT**





Summary



- Paper 1: A constitutive model to predict the hydromechanical behavior of rock joints (2007) ;
- Paper 2: A new numerical 3D-model for simulation of hydraulic fracturing in consideration of hydro-mechanical coupling effects (2013);
- Paper 3: Constitutive model for small rock joint samples in the lab and large rock joint surfaces in the field (2009);
- Paper 4: Mechanics of a discontinuity in a geomaterial (2004);
- Paper 5: A numerical procedure for the analysis of the hydromechanical coupling in fractured rock masses (1998) ;
- Paper 6: A New Model for Normal Deformation of Single Fractures under Compressive Loading (2004);





PAPER 1: A constitutive model to predict the hydro mechanical behavior of rock joints

Dominic Tremblay, Richard Simon and Michel Aubertin

Department of civil, geological & mining engineering – École Polytechnique,
Montréal, Québec, Canada.



□ Abstract

The mechanical behavior of rock joints can be strongly influenced by water flow, while the water pressure may in turn affect the joint response. These coupled phenomena should be considered simultaneously to simulate the behaviour of rock joints. The CSDS constitutive model was developed by the authors to represent the mechanical behavior of dry rock joints. In this paper, the authors show how the CSDS model can be adapted to take into account the presence of water on the joint behaviour. The modified model formulation is presented and then validated with experimental data from hydromechanical tests taken from the literature. A discussion on the significance of the model follows.





PAPER 1: A constitutive model to predict the hydro mechanical behavior of rock joints

Dominic Tremblay, Richard Simon and Michel Aubertin

Department of civil, geological & mining engineering – École Polytechnique,
Montréal, Québec, Canada.



□ **Model Description:** The CSDS model has been developed to fully describe the behaviour of dry rock joints in pre-peak and post-peak phases. **Simon (1999 – Simon et al. 1999)**

- Shear stress – shear displacement relationship

$$\tau = a + b \exp(-c u) - d \exp(-e u)$$

$$\begin{aligned} a &= \tau_r \\ b &= d - a \\ c &= 5 / u_r \end{aligned}$$

$\tau \rightarrow$ shear stress (Mpa)

$u \rightarrow$ shear displacement (mm)

$a, b, c, d, e \rightarrow$ model parameters

$$\text{conditions } \left\{ \begin{array}{l} c < e \\ a, b, c, d, e > 0 \end{array} \right.$$

$$\left\{ \begin{array}{l} \frac{d e u_r}{5(d - \tau_r)} - \exp\left[u_p \left(e - \frac{5}{u_r} \right) \right] = 0 \\ d = \frac{\tau_p - \tau_r \left[1 - \exp\left(-\frac{5u_p}{u_r} \right) \right]}{\exp\left(-\frac{5u_p}{u_r} \right) - \exp(-e u_p)} \end{array} \right.$$

System for calculating parameters d, e

$\tau_p \rightarrow$ peak strength

$\tau_r \rightarrow$ residual strength

$u_p \rightarrow$ displacement at peak strength

$u_r \rightarrow$ displacement at the onset of τ_r (independent of the normal stress level σ_n)



PAPER 1: A constitutive model to predict the hydro mechanical behavior of rock joints

Dominic Tremblay, Richard Simon and Michel Aubertin

Department of civil, geological & mining engineering – École Polytechnique,
Montréal, Québec, Canada.



- Shear stress – shear displacement relationship

$$\tau_r = \sigma_n \tan \phi_r$$

Calculation of residual shear strength:
Coulomb criterion without cohesion

σ_n → normal stress

ϕ_r → residual friction angle on the joint surface

$$\tau_p = \sigma_n (1 - a_s) \tan (i + \phi_r) + a_s S_r$$

Calculation of peak shear strength: LADAR (Ladanyi and Archambault 1970) criterion

$$i = \tan^{-1} \left[\left(1 - \frac{\sigma_n}{\sigma_T} \right)^{k_2} \tan i_0 \right]$$

i_0 → parameter that represents the initial mean angle of asperities

σ_T → transitional stress (taken as the uniaxial compressive strength C_0 ; Goodman, 1976)

k_1 e k_2 → material constants for the LADAR model determined experimentally ($k_1=1.5$ e $k_2=4.0$)

a_s → proportion of the projected sheared asperity surface to the joint surface at peak strength

S_r → shear strength of the rock making the asperities

S_0 → rock cohesion

ϕ_0 → friction angle

$$S_r = S_0 + \sigma_n \tan \phi_0$$



PAPER 1: A constitutive model to predict the hydro mechanical behavior of rock joints

Dominic Tremblay, Richard Simon and Michel Aubertin

Department of civil, geological & mining engineering – École Polytechnique,
Montréal, Québec, Canada.



- The normal displacement - shear displacement relationship

$$v = \beta_1 - \beta_2 \exp(-\beta_3 u)$$

$$\beta_1 = u_r \left(1 - \frac{\sigma_n}{\sigma_T} \right)^{k_2} \tan i_0 + \frac{\sigma_n V_m}{k_{ni} V_m - \sigma_n}$$

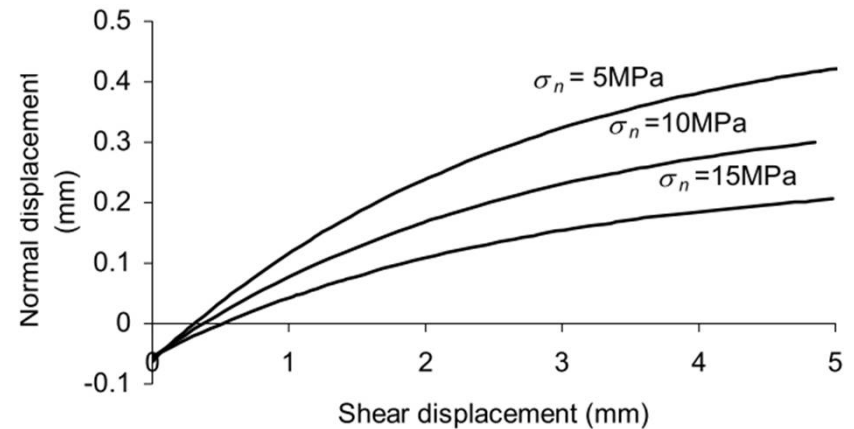
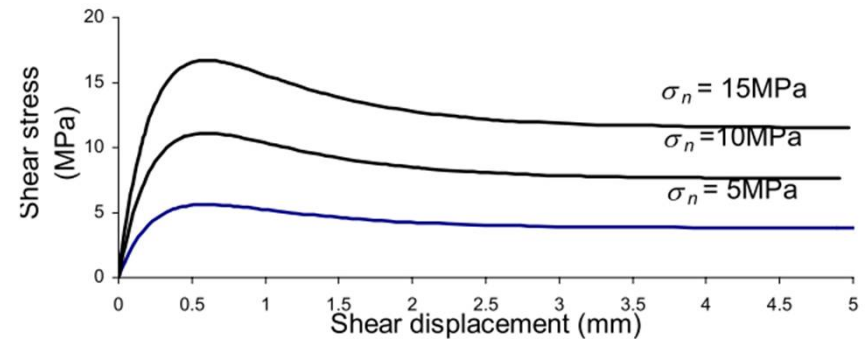
$$\beta_2 = \beta_1 - \frac{\sigma_n V_m}{k_{ni} V_m - \sigma_n}$$

$$\beta_3 \cong \frac{1.5}{u_r}$$

$\beta_1, \beta_2, \beta_3 \rightarrow$ Model Parameters

$V_m \rightarrow$ maximum closure of the joint

$k_{ni} \rightarrow$ initial normal stiffness of the joint





PAPER 1: A constitutive model to predict the hydro mechanical behavior of rock joints

Dominic Tremblay, Richard Simon and Michel Aubertin

Department of civil, geological & mining engineering – École Polytechnique,
Montréal, Québec, Canada.



- Prediction of the hydromechanical behavior with the csds model

Mechanical behavior: When a fluid pressure is acting in a rock joint, the effective normal stress (σ'_n) on the joint surface

$$\sigma'_n = \sigma_n - P_w$$

The CSDS model is modified here by replacing σ_n by σ'_n in all the above equations

σ_n → global normal stress on the rock joint

P_w → water pressure

Hydraulic behavior

using the analogy of two parallel and perfectly smooth plates to model the water flow through a rock joint. The analytical solution to the Navier-Stokes equations for a laminar fluid flow can then be used..

$$Q_f = V_f A_{sec} = - \left[\frac{\rho g b^3 w \Delta h}{12 \mu L} \right]$$

$$k_f = \frac{b^2}{12}$$

$$T_f = \frac{b^3}{12}$$

Q_f → Flow in the rock joint (m^3/s)

V_f → Mean velocity (m/s)

A_{sec} → Area perpendicular to the flow (m^2)

b → Distance between the rock joint surfaces or joint hydraulic opening (m)

Δh → Hydraulic gradient (m)

W → Joint dimension perpendicular to the flow (m)

L → Path length parallel to the flow (m)

g → Gravitational acceleration (m/s^2)

ρ → Water density (kg/m^3)

μ → Dynamic viscosity (kg/ms)

K_f → Intrinsic permeability of a joint (m^2)

T_f → Intrinsic transmissivity (m^3)



PAPER 1: A constitutive model to predict the hydro mechanical behavior of rock joints

Dominic Tremblay, Richard Simon and Michel Aubertin

Department of civil, geological & mining engineering – École Polytechnique,
Montréal, Québec, Canada.



- Prediction of the hydromechanical behavior with the csds model

Hydraulic opening - mechanical opening relation

$$\Delta b = \Delta v$$

Hydraulic opening is proportional to the mechanical opening: Mechanical opening increase (or decrease) caused by shearing of the joint will cause an equal increase (or decrease) in the hydraulic opening

$\Delta v \rightarrow$ Variation of the mechanical opening from its initial state

$$T_f(u) = \frac{(b + \Delta v)^3}{12}$$

To use this approach, the initial flow properties of the rock joint must be known so the value of the initial hydraulic opening b can be established.

$$\Delta v = \beta_2 [1 - \exp(-\beta_3 u)]$$





PAPER 1: A constitutive model to predict the hydro mechanical behavior of rock joints

Dominic Tremblay, Richard Simon and Michel Aubertin

Department of civil, geological & mining engineering – École Polytechnique,
Montréal, Québec, Canada.



References:

- Simon R. 1999. Analysis of fault-slip mechanisms in hard rock mining. Tese de Doutorado, McGill University.
- Simon R., Aubertin M. & Mitri H.S. 1999. A non-linear constitutive model for rock joints to evaluate unstable slip. Proc. 37th U.S. Rock Mech. Symp., Rock Mechanics for Industry, Amadei, Kranz, Scott & Smealli (eds), Vol.2, Balkema, Rotterdam, 1091-1098.

<https://www.onepetro.org/conference-paper/ARMA-99-1091>





PAPER 2: A new numerical 3D-model for simulation of hydraulic fracturing in consideration of hydro-mechanical coupling effects

Lei Zhou *, Michael Z. Hou **

*Energy Research Center of lower Saxony, Goslar, Germany;

**Institute of Petroleum Engineering, Clausthal University of Technology, Clausthal-Zellerfeld, Germany .



□ Abstract:

A new approach for simulating hydraulic fracture propagation, which treats fracture propagation in a 3D geometric model under 3D stress state with fully hydro-mechanical coupling, is introduced and integrated into the software FLAC3D. In the new modeling approach, the mechanical behavior of the rock formation is based on continuum mechanics. A modified tensile failure model has been used to describe fracture enlargement and closure. Meanwhile, a simplified fracture flow equation derived from the general Navier–Stokes equation and Darcy law, has been developed and used to describe fluid flow, both in the fracture and in the matrix. Fluid leakoff is no longer controlled by semi-analytical models, such as the Carter model, but resolved by means of numerical methods. In order to describe fracture propagation, the tensile failure criterion has been applied. To verify the new modeling approach, simulation of a laboratory test has been carried out. Numerical and measured results have been compared and found to be in agreement. After verification of the new modeling approach, a calculation, based on real data for a tight gas sandstone reservoir from the Northern German Basin, has been applied and graphically illustrated. Unlike conventional models, the new modeling approach not only considers the propagation of a single fracture, but also its influence on the adjacent rock formations and the neighboring fractures.





PAPER 2: A new numerical 3D-model for simulation of hydraulic fracturing in consideration of hydro-mechanical coupling effects

Lei Zhou *, Michael Z. Hou **

*Energy Research Center of lower Saxony, Goslar, Germany;

**Institute of Petroleum Engineering, Clausthal University of Technology, Clausthal-Zellerfeld, Germany .



□ **Model description:** a new approach is introduced and integrated into FLAC3D, which considers fracture propagation in 3D geometric model under 3D stress state and fully hydromechanical coupling effect between fracture and matrix. FLAC3D is a simulator for solving geotechnical problems. Mechanical effects (quasi-static + dynamic), hydraulic effects, and thermal conduction and convection (including their coupling effects). The basic modeling concept for the new approach is almost the same as for the Planar 3D (PL3D) model with a fixed rectangular mesh (Adachi et al., 2007; Garagash & Detournay, 2005). They differ only in their mathematical details to describe the mechanical and hydraulic behavior, including coupling during the calculations.

- Mechanical model

$$Cw = \int_{\Omega(t)} C(x,y)w(x,y,t)dx dy = P_f(x,y,t) - \sigma_c(x,y)$$

PL3D model: elasticity equation is used to calculate Fracture width due to pressure changes in the fracture at each grid point (on the fracture boundary) .

w → fracture width (m)

P_f → fluid pressure inside the fracture(Pa)

σ_c → closure stress(Pa)

C → contains information about the layered elastic medium.



PAPER 2: A new numerical 3D-model for simulation of hydraulic fracturing in consideration of hydro-mechanical coupling effects

Lei Zhou *, Michael Z. Hou **

*Energy Research Center of lower Saxony, Goslar, Germany;

**Institute of Petroleum Engineering, Clausthal University of Technology, Clausthal-Zellerfeld, Germany .



- Mechanical model (cont.): Actually the patterns of stress redistribution after tensile failure and that displayed by the linear elastic model with change of σ_3 are similar. All required at tensile failure is to replace $\Delta\sigma_3$ with the overloaded stress ($\sigma_3 - \sigma_t$). This stress redistribution will proportionally lead to a similar variation in displacement. The study demonstrates that changes in the stress boundary due to the pressurizing fluid in the fracture could be represented by the changes in the normal stress on the fracture wall, hence $\Delta\sigma_3 = P_f - \sigma_3$, in the fractured element:

$$\sigma_3^N = \sigma_3^O + \Delta\sigma_3$$

$$\sigma_1^N = \sigma_1^O - \Delta\sigma_3 \alpha_2 / \alpha_1$$

$$\sigma_2^N = \sigma_2^O - \Delta\sigma_3 \alpha_2 / \alpha_1$$

$K \rightarrow$ bulk modulus (Pa)

$G \rightarrow$ shear modulus (Pa)

$\varepsilon \rightarrow$ strain

$\sigma \rightarrow$ stress (Pa)

$P_f \rightarrow$ fluid pressure in fracture (Pa),

$N \rightarrow$ denotes “new”

$O \rightarrow$ denotes “old”,

$\sigma_t \rightarrow$ tensile strength (Pa)

$\alpha_1 \alpha_2 \rightarrow$ Elastic parameters





PAPER 2: A new numerical 3D-model for simulation of hydraulic fracturing in consideration of hydro-mechanical coupling effects

Lei Zhou *, Michael Z. Hou **

*Energy Research Center of lower Saxony, Goslar, Germany;

**Institute of Petroleum Engineering, Clausthal University of Technology, Clausthal-Zellerfeld, Germany .



- **Hydraulic model:** In hydraulic fracturing the flow process can be divided into three parts, i.e., flow in matrix, flow in fracture and flow exchange between matrix and fracture. In FLAC3D, however, there is no option for calculating fracture flow. To calculate the fluid flow in a fracture, a built-in flow simulator FTP3D (pseudo-3D simulator for fracture flow) is implemented in FLAC3D through the user interface.

mass balance equation and the simplified Navier– Stokes equation of flow in two planes with incompressible fluid

$$\frac{\partial w}{\partial t} + \nabla \cdot (\bar{v}w) + wq_s = 0$$

$$-\nabla P = \frac{\mu}{K(w)} v, \quad K(w) = (fw)^2 / (12\mu)$$

$w \rightarrow$ fracture width (m)

$t \rightarrow$ time (s)

$q_s \rightarrow$ source term (l/s)

$v \rightarrow$ velocity (m/s)

$P \rightarrow$ pressure (Pa)

$\mu \rightarrow$ viscosity (Pa s)

$K \rightarrow$ transmissivity (m²)

$f \rightarrow$ parameter that reflects the influence of the roughness on the transmissivity (For smooth fracture surface, f is approximately 1.0; for rough fracture surface, whereas f has values smaller than 1.0)





PAPER 2: A new numerical 3D-model for simulation of hydraulic fracturing in consideration of hydro-mechanical coupling effects

Lei Zhou *, Michael Z. Hou **

*Energy Research Center of lower Saxony, Goslar, Germany;

**Institute of Petroleum Engineering, Clausthal University of Technology, Clausthal-Zellerfeld, Germany .



- Hydraulic model: The flow option (Darcy flow) inFLAC3D is used to calculate flow in the matrix. The only problem, however, is to model the flow exchange between matrix and fracture. In order to model this flow exchange the concept of coupling was set-up. Exchange is described by an additional source term in each timestep. It is induced by the pressure difference between the matrix element and the internal fracture in the element at the previous timestep.

$$q_{sf}^{t+1} = \frac{K_m S}{\mu V_f} \left(\frac{P_m^t - P_f^t}{h_1} + \frac{P_m^t - P_f^t}{h_2} \right) \text{ in fracture}$$

$$q_{sm}^{t+1} = \frac{K_m S}{\mu V_m} \left(\frac{P_f^t - P_m^t}{h_1} + \frac{P_f^t - P_m^t}{h_2} \right) \text{ in matrix}$$

$q_s \rightarrow$ source term (l/s)

$V \rightarrow$ volume (m³)

$P \rightarrow$ pressure (Pa)

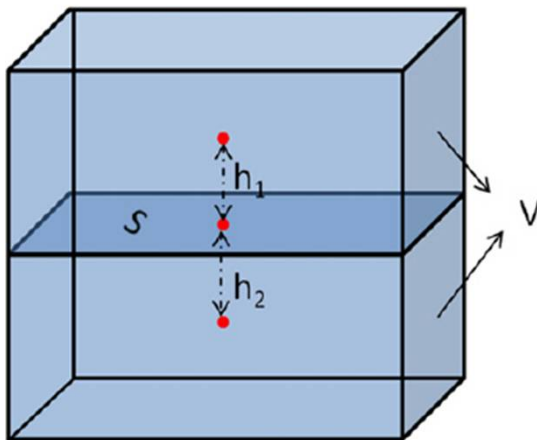
$t \rightarrow$ time (s)

$S \rightarrow$ fracture area (m²)

$m \rightarrow$ denotes “matrix”

$f \rightarrow$ denotes “fracture”

$h_1, h_2 \rightarrow$ distances between the fracture plane and the geometrical center of the two fracture





PAPER 2: A new numerical 3D-model for simulation of hydraulic fracturing in consideration of hydro-mechanical coupling effects

Lei Zhou *, Michael Z. Hou **

*Energy Research Center of lower Saxony, Goslar, Germany;

**Institute of Petroleum Engineering, Clausthal University of Technology, Clausthal-Zellerfeld, Germany .



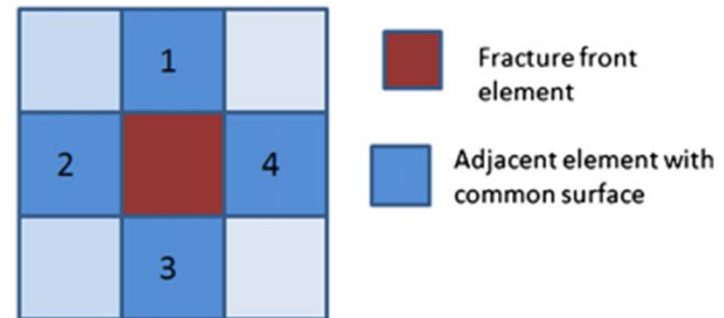
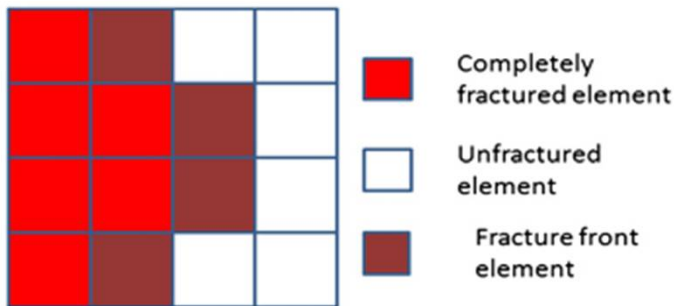
• Propagation criteria

P_{int} → interpolated fluid pressure in fracture front element (Pa)

P_{res} → reservoir pressure in the unfractured element (Pa)

g → a weighting factor (Pa) (The weighting factor depends on the rock permeability in the common surface and the distance between the center of the fracture front element and its neighbors. In the calculation the tension failure criterion is used to determine whether the fracture propagates or not. If the fluid pressure is bigger than the sum of the minimal principle stress and tensile strength ($P_{int} > \sigma_3 + \sigma_t$), then the fracture front element changes to completely fractured element.)

$$P_{int} = \sum_{i=1}^n P_f^i g_i + \sum_{o=1}^{4-n} P_{res}^o g_o \quad (n < 4)$$





PAPER 2: A new numerical 3D-model for simulation of hydraulic fracturing in consideration of hydro-mechanical coupling effects

Lei Zhou *, Michael Z. Hou **

*Energy Research Center of lower Saxony, Goslar, Germany;

**Institute of Petroleum Engineering, Clausthal University of Technology, Clausthal-Zellerfeld, Germany .



- Hydro-mechanical coupling and its solution: calculation procedure to solve the following equations:

$$\frac{\partial w}{\partial t} = \nabla \left[\frac{w(fw)^2}{12\mu} (\nabla P_f - \rho g) \right] + w(q_{inj} + q_{sf})$$

→ Can be approximated in a finite difference form by Finite Volume Method (FVM)

$$\frac{K_f}{\mu} \left(\frac{\partial^2 P}{\partial x^2} + \frac{\partial^2 P}{\partial y^2} + \frac{\partial^2 P}{\partial z^2} \right) + q_{sm} = \frac{1}{M_b} \frac{\partial P}{\partial t} + \alpha \frac{\partial e}{\partial t}$$

$\rho \rightarrow$ density (kg/m³)

$e \rightarrow$ mean strain

$a_r, a_l, a_u, a_{ab} \rightarrow$ factors calculated by the conductivity and geometrical relation [m³/(N s)]

$$q_{sf}^{t+1} = \frac{K_m S}{\mu V_f} \left(\frac{P_m^t - P_f^t}{h_1} + \frac{P_m^t - P_f^t}{h_2} \right)$$

$$q_{sm}^{t+1} = \frac{K_m S}{\mu V_m} \left(\frac{P_f^t - P_m^t}{h_1} + \frac{P_f^t - P_m^t}{h_2} \right)$$

To guarantee that the fluid volume in the fracture is equal to the integral of the fracture width over the fracture plane (fracture volume), the equation system should be fully coupled and solved together.

$$(\lambda + G) \frac{\partial e}{\partial x_i} + G \nabla^2 u - \rho \frac{\partial^2 u}{\partial t^2} = 0$$

$$\Delta \varepsilon^f = \Delta \varepsilon_3 = \frac{P_f - \sigma_3}{\alpha_1}$$

$$\Delta w = \Delta \varepsilon^f l_c$$

→ The change of the fracture width in the Eq. below can be substituted through a combination of this two Equations.

$$\left. \begin{aligned} a_l P_l^{t+1} + a_r P_r^{t+1} + a_u P_u^{t+1} + a_{ab} P_{ab}^{t+1} - (a_l + a_r + a_u + a_{ab}) P_o^{t+1} \\ = \frac{\Delta w}{\Delta t} - (q_{inj} + q_{sf}) w^t = \frac{(P_o^{t+1} - \sigma_3^t) l}{\alpha_1 \Delta t} - (q_{inje.} + q_{sf}) w^t \end{aligned} \right\}$$

Linear equation system: solved by the generalized minimal residual method (GMRS)



PAPER 2: A new numerical 3D-model for simulation of hydraulic fracturing in consideration of hydro-mechanical coupling effects

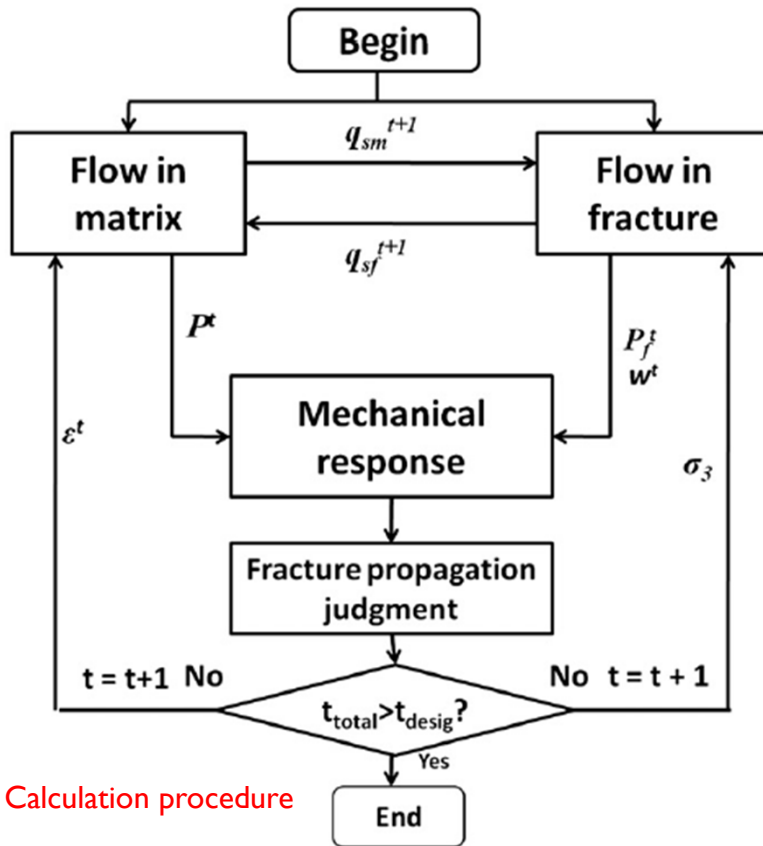
Lei Zhou *, Michael Z. Hou **

*Energy Research Center of lower Saxony, Goslar, Germany;

**Institute of Petroleum Engineering, Clausthal University of Technology, Clausthal-Zellerfeld, Germany .



- Hydro-mechanical coupling and its solution: calculation procedure to solve the following equations:



Calculation procedure

Flow chart of the computational procedure. Because of the time discretization the calculation is built in a loop with limited loop numbers. In each loop fluid flow in matrix and fracture are carried out first, but independently. With the calculated fracture and pore pressure the exchange source term for the next time step is evaluated. Secondly, the pressure and the new fracture width are transferred in the mechanical calculation, in which the stress redistribution is estimated. Finally, the new stress and elastic strain.



PAPER 2: A new numerical 3D-model for simulation of hydraulic fracturing in consideration of hydro-mechanical coupling effects

Lei Zhou *, Michael Z. Hou **

*Energy Research Center of lower Saxony, Goslar, Germany;

**Institute of Petroleum Engineering, Clausthal University of Technology, Clausthal-Zellerfeld, Germany .



□ References:

- Adachi J, Siebrits E, Peirce A, Desroches J. Computer simulation of hydraulic fractures. *Int J Rock Mech Min Sci* 2007;44:739–57.
- Garagash DI, Detournay E. Plane-strain propagation of a hydraulic fracture: small toughness solution. *J Appl Mech* 2005;72(6):916–28





PAPER 3: Constitutive model for small rock joint samples in the lab and large rock joint surfaces in the field

R. E. Barbosa

EngSolutions, Inc., Ft. Lauderdale, Florida, USA



□ Abstract:

A new constitutive model for rock joints is proposed for predicting the mechanical behavior of both small joint samples in the lab and large joint surfaces in the field. The normal and shear behavior of joints samples is predicted based on the strength and geometry of small-scale joint asperities. The behavior in the field is predicted based on the strength of smallscale asperities, determined from lab data, and the geometry of field-scale waviness determined from geologic observations. The concept of available shear strength is introduced to describe the degradation of asperities and the shape of the mobilized shear stress-displacement curve. Dilation and roughness degradation during shear is correlated to a dimensionless product of shear stress, incremental displacement, rock strength, and wavelength of irregularities. Instead of using any scaling procedures, the behavior of joints in the field is predicted by applying the model for lab samples to the actual contact areas developed in large-scale joint surfaces.





PAPER 3: Constitutive model for small rock joint samples in the lab and large rock joint surfaces in the field

R. E. Barbosa

EngSolutions, Inc., Ft. Lauderdale, Florida, USA



- **Model Description:** In the proposed model, the behavior of rock joints in the field is determined based on the strength and geometry of small-scale joint roughness determined from lab data, and the geometry of field-scale waviness determined from geologic observations. The proposed model is not a new shear strength criterion suitable for hand calculations such as limit equilibrium analysis. It is a complete fully incremental model that allows predicting the normal and shear behavior of unfilled joints subjected to general non-monotonic unidirectional loading, suitable for numerical analysis, including finite element analyses and discrete element analyses.





PAPER 3: Constitutive model for small rock joint samples in the lab and large rock joint surfaces in the field

R. E. Barbosa

EngSolutions, Inc., Ft. Lauderdale, Florida, USA



- Asperity degradation

$$\alpha = \alpha_0 e^{-cW_p}$$

$$W_p = \sum \tau \cdot d \delta_s^p, \tau$$

$\phi_r \rightarrow$ residual friction angle

$\alpha_0 \rightarrow$ initial average asperity angle

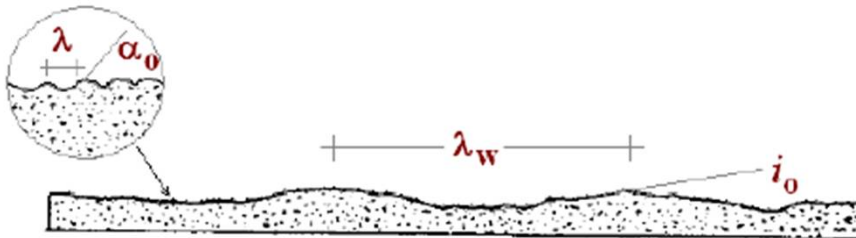
$c \rightarrow$ degradation constant

$W_p \rightarrow$ plastic work done in shear (

$\tau \rightarrow$ shear stress

$\delta_g^p \rightarrow$ plastic displacement

- Parameters of the proposed model



$\phi_r \rightarrow$ residual friction angle

$\alpha_0 \rightarrow$ initial average asperity angle

$\lambda \rightarrow$ asperity wavelength

$\sigma_c \rightarrow$ asperity compressive strength

$i_0 \rightarrow$ initial average waviness angle

$\lambda_w \rightarrow$ waviness wavelength



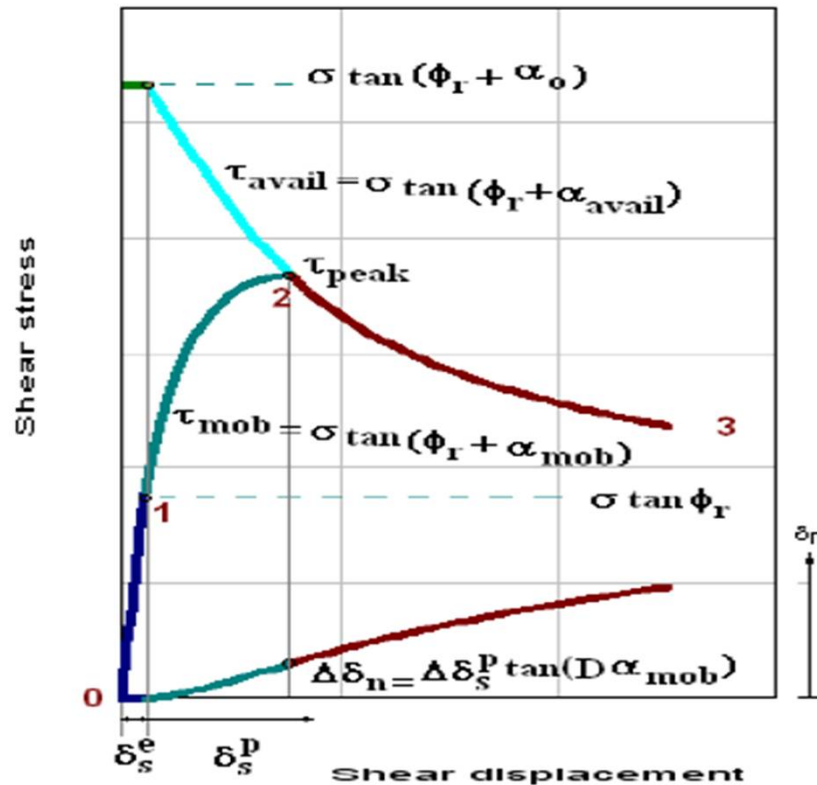
PAPER 3: Constitutive model for small rock joint samples in the lab and large rock joint surfaces in the field

R. E. Barbosa

EngSolutions, Inc., Ft. Lauderdale, Florida, USA



Shear behavior: The shear stress-displacement curve includes 3 stages: (1) mobilization of basic shear, (2) mobilization of peak strength, and (3) mobilization of residual strength.





PAPER 3: Constitutive model for small rock joint samples in the lab and large rock joint surfaces in the field

R. E. Barbosa

EngSolutions, Inc., Ft. Lauderdale, Florida, USA



- Shear behavior

$$d\alpha = -\frac{\kappa}{\lambda \cdot \sigma_c} \alpha \cdot \tau \cdot d\delta_s^p$$

Proposed degradation model: the decrement in asperity angle $d\alpha$, produced when a joint with a current asperity angle α , under a shear stress τ , undergoes an incremental sliding displacement $d\delta_s^p$

Elastic joint shear stiffness

$$K_{s_i} = \sigma_c \tan \phi_r / C$$

$$\tau_{mob} = \tau_{mob}^{old} + \Delta \tau$$

$$\alpha_{avail} = \alpha_{avail}^{old} + \Delta \alpha$$

Pre-peak plastic region

$$\alpha_{mob} = \tan^{-1}(\tau_{mob} / \sigma) - \phi_r$$

$$\tau_{avail} = \sigma \tan(\phi_r + \alpha_{avail})$$

$$K_t = K_{s_i} (1 - R_f \tau_{mob} / \tau_{avail})^2$$





PAPER 3: Constitutive model for small rock joint samples in the lab and large rock joint surfaces in the field

R. E. Barbosa

EngSolutions, Inc., Ft. Lauderdale, Florida, USA



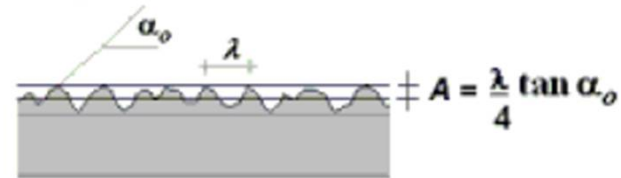
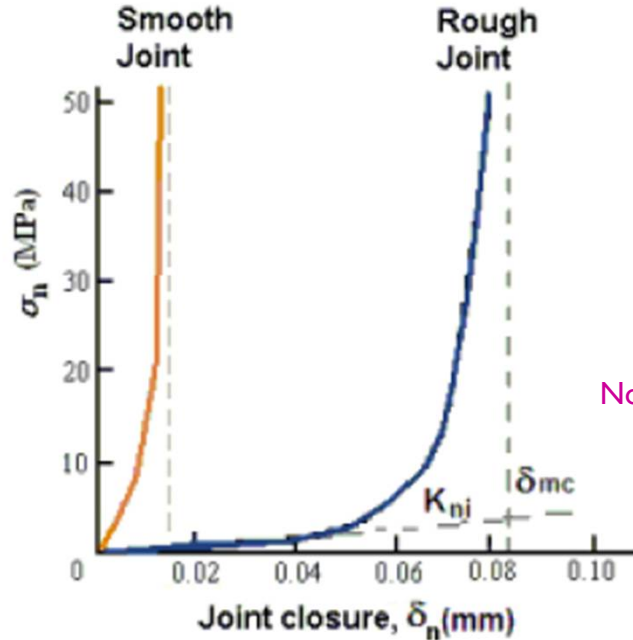
- Normal loading behavior

$$d\sigma_n = K_{ni} \left(1 - \frac{\sigma_n}{K_{ni} \delta_{mc} + \sigma_n} \right)^{-2} d\delta_n$$

hyperbolic equation to describe the normal stress-closure curves of rock joints

K_{ni} → initial normal stiffness

δ_{mc} → maximum joint closure



Normal- stress-closure curves for rock joints



PAPER 3: Constitutive model for small rock joint samples in the lab and large rock joint surfaces in the field

R. E. Barbosa

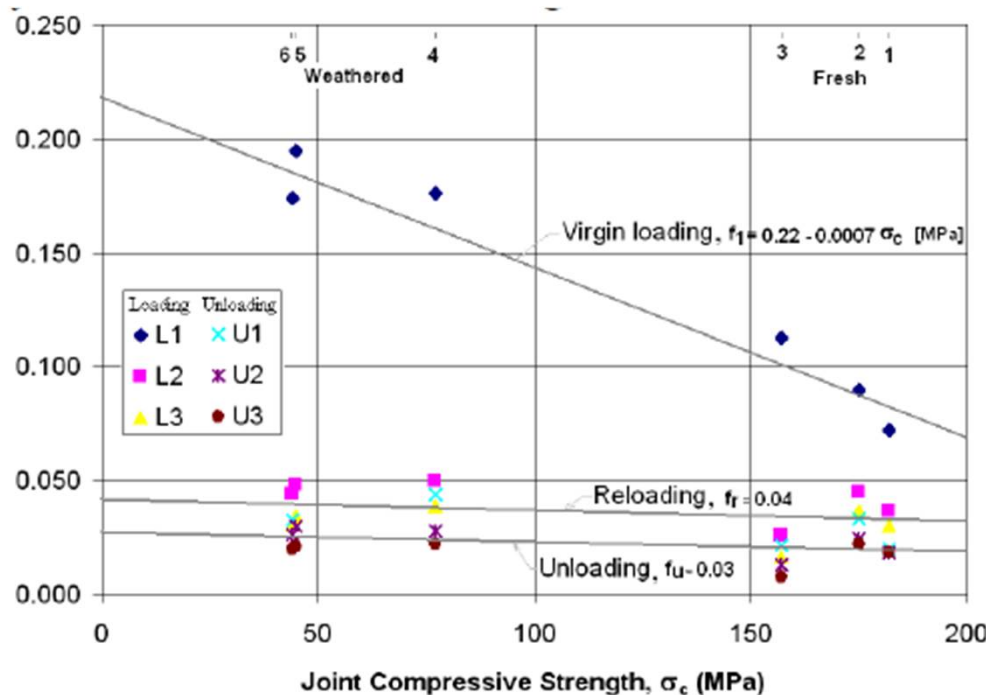
EngSolutions, Inc., Ft. Lauderdale, Florida, USA



- Normal loading behavior

$$\delta_{mc} = f \cdot \lambda \cdot \tan \alpha_0$$

Maximum joint closure: For the first loading cycle (virgin compression) of interlocked joints, the factor f is about 0.1 for fresh joints and about 0.2 for eathered joints. In general, f depends on σ_c and the loading history.



Fitting parameter f (Bandis et al., 1983)



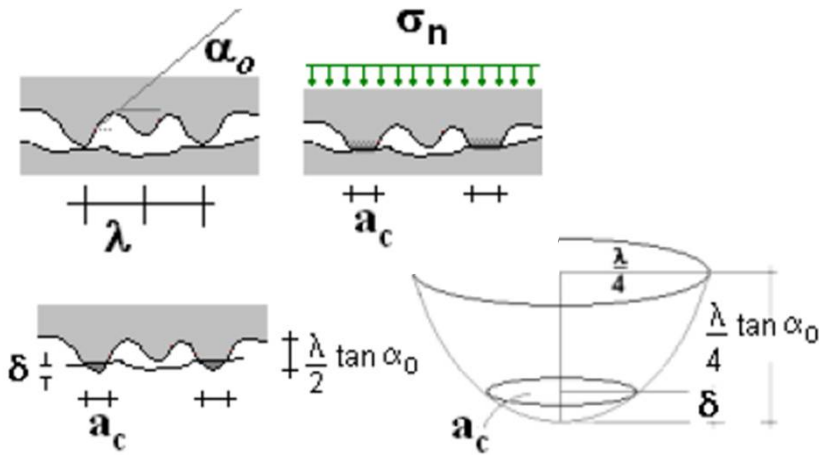
PAPER 3: Constitutive model for small rock joint samples in the lab and large rock joint surfaces in the field

R. E. Barbosa

EngSolutions, Inc., Ft. Lauderdale, Florida, USA



• Normal loading behavior



Development of contact area during normal loading and contact area for a paraboloidal asperity

$\sigma_n \rightarrow$ normal stress

$a_c \rightarrow$ contact area

$\sigma_c \rightarrow$ compressive strength of the asperity

$\eta \rightarrow$ the ratio between the number of asperities in contact and the total number of asperities.

$$\sigma_n = \frac{\pi \sigma_c \eta}{4 \lambda \tan \alpha} \delta_n$$

Normal stress-closure relation

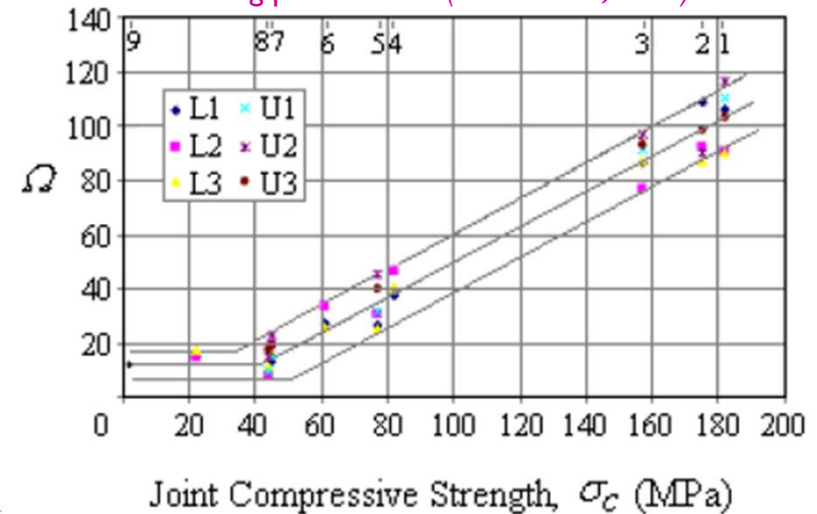
$$K_{ni} = \frac{\pi}{4} \eta_o f \frac{\sigma_c}{\delta_{mc}}$$

Initial normal stiffness

$$K_{ni} = \frac{\sigma_c}{\Omega \delta_{mc}}$$

Initial normal stiffness for real joints

Fitting parameter Ω (Bandis et al., 1983)



$$\Omega = -13.6 + 0.64 \sigma_c [MPa] \geq 12$$



PAPER 3: Constitutive model for small rock joint samples in the lab and large rock joint surfaces in the field

R. E. Barbosa

EngSolutions, Inc., Ft. Lauderdale, Florida, USA



- Normal loading behavior

Asperity degradation during normal loading

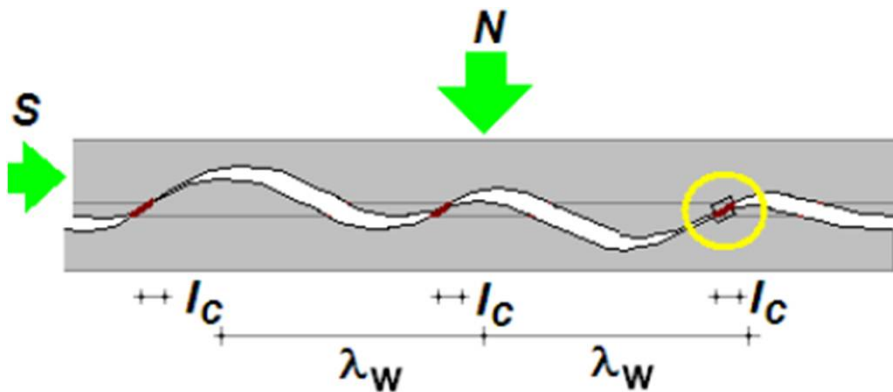
$$d\alpha = -\frac{4\cos^2 \alpha}{\lambda} d\delta_n^p$$

Decrement of the amplitude of asperities is equal to the plastic joint closure;

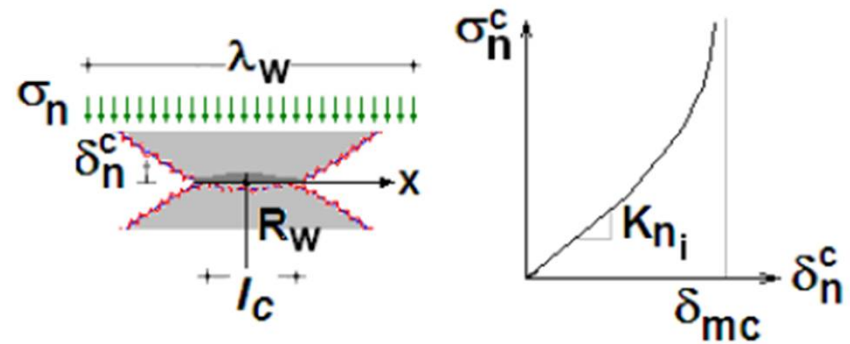
$$d\delta_n^p = d\delta_n - d\delta_n^e = (1 - f_u/f_1)d\delta_n$$

The plastic closure during virgin loading is the difference between the total closure and the elastic rebound.

- Field behavior



Reduced contact area due to waviness



contact area and contact stress-closure relation



PAPER 3: Constitutive model for small rock joint samples in the lab and large rock joint surfaces in the field

R. E. Barbosa

EngSolutions, Inc., Ft. Lauderdale, Florida, USA



- Field behavior
Contact area ratio

$$\sigma^c = \sigma_n / a$$
$$\tau^c = \tau_s / a$$

Contact stresses

In this model, the behavior in the field is determined by applying to the contact area, the behavior observed in the lab. Based on the contact area ratio, a , the applied overall normal stresses are transformed into contact stresses, and mobilized shear stresses occurring at the contacts are translated into overall stresses.

$a \rightarrow$ ratio of contact area

$$\Delta\alpha = -\frac{\kappa}{\lambda\sigma_c} \alpha \cdot \tau_s \cdot \Delta\delta_s^p / a$$

Rate of degradation of asperities:

$$\sigma_n \frac{\lambda_w}{\eta} = 2 \int_{-l_c/2}^{l_c/2} K_{ni} \cdot \delta_n^c(x) \cdot dx = \frac{K_{ni} l_c}{6R_w}$$

Equation for the contact area ratio, for a contact point on the waviness profile with radius of curvature R_w

$$a = \left(\frac{6\sigma_n R_w \eta^2}{K_{ni} \lambda^2} \right)^{1/3}$$

Contact area ratio

$$a^3 + a^2 \frac{\sigma_n}{2K_{ni} \delta_{mc}} = \frac{6\sigma_n R_w \eta^2}{K_{ni} \lambda^2}$$

cubic equation for the contact area ratio



PAPER 3: Constitutive model for small rock joint samples in the lab and large rock joint surfaces in the field

R. E. Barbosa

EngSolutions, Inc., Ft. Lauderdale, Florida, USA



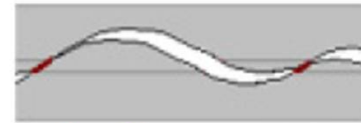
- Field behavior

Contact parameter η

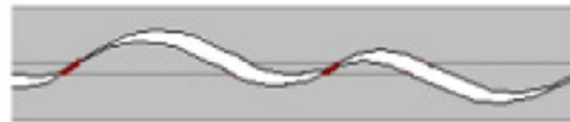
This parameter reflects the relative concentration of stresses at contacts, and it explains inverse scale effects that have been observed ([Leal Gomez, 2003](#); [Fardin, 2003](#)).



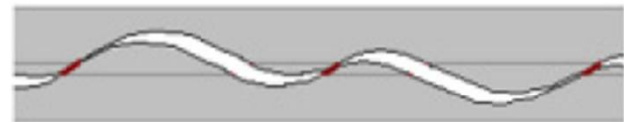
L = 36 cm $\eta = 1.66$



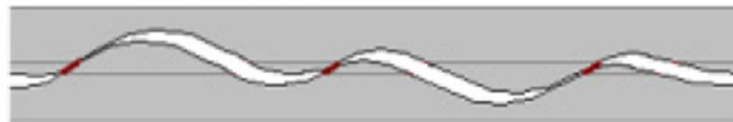
L = 45 cm $\eta = 1.33$



L = 70 cm $\eta = 0.85$



L = 75 cm $\eta = 1.20$



L = 90 cm

$\eta = 1.0$

$\lambda_w = 30$ cm $\lambda_w = 30$ cm





PAPER 3: Constitutive model for small rock joint samples in the lab and large rock joint surfaces in the field

R. E. Barbosa

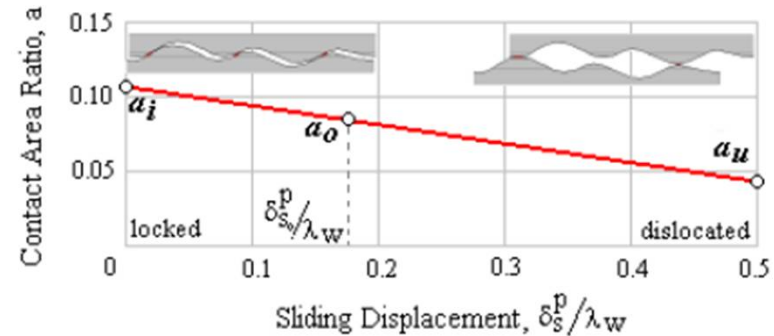
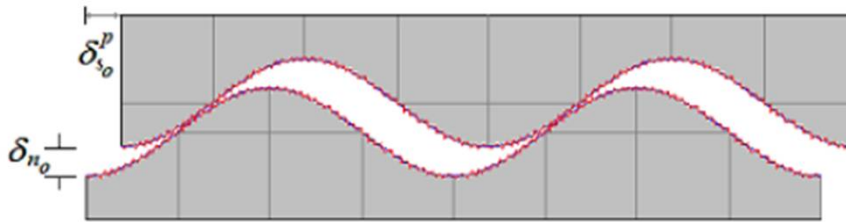
EngSolutions, Inc., Ft. Lauderdale, Florida, USA



- Field behavior

Open joint

Rock mass failures often occur along joints that are under low normal stresses and have opened and mismatched. The strength of those open joints is between that of a tightly closed joint and that of a completely dislocated joint. Interlocking and thus strength is larger for the locked joint because the initial effective waviness angle is larger, the contact parameter η is larger, the effective radius of curvature at the contact point is larger, and thus the contact area ratio is larger.



Contact ratio for open joints

Rock mass failures often occur along joints that are under low normal stresses and have opened and mismatched. The strength of those open joints is between that of a tightly closed joint and that of a completely dislocated joint. Interlocking and thus strength is larger for the locked joint because the initial effective waviness angle is larger, the contact parameter η is larger, the effective radius of curvature at the contact point is larger, and thus the contact area ratio is larger.

$$\frac{\delta_{s_0}^p}{\lambda_w} = \frac{1}{\pi} \text{Sin}^{-1} \left(\frac{2\delta_{n_0}}{\lambda_w \tan i_0} \right)$$

Initial shearing displacement:



PAPER 3: Constitutive model for small rock joint samples in the lab and large rock joint surfaces in the field

R. E. Barbosa

EngSolutions, Inc., Ft. Lauderdale, Florida, USA

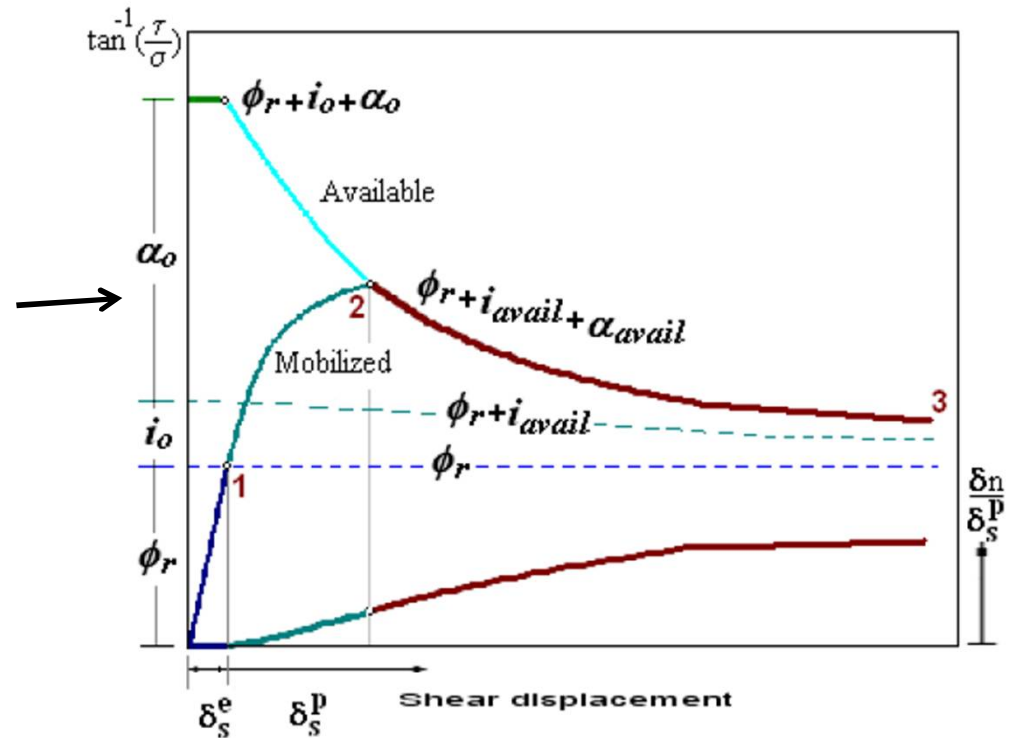


- Field behavior

Shear stress displacement curve

The shear stress-displacement curve for a large joint surface in the field includes the same three regions defined for a small sample in the lab: elastic region, pre-peak region and post-peak plastic region.

The proposed lab-scale model is applied to the contact area and contact stresses are converted to overall values to determine the field stress-displacement curve in these regions..





PAPER 3: Constitutive model for small rock joint samples in the lab and large rock joint surfaces in the field

R. E. Barbosa

EngSolutions, Inc., Ft. Lauderdale, Florida, USA



- Field behavior

Contact ratio for open joints

$$K_{field} = a_o \cdot K_s$$

Shear stiffness in the field

$$\Delta\alpha = -\frac{\kappa}{\lambda_w \sigma_c} \cdot \alpha_{avail} \cdot \tau / a \cdot \Delta\delta_s^p$$

Degradation of asperities

$$\Delta i = -\frac{\kappa}{\lambda_w \sigma_c} \cdot i_{avail} \cdot \tau \cdot \Delta\delta_s^p - \frac{2i_0}{\lambda_w} \Delta\delta_s^p$$

Degradation of waviness

$$\Delta a = -\frac{2(a_i - a_u)}{\lambda_w} \Delta\delta_s^p - \frac{a}{3 + \frac{\Omega \sigma_n}{a \sigma_c}} \frac{\Delta\sigma_n}{\sigma_n}$$

Change of contact area ratio





PAPER 3: Constitutive model for small rock joint samples in the lab and large rock joint surfaces in the field

R. E. Barbosa

EngSolutions, Inc., Ft. Lauderdale, Florida, USA

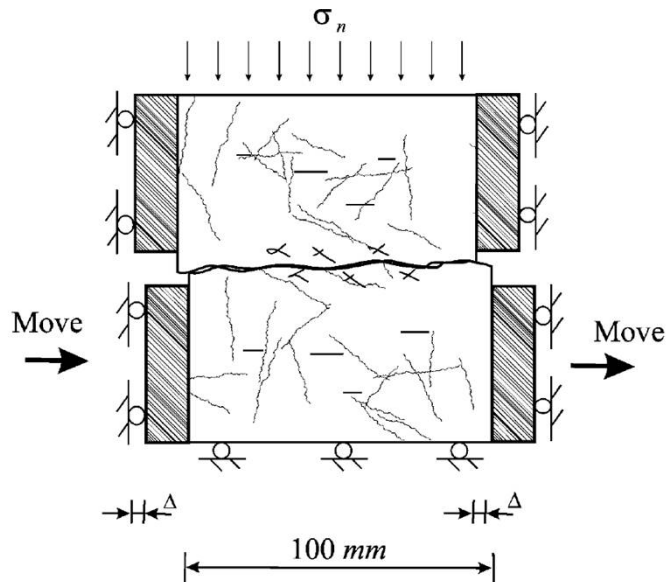


References:

- Bandis, S.C., Lumsden, A.C. and Barton, N.R. 1983. Fundamentals of rock joint deformation, *Int. J. Rock Mech. Min. Sci. & Geomech. Abstr.* **20(6): 249-268**



- Discontinuity in a geomaterial region that is subjected to relative shear movement with provision for dilation of the discontinuity.
- The evaluation focuses on the assessment of the influence of the surface topography of the discontinuity, frictional contact mechanisms, failure of the parent material composing the discontinuity and incompatible movements at the contacting planes on the behavior of the discontinuity.
- The computational modeling is used to examine the shearing tests conducted by Bandis et al. (1983)



- The two-dimensional contact between the two deformable surfaces has been modeled by **finite-sliding** interaction provided in the **ABAQUS/Standard** software



Paper 5: A numerical procedure for the analysis of the hydromechanical coupling in fractured rock masses

C. Duarte Azevedo*, L. E. Vaz**, E. A. Vargas**

*Civil Engineering Department, Federal University of Viçosa, Minas Gerais, 36571-000 Brazil

**Civil Engineering Department, Catholic University, Rio de Janeiro, Brazil



□ Abstract

This work presents a finite element implementation to treat the Hydromechanical Coupling (HM) in fractured rock masses under the framework of the so-called 'Equivalent continuum' approach. The multilaminar concept (Zienkiewicz and Pande, 1977) is used to simulate the mechanical behaviour of both the intact rock and the families of fractures. In that concept, the non-linearities in the constitutive relations are dealt by means of fictitious viscoplasticity. In the present implementation, the mechanical behaviour of the fractures is modelled by means of Barton - Bandis model. The shear stress/shear displacement/dilatancy relationship is modelled as viscoplastic and the normal stress/normal displacement as non-linear viscoelastic. Flow along fractures is considered to occur as a sequence of permanent states. The permeability tensor of the equivalent continuum is determined from the hydraulic apertures, in accordance of Barton et al (1985). From the numerical point of view, the basic aim of the work is the implementation of an efficient scheme to solve the above described problem. This is done by designing a self-adaptive time step control, transparent to the user, which determines the highest possible time step while assuming the conditions of precision, stability and convergence.





Paper 5: A numerical procedure for the analysis of the hydromechanical coupling in fractured rock masses

C. Duarte Azevedo*, L. E. Vaz**, E. A. Vargas**

*Civil Engineering Department, Federal University of Viçosa, Minas Gerais, 36571-000 Brazil

**Civil Engineering Department, Catholic University, Rio de Janeiro, Brazil



Model Description: The present work addresses an implementation of the HM coupling as an 'equivalent continuum' under the multilaminar concept with fluid flow taking place as a sequence of permanent states. Barton-Bandis (B-B) model, which incorporates the hydromechanical coupling, is the constitutive law adopted for the joints. The shear stress/shear displacement/dilatancy relationship is modelled as viscoplastic and the normal stress/normal displacement as non-linear viscoelastic. The intact rock is considered as a linear and elastic material. The multilaminar concept was introduced by Zienkiewicz and Pande in order to describe the behaviour of fractured rock masses as an 'equivalent continuum'. The rheological idealization of the multilaminar material is such that non-linearities such as sliding and separation of joints can be incorporated. It presupposes that joints are planar, persistent and parallel. Any number of joint families can be considered.



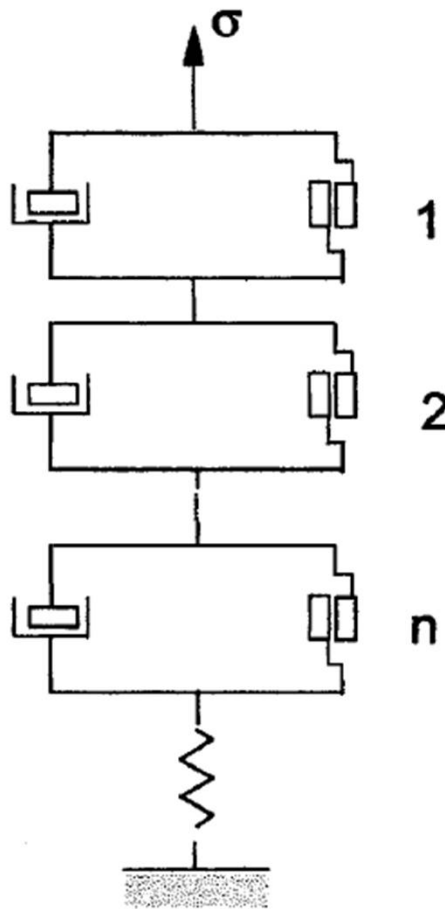


Paper 5: A numerical procedure for the analysis of the hydromechanical coupling in fractured rock masses

C. Duarte Azevedo*, L. E. Vaz**, E. A. Vargas**

*Civil Engineering Department, Federal University of Viçosa, Minas Gerais, 36571-000 Brazil

**Civil Engineering Department, Catholic University, Rio de Janeiro, Brazil



Viscoplastic idealization for the rheology of the multilaminar material. It consists of a spring and viscoplastic units associated in series: the lone spring represents the elastic character of the material and each viscoplastic unit represents one family of joints.

$$\begin{cases} F = F(\sigma, \eta^{vp}) \\ Q = Q(\sigma, \eta^{vp}) \end{cases}$$

Properties of each viscoplastic unit: (yield function, F , and a plastic potential, Q) F and Q are functions of stresses and the viscoplastic strains.

$$\mathbf{u}_i = \begin{Bmatrix} v \\ u \end{Bmatrix}_i = \begin{Bmatrix} v_{ns} \\ u_{ss} \end{Bmatrix}_i + \begin{Bmatrix} v_{nn} \\ u_{sn} \end{Bmatrix}_i$$

Displacements induced by the application of stresses on the plane of a joint family.

$$\sigma_i = \begin{Bmatrix} \sigma_c \\ \tau \end{Bmatrix}_i$$

Stress vector on a joint family i

$$\eta_i = \frac{\mathbf{u}_i}{S_i}$$

Deformation of a joint family i : displacement divided by its spacing

$$\eta_i = \begin{Bmatrix} \eta_v \\ \eta_u \end{Bmatrix}_i = \begin{Bmatrix} \eta_{ns} \\ \eta_{ss} \end{Bmatrix}_i + \begin{Bmatrix} \eta_{nn} \\ \eta_{sn} = 0 \end{Bmatrix}_i$$

Rheological analogue of multilaminar material





Paper 5: A numerical procedure for the analysis of the hydromechanical coupling in fractured rock masses

C. Duarte Azevedo*, L. E. Vaz**, E. A. Vargas**

*Civil Engineering Department, Federal University of Viçosa, Minas Gerais, 36571-000 Brazil

**Civil Engineering Department, Catholic University, Rio de Janeiro, Brazil



Viscoplastic modelling of shear behaviour

$$\dot{\eta}^{VP} = \left\{ \begin{matrix} \dot{\eta}_{ns}^{VP} \\ \dot{\eta}_{ss}^{VP} \end{matrix} \right\}_i = \Phi_i(\sigma, k) \quad \text{rate of viscoplastic strains for each joint family.}$$

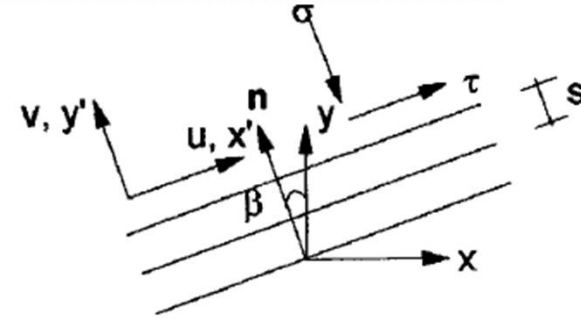
γ : fluidity parameter
 k : hardening parameter

$$\Phi_i(\sigma, k) = \bar{\gamma} \langle \phi(F) \rangle \left(\frac{\partial Q}{\partial \sigma} \right)_i$$

$$\langle \phi(F) \rangle = \begin{cases} \phi(F) & \text{if } F > 0 \\ 0 & \text{if } F \leq 0 \end{cases}$$

$$\dot{\eta}^{VP} = \sum_{i=1}^n \dot{\eta}_i^{VP}$$

'Equivalent continuum' viscoplastic strain rate vector: All units are subjected to the same stress and that the total viscoplastic strain rate corresponds to the sum of the viscoplastic strain rates of each individual component.



β : angle between local and global co-ordinate axes of joint family i

$$T_{M_i} = \begin{bmatrix} \sin^2 \beta_i & \cos^2 \beta_i & -2 \sin \beta_i \cos \beta_i \\ -\sin \beta_i \cos \beta_i & \sin \beta_i \cos \beta_i & \cos^2 \beta_i - \sin^2 \beta_i \end{bmatrix}$$

$$\sigma_i = T_{M_i} \sigma$$

$$\gamma = T_{M_i}^T \gamma_i$$

Matrix which transforms stresses from global to local co-ordinate systems: Each joint family may have a different orientation in the rock mass, it is necessary to define a local co-ordinate system for each joint family and a global co-ordinate system for the 'Equivalent continuum'

$$\gamma_i^T = \{ \gamma_v, \gamma_u \}$$

Total strain vector of joint family i

} local co-ordinate system

$$\gamma^T = \{ \gamma_x, \gamma_y, \gamma_{xy} \}$$

Total strain vector of 'equivalent continuum'

} global co-ordinate system

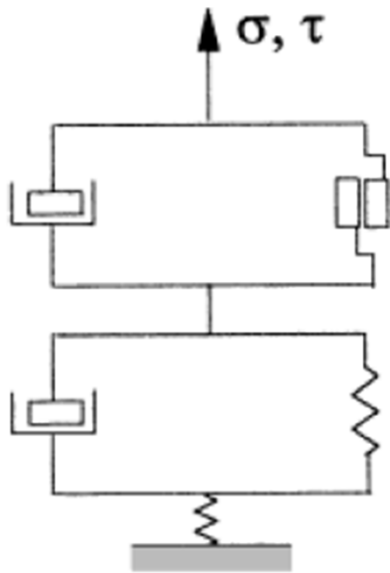
$$\sigma^T = \{ \sigma_{xx}, \sigma_{yy}, \sigma_{xy} \}$$

Stress vector



• Non-linear viscoelastic modeling of normal stress/normal displacement relationship

Taking advantage of the fact that viscoplasticity incorporates time as a fictitious independent variable Non-linear normal stress vs. normal displacement relationship is modelled by means of non-linear viscoelasticity .



$$\frac{1}{\bar{\gamma}} \dot{v}_{nn}^{ve} + k_{nn}(v_{nn}^{ve}) v_{nn}^{ve} = \sigma_c$$

Viscoelastic normal displacement

Joint secant normal stiffness

$$\mathbf{u}_i = \begin{Bmatrix} v_{ns}^{vp}(\sigma_c, \tau) \\ u_{ss}^{vp}(\sigma_c, \tau) \end{Bmatrix}_i + \begin{Bmatrix} v_{nn}^{ve}(\sigma_c) \\ 0 \end{Bmatrix}_i$$

$$\boldsymbol{\eta}_i = \begin{Bmatrix} \eta_{ns}^{vp}(\sigma_c, \tau) \\ \eta_{ss}^{vp}(\sigma_c, \tau) \end{Bmatrix}_i + \begin{Bmatrix} \eta_{nn}^{ve}(\sigma_c) \\ 0 \end{Bmatrix}_i$$

displacements and strains, for a given joint family, induced by normal and shear stresses applied in the plane of the joint.

Each pair of viscoplastic and viscoelastic units represents one family of joints and the lone spring represents the elastic character of the intact rock





- Description of B-B joints as viscoplastic/viscoelastic material

$$F = |\tau| - \sigma_c \operatorname{tg} \left[\operatorname{JRC}_{\text{mob}} \log \left(\frac{\operatorname{JCS}}{\sigma_c} \right) + \phi_r \right]$$

$$\frac{\partial Q}{\partial \sigma_c} = \operatorname{tg} \left[\frac{1}{M} \operatorname{JRC}_{\text{mob}} \log \left(\frac{\operatorname{JCS}}{\sigma_c} \right) \right]$$

$$\frac{\partial Q}{\partial \tau} = \pm 1$$

Yield and the potential functions (B-B model)

$$\sigma_c = \frac{k_{ni} V_m}{V_m - v_{nn}} v_{nn}$$

Normal stress-normal displacements for the joints (Barton et al.).

V_m e K_{ni} : Parameters determined by empirical relationships as functiond of JRC and JCS

Joint maximum closure





Paper 5: A numerical procedure for the analysis of the hydromechanical coupling in fractured rock masses

C. Duarte Azevedo*, L. E. Vaz**, E. A. Vargas**

*Civil Engineering Department, Federal University of Viçosa, Minas Gerais, 36571-000 Brazil

**Civil Engineering Department, Catholic University, Rio de Janeiro, Brazil



- **Fluid Flow**

Fluid flow is considered to take place exclusively along joints. Fracture conductivity is a function of the hydraulic aperture. BDB model2 allows the determination of the hydraulic aperture as function of JRC and the mechanical aperture. As the joint deforms, both mechanical and hydraulic apertures change. The cubic law is assumed valid for flow along fractures

$$\mathbf{k}_{eq_i} = \frac{e_i}{s_i} \begin{bmatrix} k_{fi} & 0 \\ 0 & 0 \end{bmatrix} \quad \text{Equivalent permeability tensor of joint family } i$$

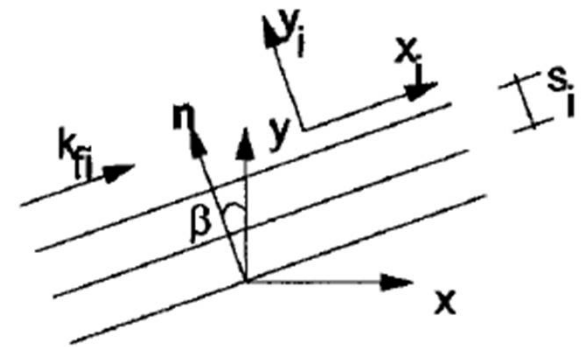
$$k_{fi} = \frac{ge_i^2}{12\mu} \quad \text{Hydraulic conductivity of joint family } i \text{ described as planar joint}$$

If n families of joints are present in the rock mass, the equivalent permeability tensor, \mathbf{K} , for the assemblage of all families is determined as:

$$\mathbf{K} = \sum_{i=1}^n \mathbf{K}_i$$

$$\mathbf{K}_i = \mathbf{T}_{H_i}^T \mathbf{k}_{eq_i} \mathbf{T}_{H_i} \quad \text{Permeability tensor of joint family } i \text{ referred to the 'equivalent continuum' co-ordinate system (global system).}$$

$$\mathbf{T}_{H_i} = \begin{bmatrix} \cos \beta_i & \sin \beta_i \\ -\sin \beta_i & \cos \beta_i \end{bmatrix} \quad \text{Transformation matrix.}$$



Hydraulic conductivity of joint family i





Paper 5: A numerical procedure for the analysis of the hydromechanical coupling in fractured rock masses

C. Duarte Azevedo*, L. E. Vaz**, E. A. Vargas**

*Civil Engineering Department, Federal University of Viçosa, Minas Gerais, 36571-000 Brazil

**Civil Engineering Department, Catholic University, Rio de Janeiro, Brazil



□ References:

- O. C. Zienkiewicz and G. N. Pande. Time dependent multilaminate model of rocks - A numerical study of deformation and failure of rock masses. Int. J. Numer. Anal. Meth. Geomech., 1, 219-247 (1977).
- N. Barton, S. Bandis and K. Bakhtar. Strength deformation and conductivity of rock joints. Int. J. Rock Mech. Min. Sci. Geomech., 22 (3), 121-140 (1985).





□ Abstract:

A new semi-empirical model that predicts fracture deformation under normal compressive loading is presented. The development of a simple exponential model is given first after which a modified and more general exponential model, with an additional degree of freedom in the model parameters, is presented. The simple and the modified exponential models are then compared to available fracture closure models, namely the empirical **Barton-Bandis hyperbolic model**, and a power-law model based on Hertzian contact theory, to determine how good they fit the results of fracture closure experiments conducted under monotonically increasing normal compressive loading. A new parameter called the half-closure stress, $\sigma_{1/2}$, is introduced and is used, in addition to the maximum fracture closure, Δv_m , in the model fitting procedures for the Barton-Bandis and the simple and generalized exponential models. The half-closure stress is shown to be related to the initial normal stiffness, K_{ni} , used in the original Barton-Bandis model. An additional parameter, n , is used in fitting the modified exponential model to the experimental data. Of the models presented herein, the modified exponential model was found to provide the best fit to the experimental data, for the same values of $\sigma_{1/2}$ and Δv_m , over the entire range of compressive stresses. The power-law model based on Hertzian contact theory was found to be unsuitable for accurate prediction of fracture normal deformation behavior .





- **Model description:** Fracture closure under normal compressive loading is conventionally described by stress-deformation relations in which the normal-stiffness, K_n , and the maximum normal joint closure, Δv_m , are used as the characteristic parameters (Goodman et al., 1968). It has been suggested however, that given the manner in which shear and normal fracture deformation tests are conducted, the displacement and not the stress, should be taken to be the dependent variable. In that event the measured fracture properties are best expressed in terms of the respective shear and normal compliances, C_s and C_n , rather than the corresponding stiffnesses (Sun et al. 1985). In the simple one dimensional normal deformation problem this may seem to be a trivial technicality since $C_n = 1 / K_n$. In the general case, however, matrix inversion is required given the tensorial nature of these parameters.

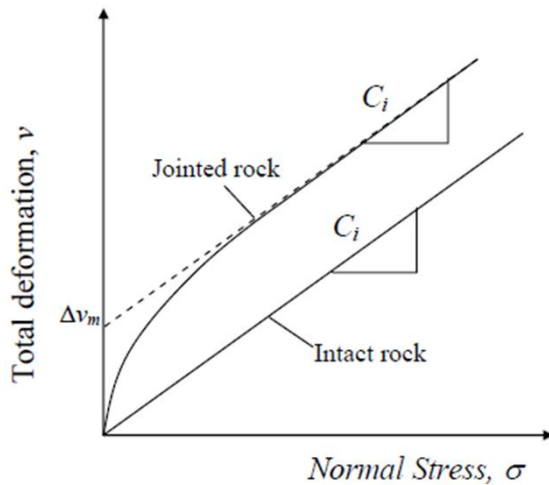




- Model development for fracture closure :

$$v_i = C_i \sigma$$

For intact rock, linear-elasticity is assumed and the deformation: function of normal stress (σ). C_i (constant) is the intact rock compliance. For jointed rock, the relation between the total deformation, v , and the compressive stress, σ , normal to the fracture plane, is non-linear.



C_j : compliance of a jointed rock. It's not a constant but a continuous function of σ .

$$\frac{\partial C_j}{\partial \sigma} = -f(\sigma)$$

Rate of decrease of the jointed rock normal compliance, C_j , with increasing normal compressive stress.

$$\left. \begin{array}{l} \lim_{\sigma \rightarrow \infty} f(\sigma) = 0 \\ \lim_{\sigma \rightarrow \infty} C_j = C_i = \text{constant.} \end{array} \right\}$$

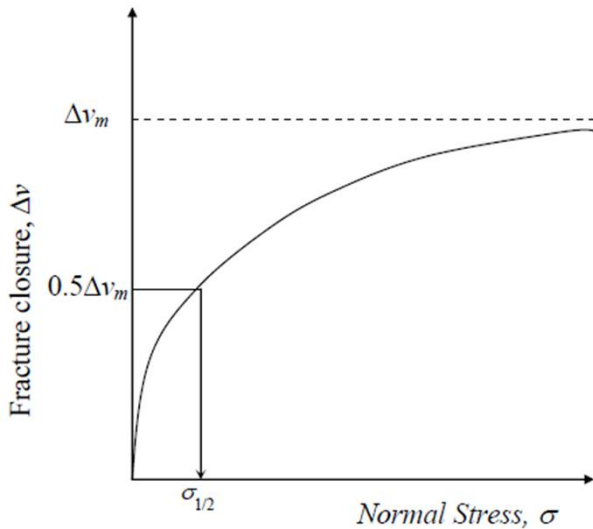




- Model development for fracture closure :

$f(\sigma) = ae^{-b\sigma}$ \longrightarrow This exponential function of the following form satisfies the condition

a and b are constants which give the initial rate of decay of the jointed rock compliance and the decay constant, respectively. These two parameters are related to the maximum fracture closure, Δv_m , and to the normal stress value at $\Delta v_m / 2$



$$\frac{\partial^2 v}{\partial \sigma^2} = -ae^{-b\sigma}$$

$$\left\{ \begin{array}{l} v(\sigma = 0) = 0 \\ \lim_{\sigma \rightarrow \infty} \frac{\partial v}{\partial \sigma} = C_i \end{array} \right.$$

$v = \frac{a}{b^2} [1 - e^{-b\sigma}] + C_i \sigma$ Non-linear relation between the total deformation and the normal stress.

$$\Delta v = \Delta v_m \left[1 - e^{-\left(\frac{\sigma}{\sigma_{1/2}}\right) \ln 2} \right]$$

Equation for fracture closure



Model development for fracture closure

$$v_i = C_i \sigma$$

$$\frac{\partial C_j}{\partial \sigma} = -f(\sigma)$$

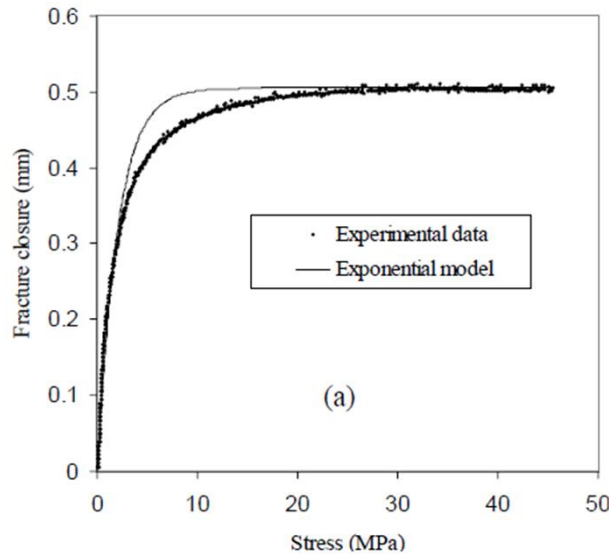
$$f(\sigma) = ae^{-b\sigma}$$

$$\frac{\partial^2 v}{\partial \sigma^2} = -ae^{-b\sigma}$$

$$\left\{ \begin{aligned} v(\sigma = 0) &= 0 \\ \lim_{\sigma \rightarrow \infty} \frac{\partial v}{\partial \sigma} &= C_i \end{aligned} \right.$$

$$v = \frac{a}{b^2} [1 - e^{-b\sigma}] + C_i \sigma$$

$$\Delta v = \Delta v_m \left[1 - e^{-\left(\frac{\sigma}{\sigma_{1/2}}\right)^{\ln 2}} \right]$$

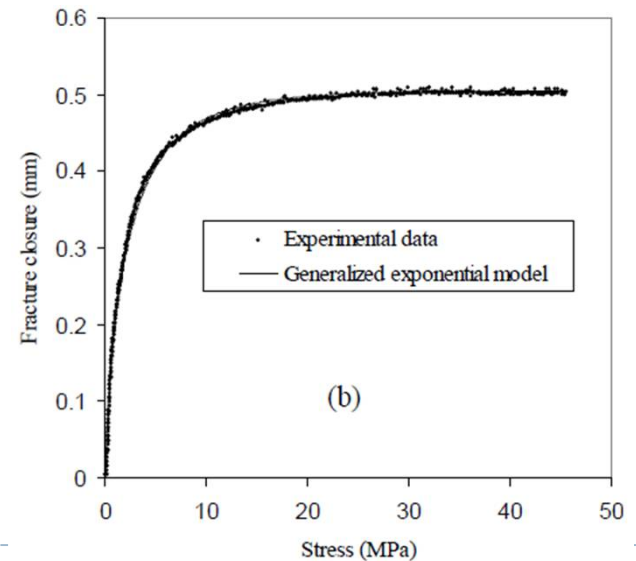


General exponential model for closure

$$f(\sigma) = a(\sigma)e^{-b\sigma^n}$$

$$\Delta v = \Delta v_m \left[1 - e^{-\left(\frac{\sigma}{\sigma_{1/2}}\right)^n \ln 2} \right]$$

$$0 < n < 1.0$$





□ References:

- Bandis, S.C., A.C. Lumsden and N.R. Barton. 1983. Fundamentals of rock joint deformation. Int. J. Rock Mech. Min. Sci. & Geomech. Abstr. 20(6): 249-268.
- Barton, N.R., S.C. Bandis and K. Bakhtar. 1985. Strength, deformation and conductivity coupling of rock joints. Int. J. Rock Mech. Min. Sci. & Geomech.
- Goodman, R.E., R.L. Taylor and T.A. Brekke. 1968. A model for the mechanics of jointed rock. J. Soil Mech. Fdns. Div., Proc. Am. Soc. Civ. Engrs. 94(SM3): 637-659.
- Sun, Z., C. Gerrard and O. Stephansson. 1985. Rock joint compliance tests for compression and shear loads. Int. J. Rock Mech. Min. Sci. & Geomech. Abstr. 22(4): 197-213.
- Swan, G. 1983. Determination of stiffness and other joint properties from roughness measurements. Rock Mech. Rock Engng. 16:19-38.





Rock Joint Compliance Tests Compression for and Shear Loads

Sun et al., (1985)

INT. J. ROCK MECH. MIN. SCI. & GEOMECH.





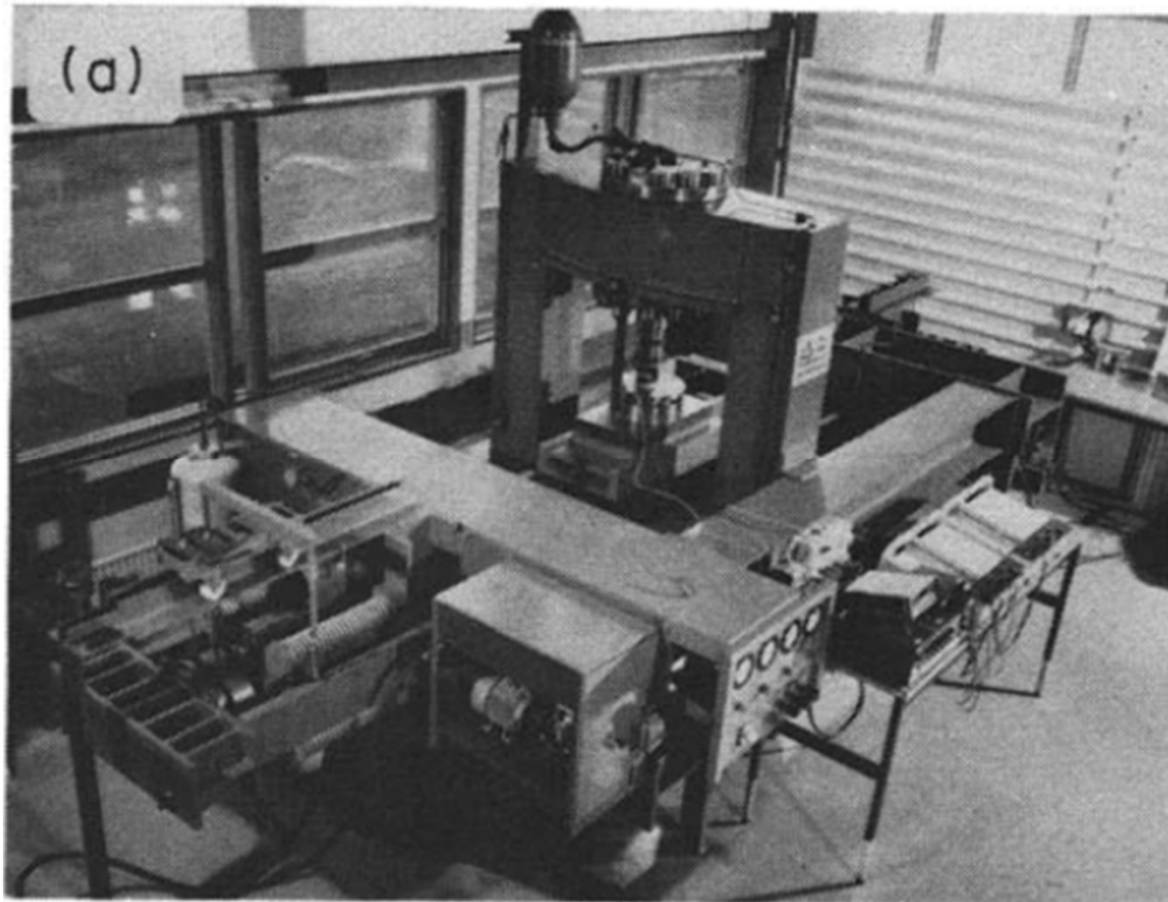
Abstract



- ▶ A series of compression and shear tests were conducted at **large scale** on joint surfaces in granite and slate specimens, with special equipment being used to isolate the deformations of the joints from those of the rock material.
- ▶ Any attempt to base predictions of rock mass behaviour on the combined use of these two pairs of components should take into account the different stress paths to which they relate.
- ▶ For the compression tests, the results indicate a pattern of decreasing compliance with load, an increase in compliance with initial aperture, and high levels of recoverability of deformation.
- ▶ In the shear tests, the curves for the relative displacements indicate there are three zones of different behaviour, elastic, transition and sliding.



■ ROCK JOINT TESTING TECHNIQUES



■ ROCK JOINT TESTING TECHNIQUES

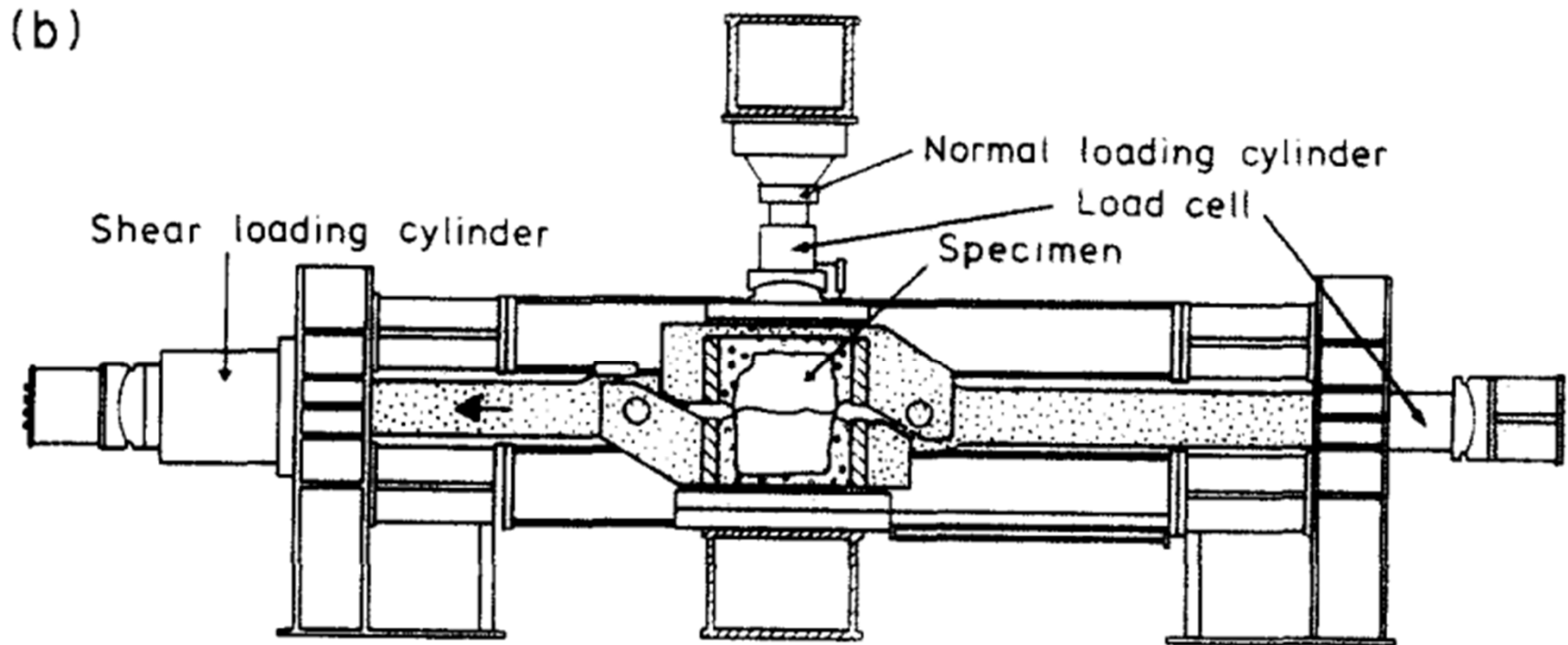
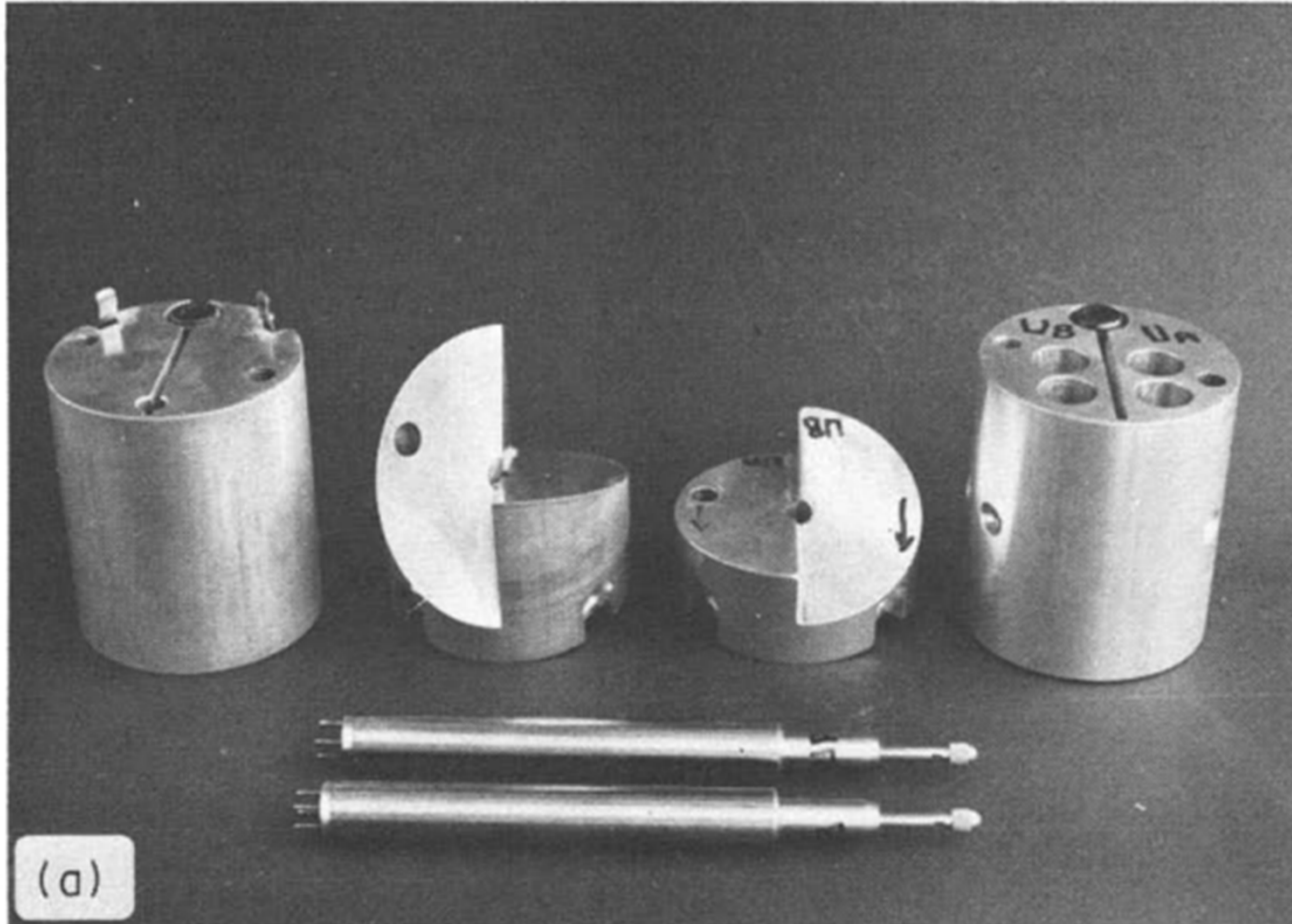
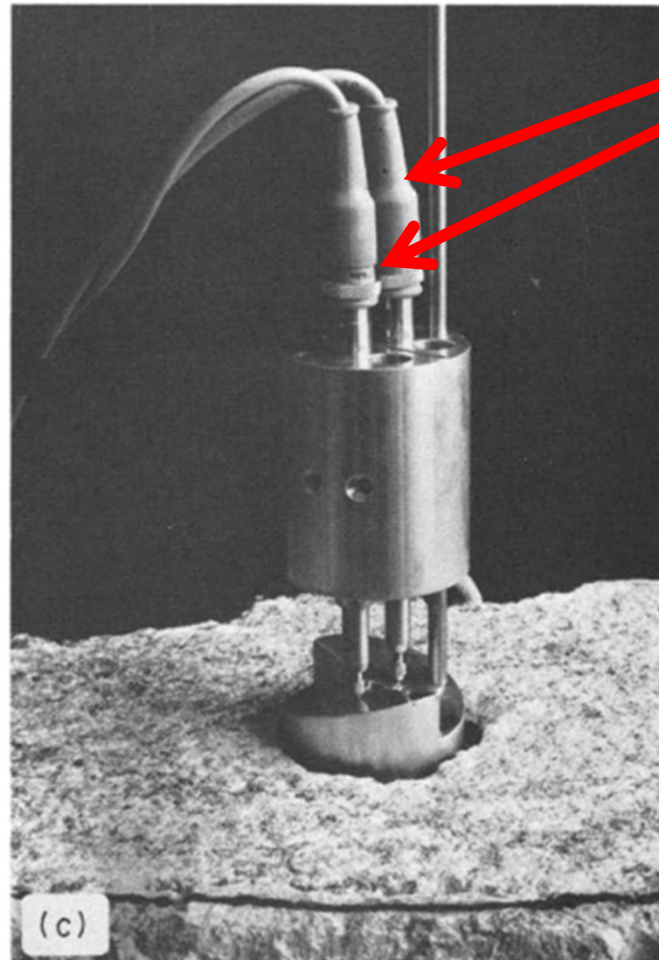
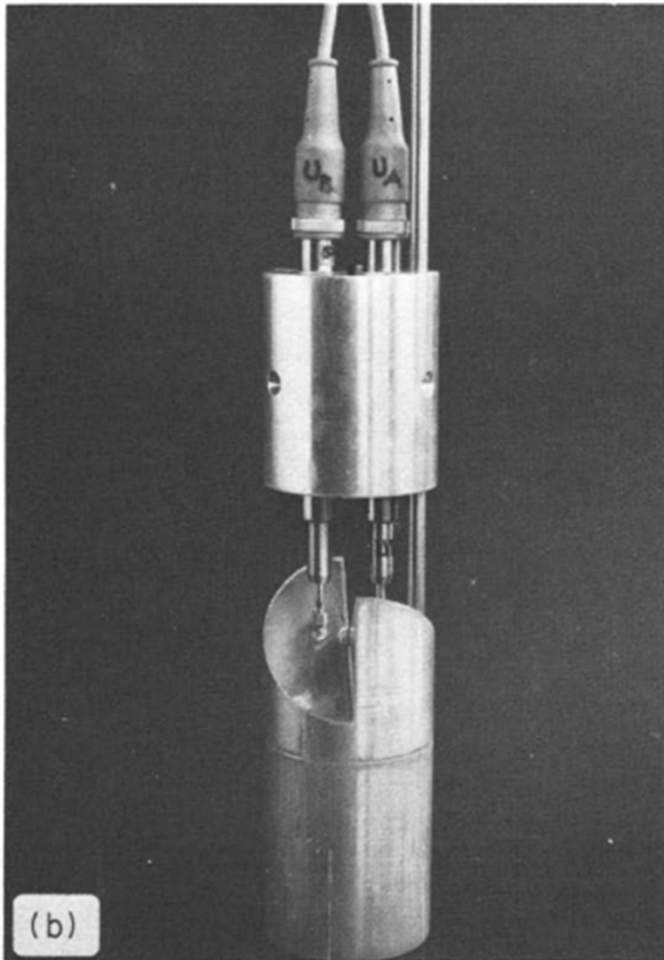


Fig. 2. Large scale shear rig, (a) photograph, (b) diagrammatic representation.

■ ROCK JOINT TESTING TECHNIQUES



ROCK JOINT TESTING TECHNIQUES



LVDT

Fig. 3. Apparatus for normal and shear relative displacement measurements of rock joints, (a) disassembled apparatus, (b) assembled apparatus, (c) installed apparatus.



Methodology



▪ **ROCK JOINT TESTING TECHNIQUES**

- ▶ The shear box was 0.5 m long and 0.35 m wide with.
- ▶ The applied normal and shear forces being generated by a hydraulic system and measured by load cells.
- ▶ The maximum possible values of these forces were 1500 kN (normal forces) and 3000 kN (shear forces).
- ▶ The accuracy of measurement being of the order of ± 0.5 kN.
- ▶ The relative velocity between the two halves of the shear box was usually about 0.5 mm/min, with the maximum being 2 mm/min.
- ▶ The maximum possible relative shear displacement was 100 mm.



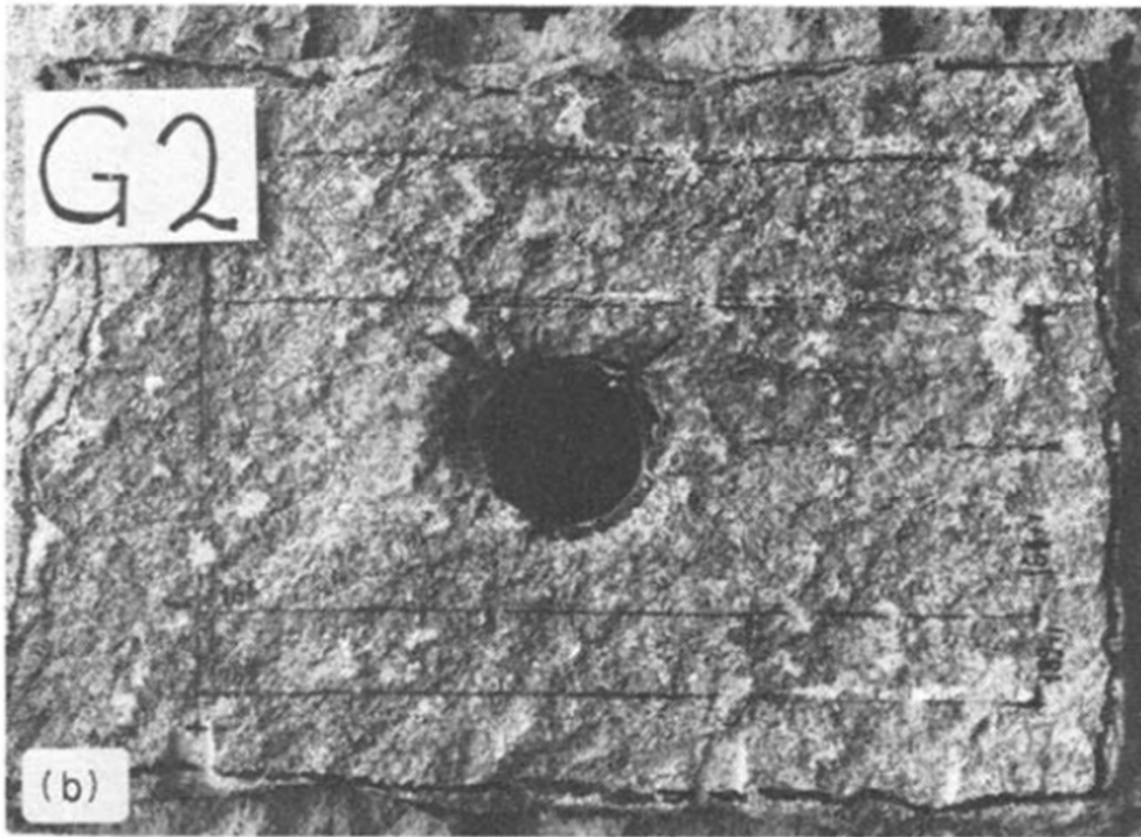
■ ROCK JOINT TESTING TECHNIQUES



Red Granite



■ ROCK JOINT TESTING TECHNIQUES



Grey
Granite

Fig. 4. Photographs showing surface texture of rock joint specimens,
(a) Red granite, (b) Grey granite.

ROCK JOINT TESTING TECHNIQUES

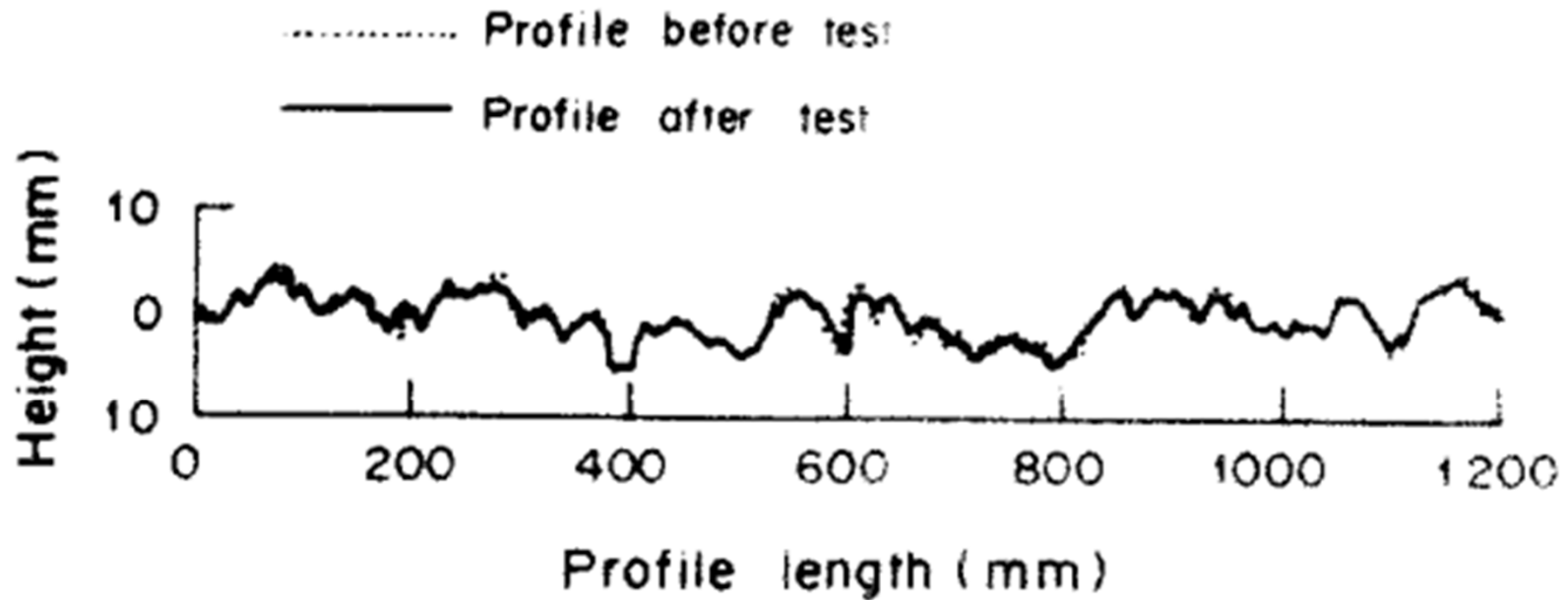


Fig. 5. Normal stress–normal relative displacement curves for Red granite.





▪ ROCK JOINT TESTING TECHNIQUES

Table 1. Rock material properties

Rock type	Uniaxial compression strength q_u (MPa)	Young's modulus E (GPa)	Poisson's ratio ν	Reference
Red coarse-grained granite	233.9	67.9	0.29	Bjurström [20]
Grey medium-grained granite	207.5	$E_t = 60.2^a$ $E_s = 50.7^b$	$\nu_t = 0.22^a$ $\nu_s = 0.14^b$	
Slate	320.0	68.0	0.20	Stillborg and Swan [21]

^a E_t , ν_t = tangent Young's modulus and tangent Poisson's ratio.

^b E_s , ν_s = secant Young's modulus and secant Poisson's ratio.



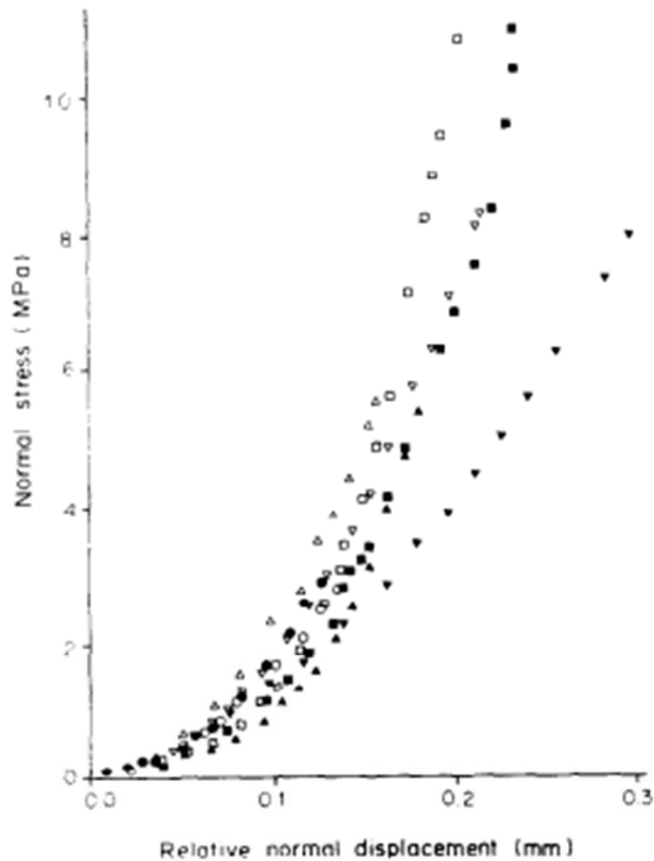
Results



- ▶ Since the curves are monotonic this means that the normal compliance decreases with increase in either the normal stress or normal relative displacement.
- ▶ There appear to be two reasons why the normal compliance should decrease at higher displacements:
 - ▶ (a) for points initially in contact, the area of contact will have significantly increased, and
 - ▶ (b) new points of contact will have been gradually brought into action.



► COMPRESSION TEST



Nominal maximum applied normal stress (MPa)	No	1st test series	No	2nd test series
10.9	15	■	69	□
8.2	14	▼	60	▽
5.5	13	▲	63	△
2.7	12	○	66	●

Fig. 6. Joint surface profile of Grey granite before and after shear testing.

► COMPRESSION TEST

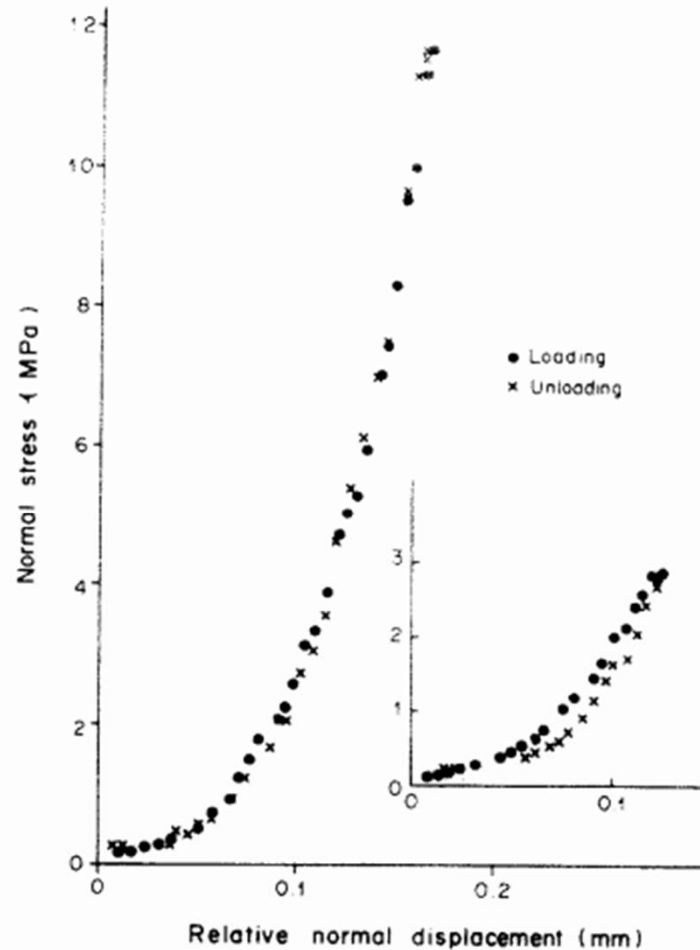


Fig. 11. Repeated normal loading and unloading of the Red granite joint.

► COMPRESSION TEST

It gives rise to the following relations between delta, sig, C_{11} :

$$\delta_1 = a_0 + a_1 \ln \sigma_1,$$

$$\sigma_1 = \exp\left(\frac{\delta_1 - a_0}{a_1}\right),$$

$$C_{11}^t = a_1 / \sigma_1 = a_1 / \exp\left(\frac{\delta_1 - a_0}{a_1}\right),$$

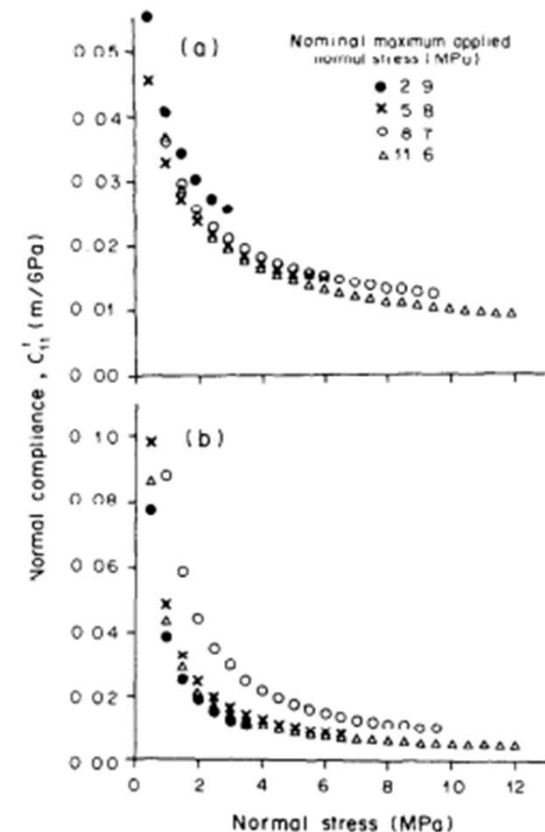


Fig. 8. Tangential normal compliance–normal stress curves for Red granite. (a) power law fitted to test 12–15. (b) exponential law fitted to tests 60, 63, 66 and 69.

■ SHEAR TEST RESULTS

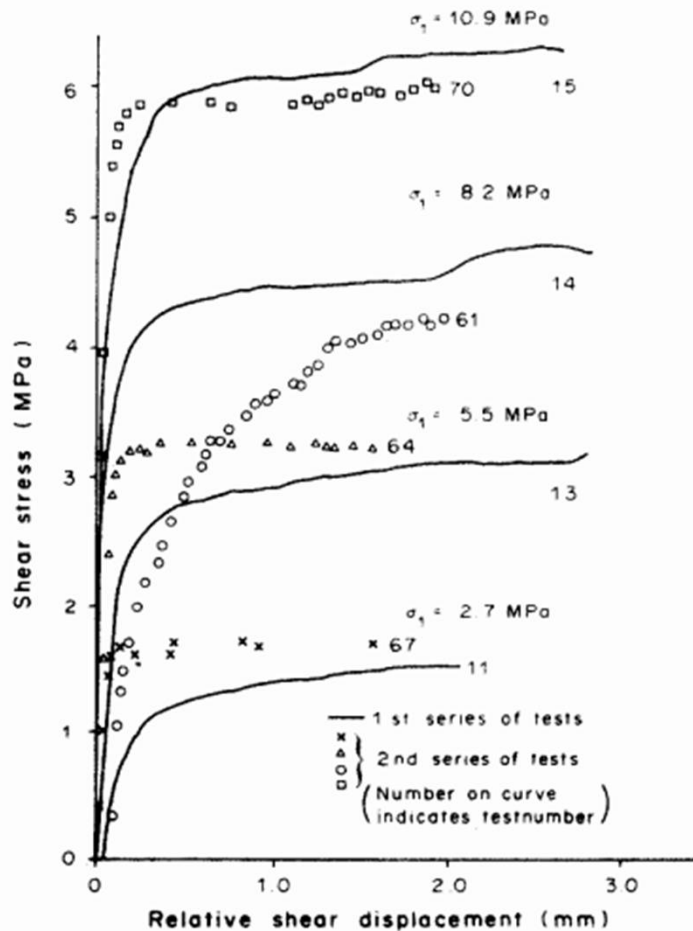


Fig. 15. Plots of shear stress vs shear relative displacement for Red granite.

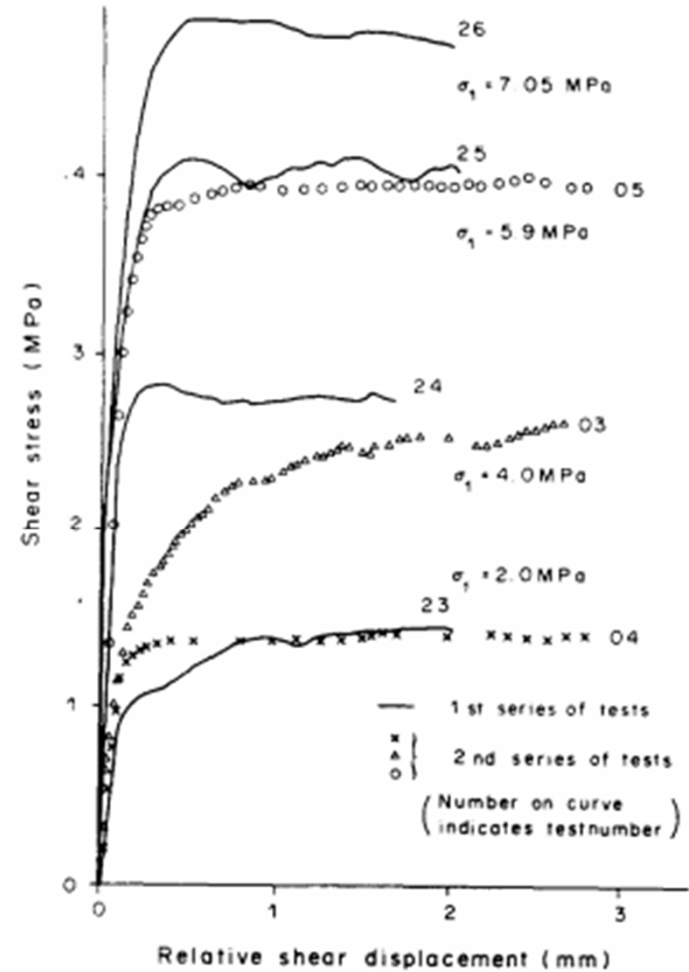


Fig. 16. Plots of shear stress vs shear relative displacement for Grey granite.

■ SHEAR TEST RESULTS

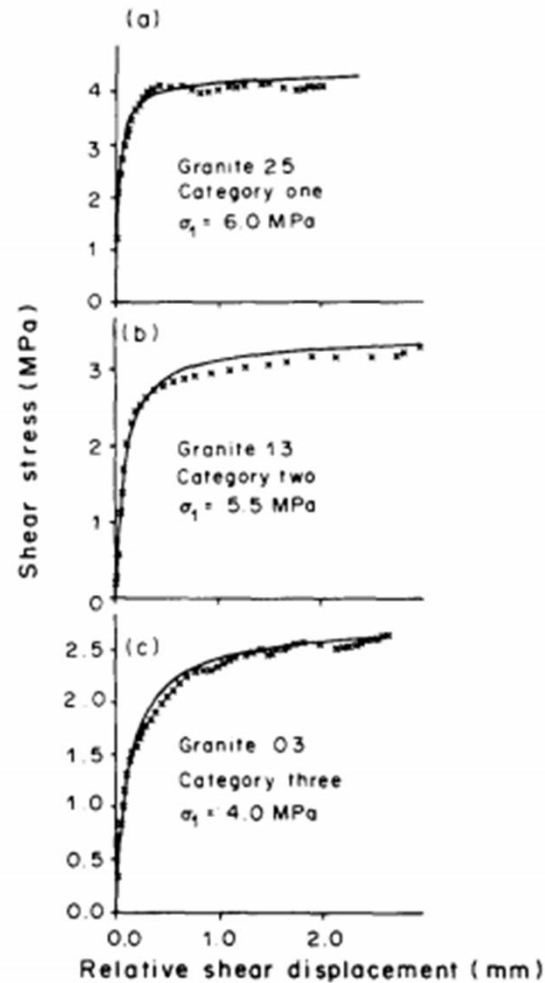


Fig. 17. Three categories of curves of shear stress vs shear relative displacement.

▪ SHEAR TEST RESULTS

The empirical relations involving the relative shear displacements:

$$\delta_2 = \frac{(\tau_2 - m_0)m_1}{1 - (\tau_2 - m_0)m_2},$$

or

$$\tau_2 = \frac{\delta_2}{m_1 + m_2\delta_2} + m_0,$$

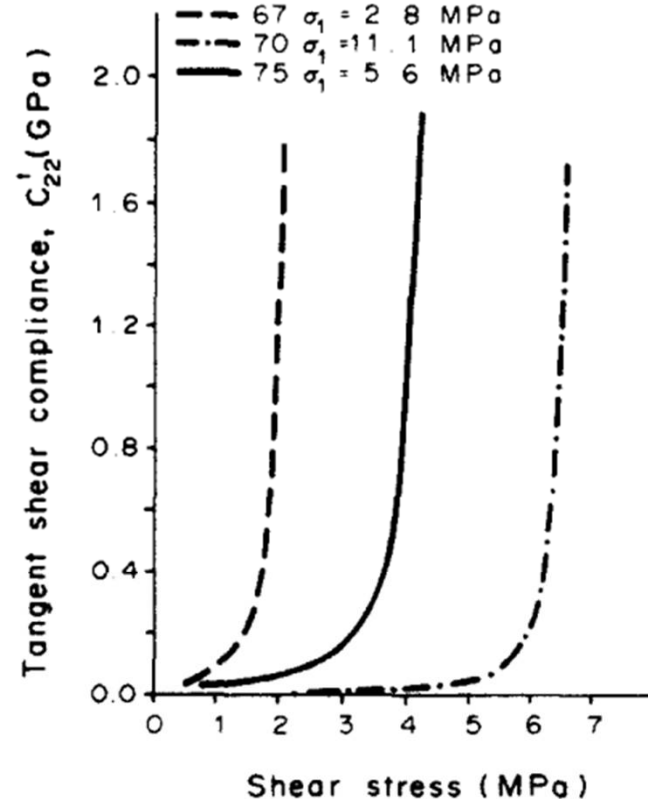


Fig. 19. Tangential shear compliance vs shear stress for Red granite.



Experimental study of the effect of fracture size on closure behavior of a tensile fracture under normal stress

A.A.Giwelli , K.Sakaguchi, K.Matsuki (2009)

INTERNATIONAL JOURNAL OF ROCK MECHANICS & MINING SCIENCES





Introduction



- The mechanical and hydraulic properties of rock mass are mainly governed by the fractures it contains. As a consequence, over the past decade, many researchers have focused on the mechanical and hydraulic properties of rock fractures.
- In particular, the estimation of the hydraulic conductivity of a hydraulic fracture is essential for hydraulic stimulation of oil and geothermal reservoirs.
- A fracture under normal stress consists of two rough surfaces in partial contact.
- The mechanical response of a fracture is closely related to the amount and geometry of the contact area, while the hydrological response is governed by the connectivity and size of the voids.





Introduction



- Brown [5] showed that a fracture that is closed macroscopically due to normal stress may, nevertheless, provide a path for fluid flow because the fracture surfaces do not match perfectly and an aperture exists between the surfaces.
- The aperture distributions in a fracture are governed by rock stresses, the mechanical properties of rock, and the topography of the fracture surfaces.
- To estimate the permeability of a given fracture under a given normal stress, it is necessary to estimate the mean aperture of the fracture by determining the closure of the fracture under normal stress.
- The closure of a fracture under normal stress is a highly nonlinear process that depends on the matedness of the surfaces during loading/unloading. The non linearity arises because the contact area increases as normal stress increases, which results in stiffening of the fracture.



Introduction



- There have been only a few experimental studies on the size effect on the mechanical behavior of a fracture under normal stress.
- Raven and Gale studied the effect of sample size ranging from 100 to 249mm in diameter on the closure and permeability of a natural fracture in granite under uniaxial compression of up to 30MPa. They showed that the closure of the fracture tends to increase with the sample size and the fracture flow rate decreases with increasing the sample size.
- Yoshinaka and Yamabe experimentally investigated the deformation of artificially created joints with different roughness and different sizes ranging from 60 to 422mm, and showed that the normal stiffness decreases with the joint size and the maximum closure increases approximately in proportion to the joint size.
- Recently, Fardin showed that the closure under uniaxial compression increases with the sample size for concrete replicas of a natural joint with a size of from 50 to 200mm. Thus, these previous studies have shown that closure of a fracture state of stress in a rock mass, due to both natural phenomena and those induced by engineering activities, can have a substantial effect on the fluid flow and material/heat transport in a fracture.



Objective



- However, the aperture was not measured in these studies, and accordingly, the mechanism for the size effect is not yet clear, since an aperture of a fracture is produced by mismatching between the two surfaces of the fracture, which causes a nonlinear behavior of the closure.
- The main goal of this study was to experimentally clarify the size effect on the closure behavior of a single rock fracture under normal stress. For that purpose, tensile fractures that measured from 37.5mmx37.5mm to 260mmx260mm were created in sandstone by intending steel wedges. After the surface topography was measured by a laser profilometer to determine the aperture distribution, the size effect on fracture closure was examined under normal stress by conducting cyclic loading tests in the laboratory.





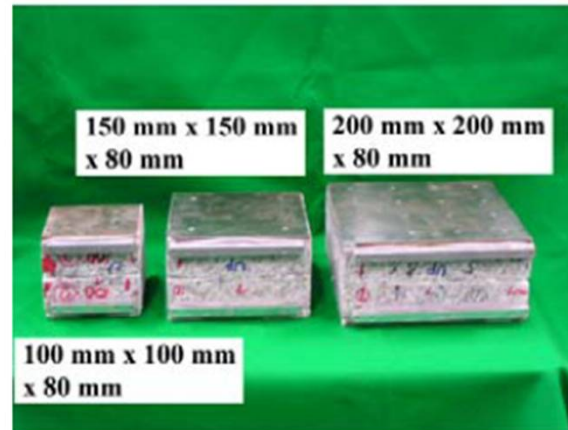
Sample preparation



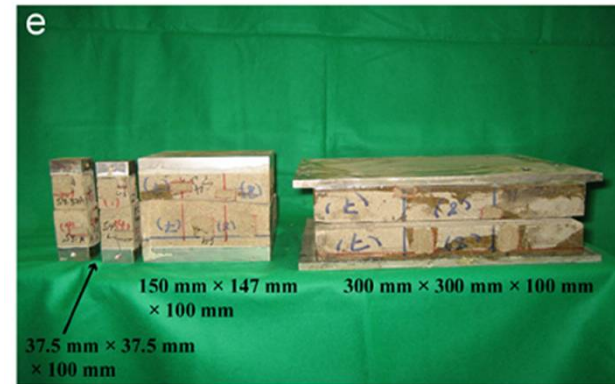
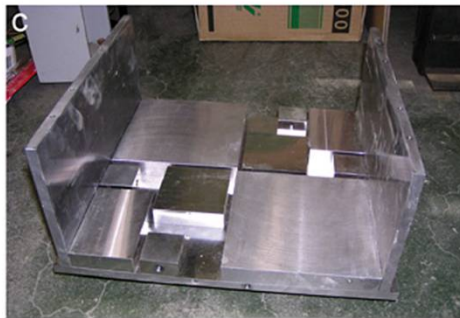
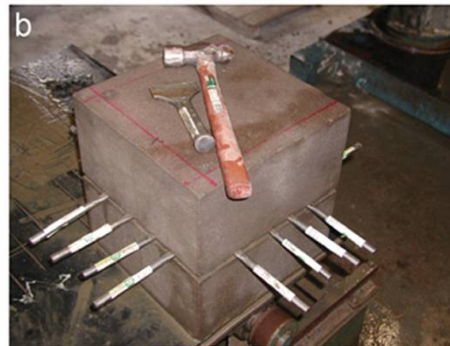
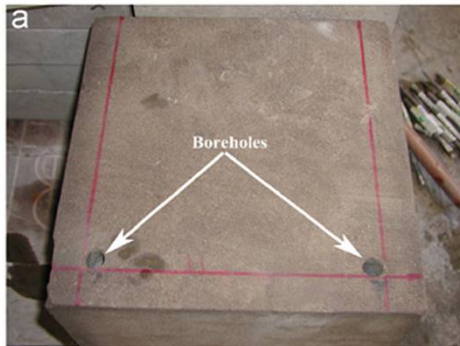
- To determine the aperture distribution of the tensile fracture, they need to measure the heights of the two surfaces at the same positions along matched paths for all measurement lines. Thus, a special method was used to create the fracture.
- A tensile fracture that did not penetrate through out the block was then created by indenting several steel wedges into a shallow groove that was made along the center of the side planes of the block.
- After the tensile fracture was created, the block was cut to a height of 100mm to have a size of L (300mm)xW (300mm)xH (100mm), and a reference-setting jig was inserted into the bore holes to locate the reference-setting pipes at the level of the fracture and to fix them to each part of the rock with glue. Reference plates for each specimen size (37.5mmx37.5mm, 150mmx147mm, 260mmx260mm) were glued to both the upper and lower surfaces of the block, and thus, ensured that they were parallel to each other by using height gauges.



□ granite



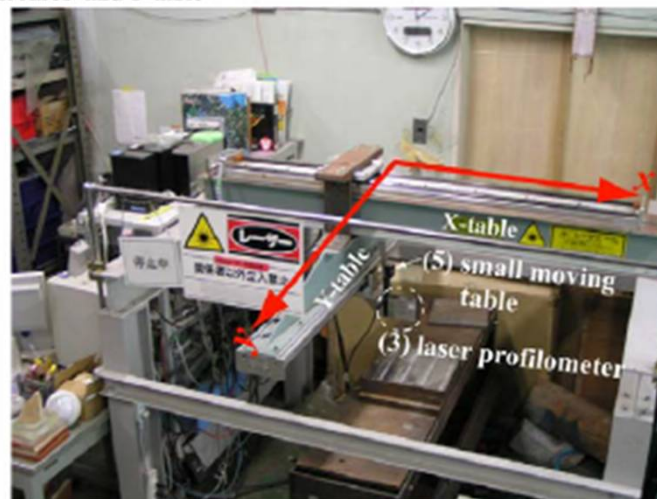
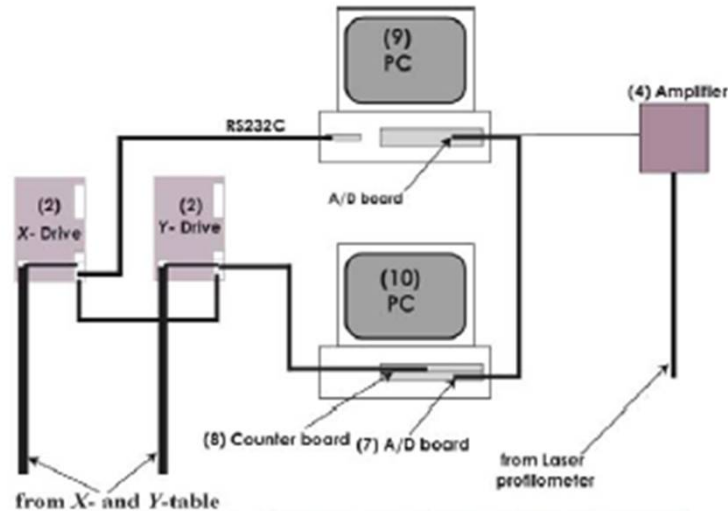
□ sandstone



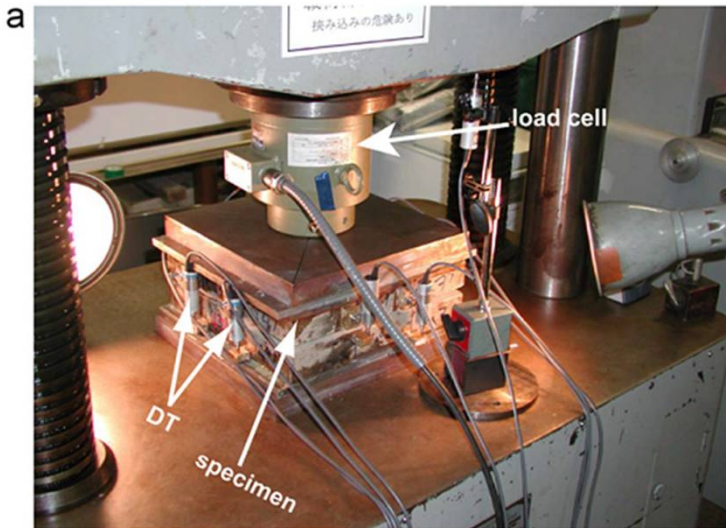


Determination of the opening surface height measurement.

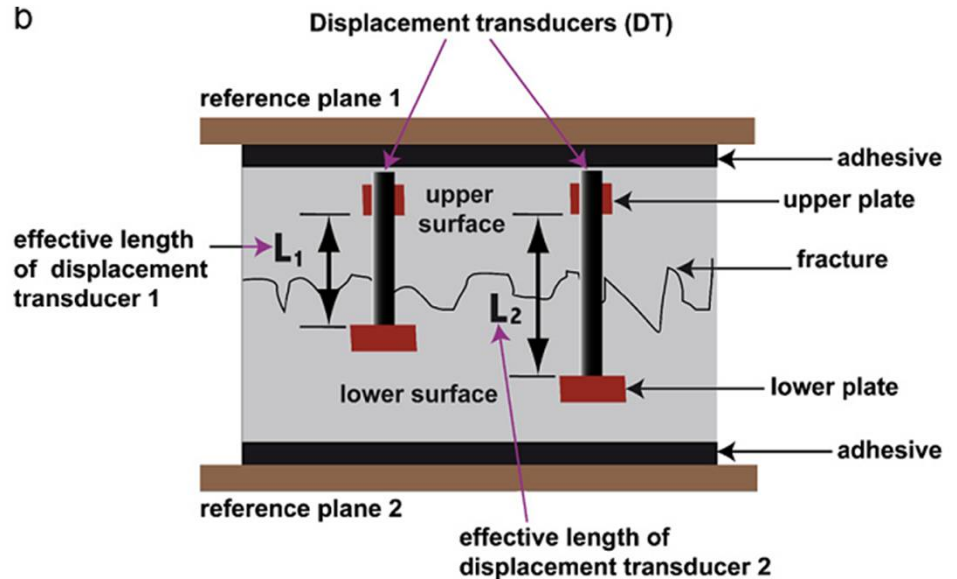
- Measurement System – Laser scanning apparatus for measurement of surface height



□ Uniaxial compression test

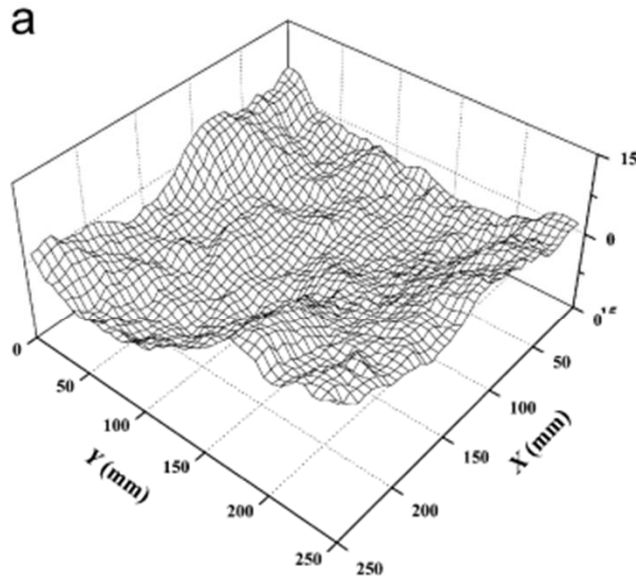


- ✓ Normal stress by using a loading machine with a capacity of 10kN,
- ✓ The outputs of the load cell and the displacement transducers (DTs) were digitally recorded every 1s with a PC. To measure deformation across the fracture, two to four pairs of strain-gauge-type DTs with two effective lengths were used.

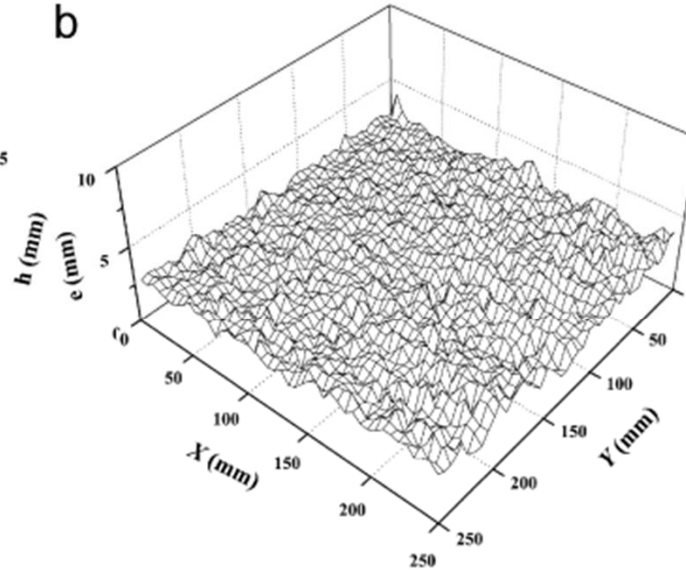


- ✓ The schematic of closure measurement by DTs with different effective lengths
- ✓ When a pair of DTs has different effective lengths (L_1 and L_2), the difference in deformation gives the deformation of the intact rock with a length of $(L_2 - L_1)$.

$$\delta = \delta_1 - \frac{\delta_2 - \delta_1}{L_2 - L_1} L_1.$$



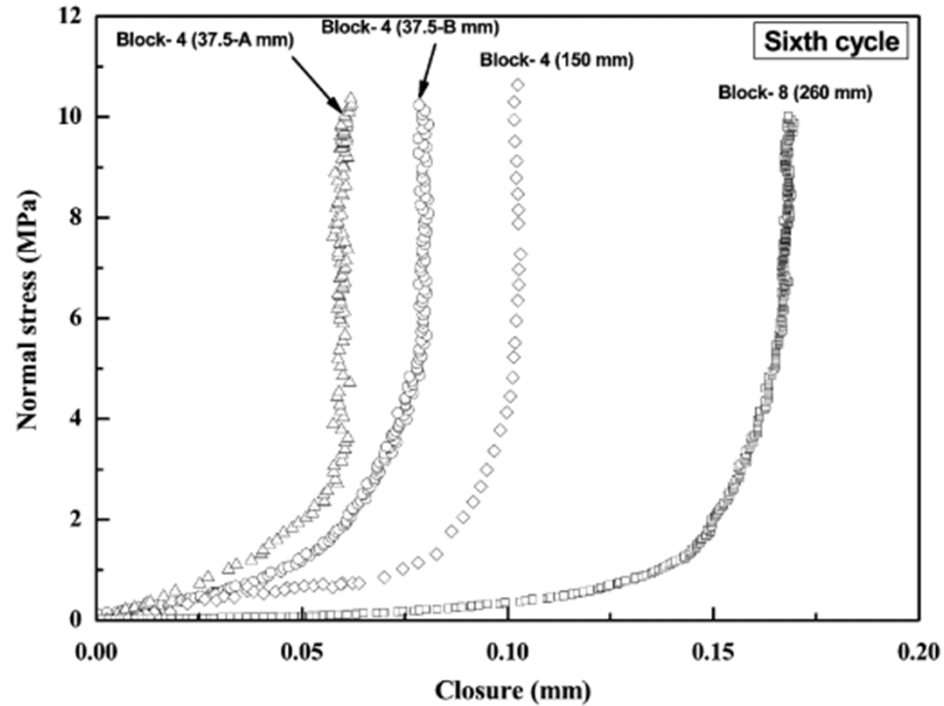
Fracture size = 255 mm, (block- 4)



Fracture size = 255 mm, (block- 4)

□ Examples of: (a) height distributions of the lower surface and (b) the initial aperture distribution for the block.





□ The figure shows the effect of fracture size on the normal stress versus closure curve of the tensile fracture, obtained in the sixth cycle. Note that the closure curve was not obtained for some of the largest fractures since the specimens failed during the loading test. Closure of the tensile fracture significantly increases with fracture size. This is consistent with previous experimental results.





Presentation:

Hydraulic and Hydromechanical Laboratory Testing of Large Crystalline Rock Cores

Thörn J, Ericsson L, Fransson Å (2014)

ROCK MECHANICS AND ROCK ENGINEERING



Introduction



- The mechanical and hydrological behavior of a rock fracture is determined using several parameters related to the geometry of the void space between the adjacent surfaces of a fracture.
- Hakami (1995) mentions eight such parameters: aperture, which is the distance between the surfaces; the contact area between the surfaces; the roughness and matedness of the surfaces, i.e. how coarse the surfaces are and how well they fit together; the spatial correlation length of the aperture; the presence of channeling, i.e. wider, continuous paths that may transmit water; the tortuosity of the flow paths and the fracture stiffness, which is a measure of the stress needed to bring the fracture surfaces one unit of length closer to each other.
- The water-conducting ability of a rock fracture can be expressed as the hydraulic aperture. The cubic law (e.g. Snow 1968) is a common idealization of the hydraulic aperture as the solution to the Navier-Stokes equations for a constant distance between two smooth parallel plates between which laminar flow occurs.



Introduction



- Efforts have been made to establish a link between the hydraulic and mechanical apertures of rock fractures. An example of this is provided by Barton et al. (1985), updated in Olsson and Barton (2001), showing an empirical link using the joint roughness coefficient, JRC.
- Another example are cubic law-based models, see e.g. Konzuk and Kueper (2004), for the evaluation of certain models. Pyrak-Nolte and Morris (2000) set fracture flow properties in relation to fracture stiffness in the light of aperture correlation.





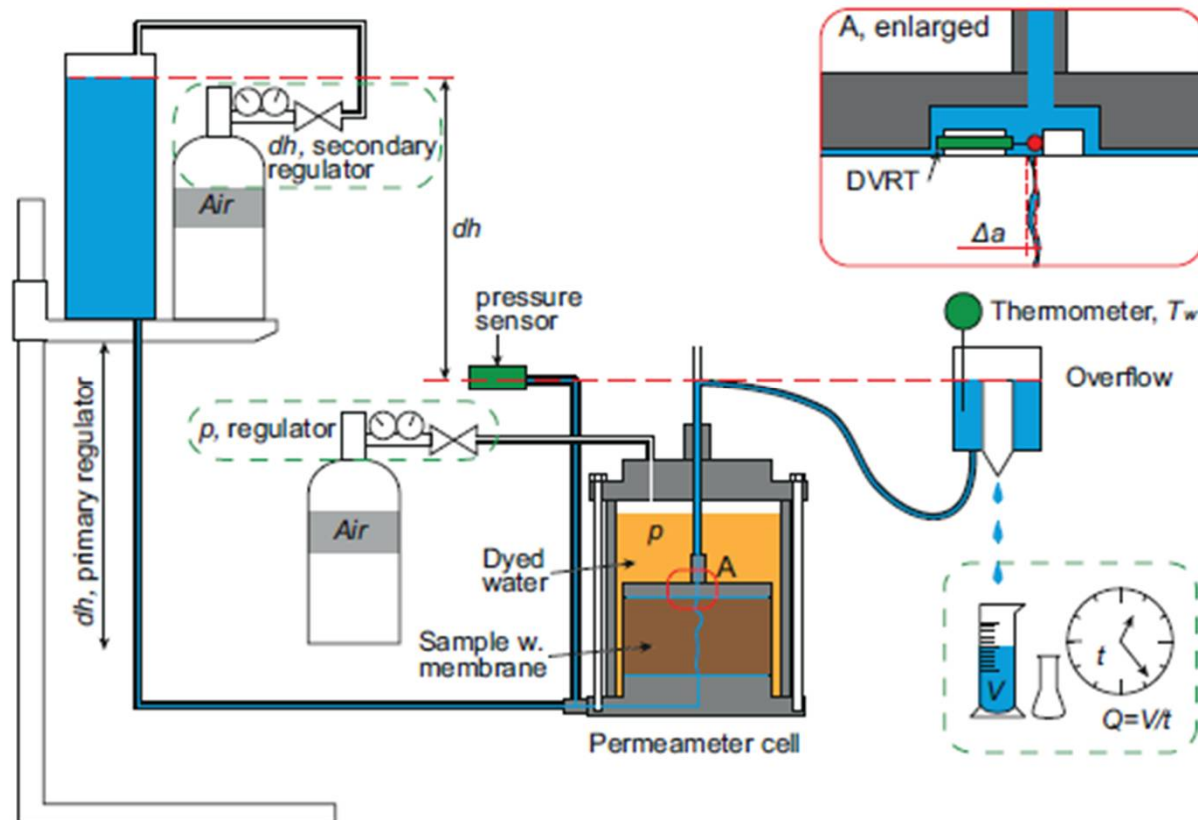
Objectives



□ The aim behind the experiments described in this paper is to develop and improve a sampling and testing method that provides information on hydraulic aperture variation linked to mechanical aperture variation in a fracture normal stress range of 0-2.5MPa. It is proposed that unmated fractures, where the surfaces fit each other poorly, have large apertures and low normal stiffness. Well-mated fractures, where the surfaces fit each other well, are assumed to have a small aperture and large normal stiffness.



- hydrostatic compression test - undisturbed samples – up to 2.5MPa (radial and axial stress)



□ For the hydromechanical procedure, a deformation sensor was mounted in plastic brackets, which were epoxy-glued to the sample, perpendicular to the fracture trace in the center of the top surface of the core.



- 1 Bottom plate
- 2 Sample
- 3 Sensor w. brackets
- 4 Top plate
- 5 Membrane seal





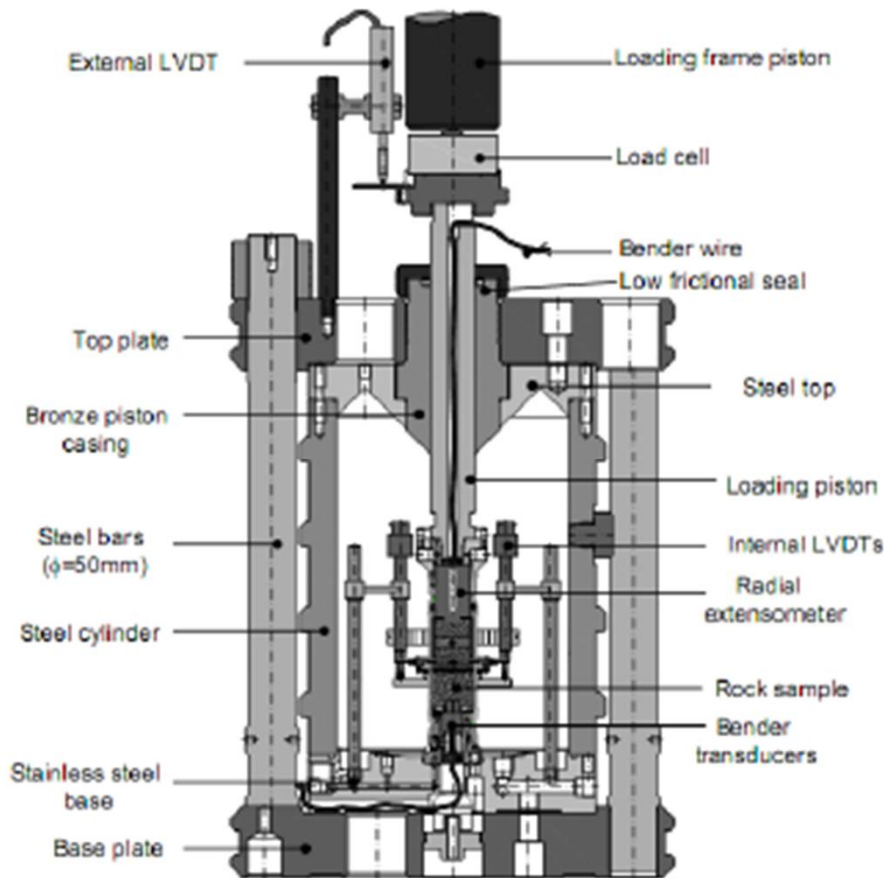
Proposed test programme for aperture and closure of fractures



- There are different ways of carrying out hydro-mechanical laboratory tests on rock samples. The review by Heiland (2003) distinguishes three general types of experimental set-ups: 1) hydrostatic compression, where a sample is subjected to the same stress in all three dimensions; 2) triaxial compression, where the axial and circumferential stress levels can be set individually; 3) uniaxial strain, where the lateral strain of the sample is kept constant by adjusting the confining pressure.
- In order to choose a test program to verify natural fractured rocks and consequently the aperture and closure of fractures is important to check three types of tests:



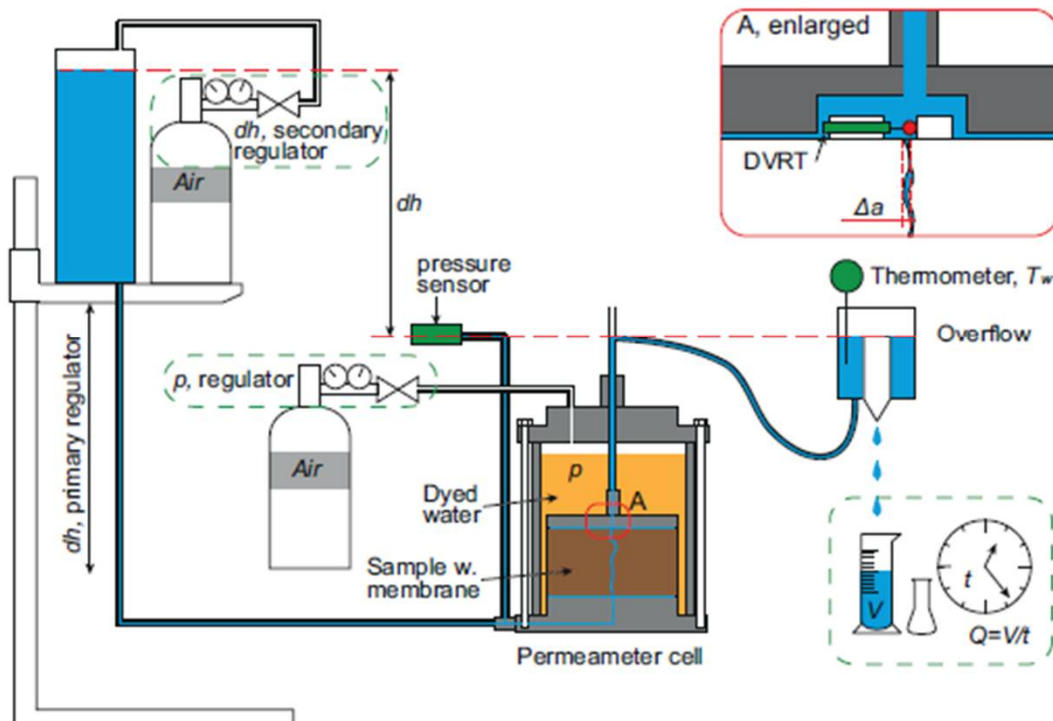
High pressure triaxial test



Characteristics

- ❑ Maximum dimension samples of 50mm of diameter and 100mm of height
- ❑ Application of high axial and radial stress (in order to 40 to 200 MPa)
- ❑ Measurement of radial and vertical displacements
- ❑ Fluid injection in order to measure the permeability and verify the aperture and closure of fractures

Permeameter cell (with high pressures)

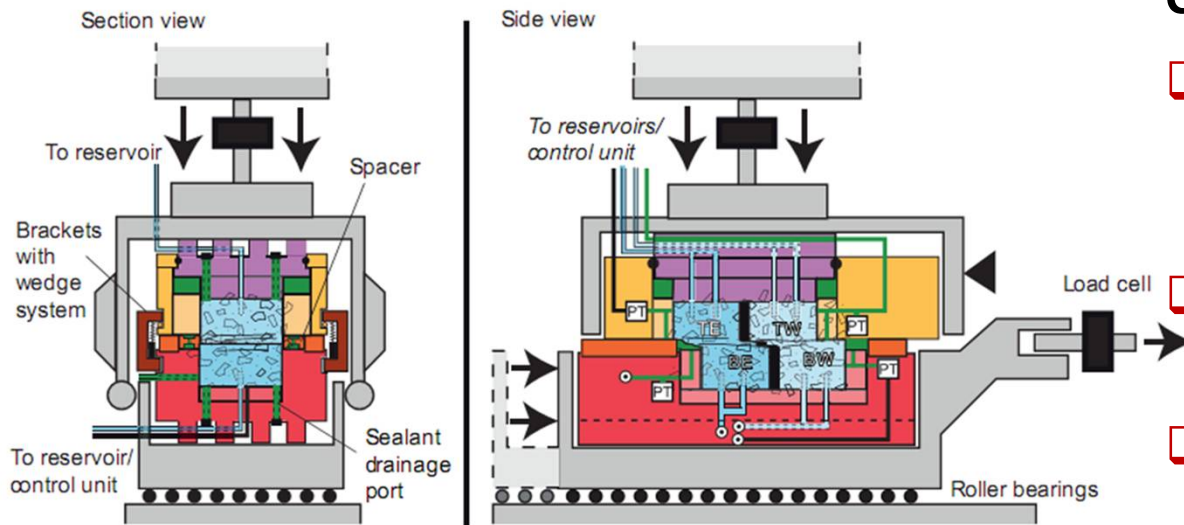


Thörn et al. (2014)

Characteristics

- ❑ Maximum dimension samples of 190mm of diameter and 100mm of height
- ❑ Application of high hydrostatic compression
- ❑ Measurement of aperture and closure of fractures with strain gauges glued in the rock
- ❑ Fluid injection in order to measure the permeability and verify the aperture and closure of fractures

Direct shear test for rock samples – with fluid injection

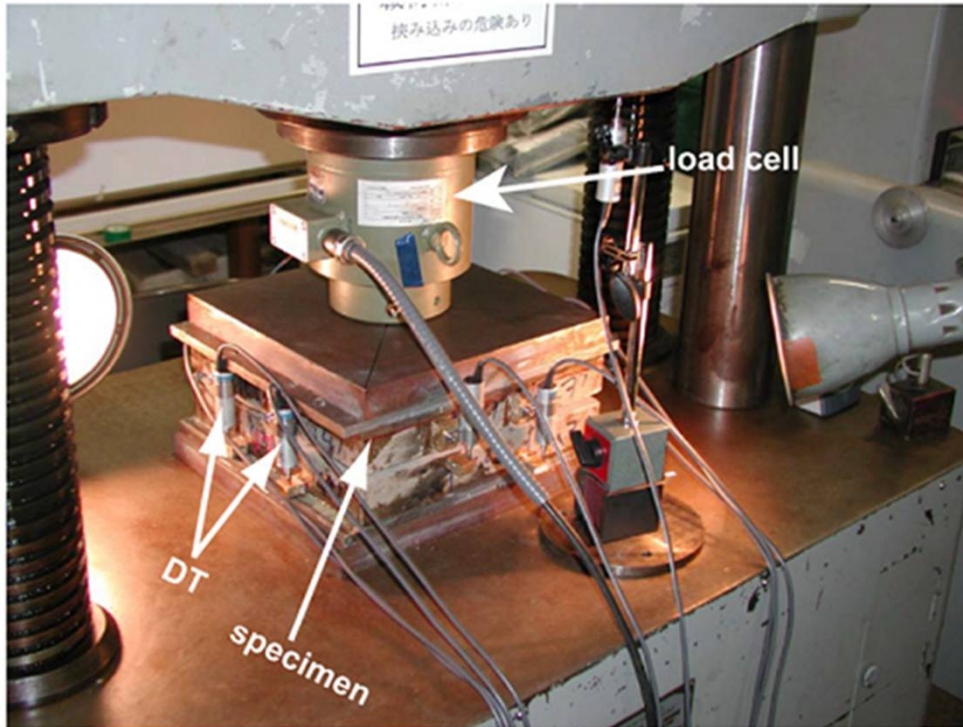


Giwelli (2010)

Characteristics

- ❑ Maximum dimension samples of 600 x300x 300 mm³
- ❑ Application of high vertical stress
- ❑ Direct shear test closed to ensure the sealing for fluid injection
- ❑ Fluid injection in order to measure the permeability and verify the aperture and closure of fractures

Vertical compression test with measurement of closure of fractures



Characteristics

- ❑ Maximum dimension samples of 200x200x80mm (it is possible to vary the dimensions)
- ❑ Application of high vertical stress
- ❑ Measurement of vertical displacement with strain gauges in order to verify the closure of fractures

Giger et al. (2011)





Commercial software used for Naturally and Hydraulically Fractured Reservoir Modeling





Commercial software used for Naturally and Hydraulically Fractured Reservoir Modeling



- CMG Package
- Abaqus





CMG'S PRODUCTS

IMEX – Black Oil reservoir simulator

GEM – EOS-compositional reservoir simulator

STARS – Thermal/Reactive-Transport reservoir simulator

GEOMECH – Geomechanics simulator (GEM & STARS)

BUILDER – Model creation/editing GUI

RESULTS – Simulator output display GUI

WINPROP – PVT modelling

CMOST – SA, UA, Aided History-Matching & Optimization



STARS

Steam, Thermal and Advanced processes Reservoir Simulator

STARS is a thermal, K-value compositional, chemical reaction and geomechanics reservoir simulator ideally suited for advanced modelling of recovery processes involving the injection of steam, solvents, air and chemicals.

STARS is the industry's leading thermal and advanced processes reservoir simulator. Its robust reaction kinetics and geomechanics capabilities make it the most complete and flexible reservoir simulator available for modelling the complex oil and gas recovery processes being studied and implemented today.

The following is a general list of reservoir processes being modeled with STARS:

Thermal

- Steam flooding
- Cyclic Steam
- SAGD - (Steam Assisted Gravity Drainage)
- ES-SAGD - (Expanding Solvent - Steam Assisted Gravity Drainage)
- Thermal VAPEX
- Hot Water Flooding
- Hot Solvent Injection
- Combustion (Air Injection)
 - HTO & LTO (High & Low Temperature Oxidation)
 - THAI (Toe-to-Heel Air Injection)
- Electrical Heating
- Differential Temperature Water Injection

Chemical

- Gellation, simple or multi-stage, multi-component
- Foams, Emulsions & Foamy Oil
- ASP (Alkaline-Surfactant-Polymer) flooding
- Microbial EOR
- VAPEX
- Low salinity waterflooding
- Reservoir souring

Non Oil & Gas Related Applications of STARS:

- Ground-water movement
- Pollutant clean-up and recovery
- Hazardous waste disposal and re-injection
- Geothermal reservoir production
- Solution mining operations
- Near wellbore exothermic reactions

Solids Transport & Deposition

- Fines transport
- CHOP (Cold Heavy Oil Production)
 - Sand transport and production (Worm-holes)
- Asphaltene precipitation, flocculation, deposition and plugging
- Wax precipitation

Geomechanics

- Compaction and subsidence
- Rock failure
- Dilation
- Creep

Naturally and Hydraulically Fractured Reservoir Modelling

- Dual porosity
 - Multiple interacting continua
 - Vertical refinement
- Dual permeability
- Integrated to Pinnacle Technologies, Inc.'s FracProPT fracture design software
- Integrated to Fracture Technologies Ltd's WellWhiz well, completion and fracture design software



STARS

GEM

Generalized Equation of State Model Reservoir Simulator

GEM is a full Equation of State compositional reservoir simulator with advanced features for modelling recovery processes where the fluid composition affects recovery. GEM also models Asphaltenes, Coal Bed Methane and the Geochemistry for the sequestration of various gases including Acid Gases and CO₂.

GEM provides reservoir simulation capabilities that go beyond the abilities of conventional black oil and K-value compositional simulators, including the effects of asphaltene precipitation and plugging. It is also the industry's leading Coal Bed Methane (CBM) simulator, as it can provide accurate early time water and methane production predictions, as well as multi-component production predictions for Enhanced CBM (ECBM) recovery. The ECBM features include extended Langmuir Isotherms to model the preferential adsorption of CO₂ and other gases and models for coal shrinkage and swelling. The extensive capabilities for representing asphaltene behavior and geochemical effects make GEM the most robust compositional simulator available today.

The following is a general list of applications of GEM:

Hydrocarbon and Acid Gas Injection

- Multiple contact miscibility
- Swelling
- Viscosity reduction
- Lowering of interfacial tension
- Gas solubility in the aqueous phase
- WAG process
- Relative permeability hysteresis
- VAPEX processes for heavy oil
- Molecular diffusion and convective dispersion
- Asphaltene precipitation, flocculation, deposition and plugging

Gas, Gas Condensate and Volatile Oil

- Gas Cycling and Re-cycling
- Condensate blocking
- Underground Gas Storage

Primary & Enhanced Coal Bed Methane

- Primary Depletion
- Coal Shrinkage and Swelling
- Flue Gas, CO₂ and N₂ Injection for enhanced CBM recovery

Green House Gas Sequestration

- CO₂ and other acid gas storage
- Aqueous equilibrium chemical reactions
- Mineral dissolution and precipitation

Thermal Effects

- Joule-Thompson near wellbore cooling
- Deferential temperature water injection

Fractured Reservoirs

- Naturally Fractured Reservoirs
- Hydraulically Fractured Reservoirs
- Fractured Gas Condensed Wells
- Gas-Oil Gravity Drainage



Advanced features of GEM include:

Naturally and Hydraulically Fractured Reservoir Modelling

- Dual porosity
- Dual permeability
- Sub-domain dual permeability
- Matrix-fracture diffusion
- Multi-phase non-Darcy flow
- Rate dependant relative permeability
- Integrated to Pinnacle Technologies, Inc.'s FracProPT fracture design software
- Integrated to Fracture Technologies Ltd's WellWhiz well, completion and fracture design software

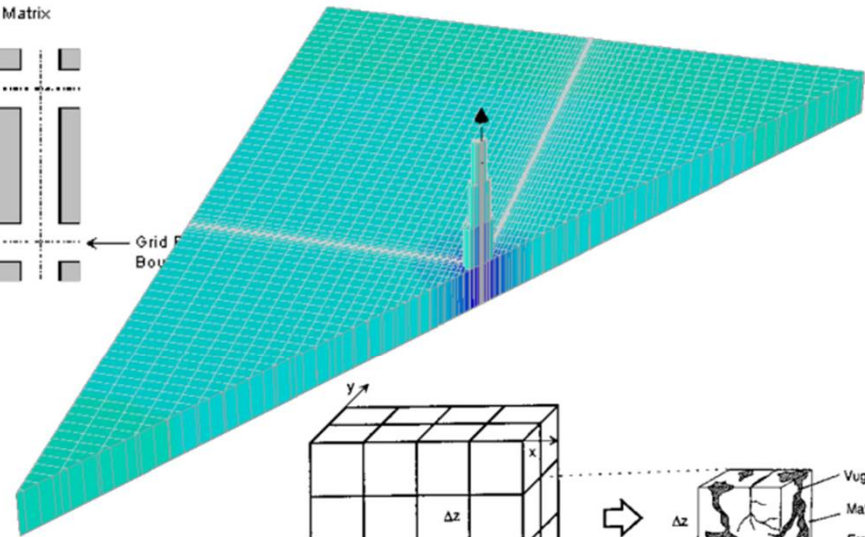
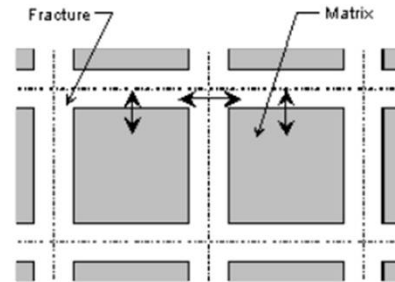


Commercial software used for Naturally and Hydraulically Fractured Reservoir Modeling



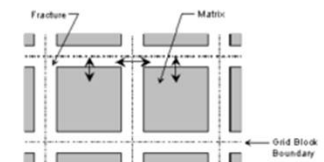
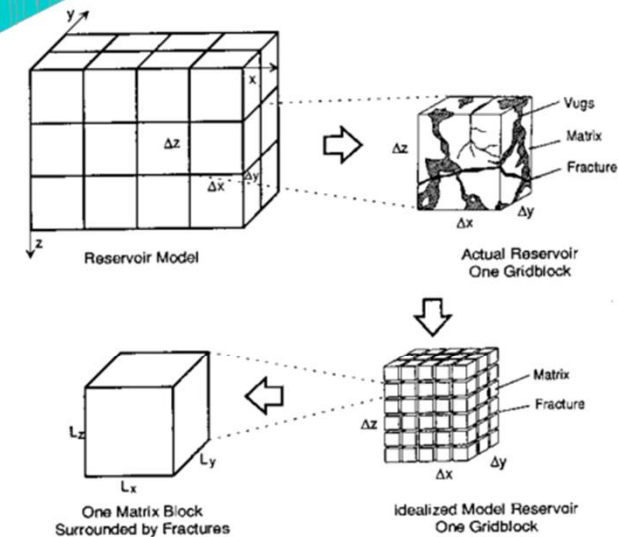
Natural Fractures

- ✓ Dual Porosity
- ✓ Dual Permeability
- ✓ Matrix subdivision via:
 - ✓ Multiple Interacting Continua (MINC)
 - ✓ Subdomain (SD)



Hydraulic Fractures

- ✓ Wizard to generate Locally Refined Grids to model Bi-wing and Complex fractures placed along horizontal wells accurately and efficiently
- ✓ Wizard to import Microseismic Data to delineate Stimulated Reservoir Volume (SRV)

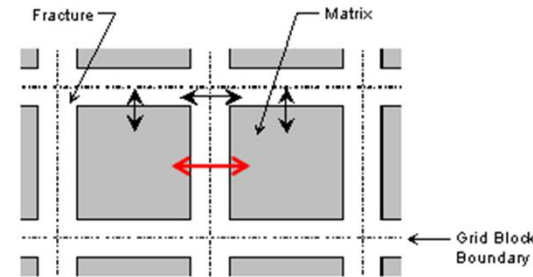




MODELLING FEATURES

❑ Single vs Dual Porosity

- Single Porosity if no open natural fractures
- Dual Permeability if open natural fractures



❑ Relative Perm & Capillary Pressure

- Independent curves for matrix, natural fractures & propped fractures
 - Usually straight line for natural & propped fracs
 - Matrix can be oil-wet or water-wet (which is it?)
 - Can include hysteresis if modelling solvent injection
 - Can also include wettability alteration via relative permeability interpolation (new in GEM for 2012)



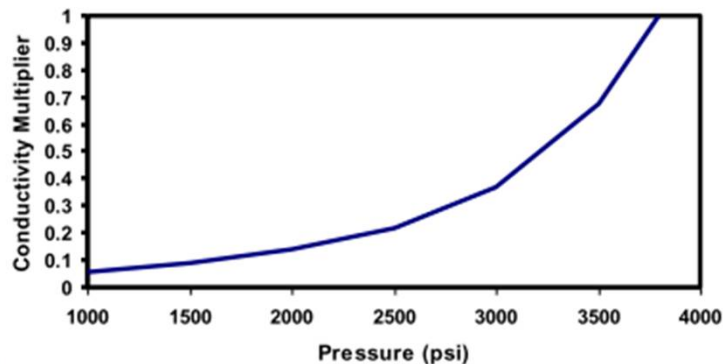


MODELLING FEATURES (cont.)

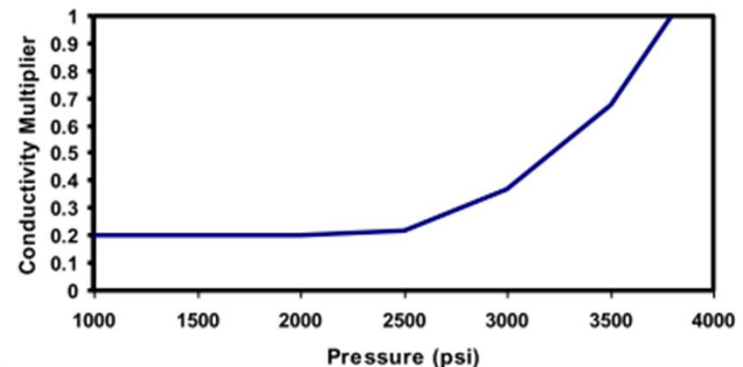
❑ Compaction/Dilation

- Pressure-dependent Compaction/Dilation tables for modelling degradation of permeability & porosity
 - In propped fractures, natural fractures & matrix, including hysteresis for modelling shut-in periods
- Effective Stress-dependent Compaction/Dilation tables when using GEOMECH (GEM)
 - Barton-Bandis approach for modelling of natural fracture perm vs Effective Stress

Unpropped Fracture
Compaction Table



Propped Fracture
Compaction Table





Commercial software used for Naturally and Hydraulically Fractured Reservoir Modeling



□ References:

- Unconventional Reservoirs Flow modelling challenges (Presentation) by Victor Salazar. November, 2013.

Available in: <http://pt.slideshare.net/SistemaFIEB/unconventional-reservoirs-flow-modelling-challenges>

- Shale & Tight Reservoir Simulation (Presentation) by Jim Erdle, VP-USA & LA . October, 2012.

Available in: www.cup.edu.cn/fcg/docs/20121205163502065462.pdf

- **SPE166201:** A.S.Padmakar, Chevron. Geomechanics Coupled Reservoir Flow Simulation for Diagnostic Fracture Injection Test Design and Interpretation in Shale Reservoirs. 2013.

Available in: <https://www.onepetro.org/conference-paper/SPE-166201-MS>

- **SPE132093 :** Barry Rubin (Computer Modelling Group Inc). Accurate Simulation of Non Darcy Flow in Stimulated Fractured Shale Reservoirs. 2010.

Available in: <https://www.onepetro.org/conference-paper/SPE-132093-MS>





ABAQUS

Constitutive model for jointed materials

The jointed material model is intended to provide a simple, continuum model for materials containing a high density of parallel joint surfaces in different orientations. The spacing of the joints of a particular orientation is assumed to be sufficiently close compared to characteristic dimensions in the domain of the model that the joints can be smeared into a continuum of slip systems. An obvious application is the modeling of geotechnical problems where the medium of interest is composed of significantly faulted rock. In this context, models similar to the one described next have been proposed in the past; see, for example, the model formulated by [Zienkiewicz and Pandle \(1977\)](#).

The model implemented in Abaqus/Standard provides for opening of the joints, or frictional sliding of the joints, in each of these systems (a “system” in this context is a joint orientation in a particular direction at a material calculation point). In addition to the joint systems, the model includes a bulk material failure mechanism. This is based on the Drucker-Prager failure criterion.





Joint system definitions

It's considered a particular joint a oriented by the normal \mathbf{n}_a to the joint surface. We define $\mathbf{t}_{a\alpha}, \alpha = 1, 2$ as two unit, orthogonal vectors in the joint surface. The local stress components are:

$$\left\{ \begin{array}{l} p_a \stackrel{\text{def}}{=} \mathbf{n}_a \cdot \boldsymbol{\sigma} \cdot \mathbf{n}_a, \\ \tau_{a\alpha} = \mathbf{n}_a \cdot \boldsymbol{\sigma} \cdot \mathbf{t}_{a\alpha}, \end{array} \right.$$

the pressure stress across the joint

and

Shear stresses across the joint

With: $\boldsymbol{\sigma} \rightarrow$ Stress tensor

We define the shear stress magnitude as

$$\tau_a = \sqrt{\tau_{a1}\tau_{a1} + \tau_{a2}\tau_{a2}}$$

The local strain components are

$$\left\{ \begin{array}{l} \varepsilon_{an} = \mathbf{n}_a \cdot \boldsymbol{\varepsilon} \cdot \mathbf{n}_a, \\ \gamma_{a\alpha} = \mathbf{n}_a \cdot \boldsymbol{\varepsilon} \cdot \mathbf{t}_{a\alpha} + \mathbf{t}_{a\alpha} \cdot \boldsymbol{\varepsilon} \cdot \mathbf{n}_a, \end{array} \right.$$

Normal strain across the joint

and

Shear strain in the α direction in the joint surface

Where: $\boldsymbol{\varepsilon} \rightarrow$ Stress tensor





Strain rate decomposition

A linear strain rate decomposition is assumed:

$$d\varepsilon = d\varepsilon^{el} + d\varepsilon^{pl}$$

With: $d\varepsilon^{el}$ → Elastic strain rate

$d\varepsilon^{pl}$ → Inelastic (plastic) strain rate

Supposing that several systems are active (we designate an active system by i , where $i=b$ indicates the bulk material system and $i=a$ is a joint system a)

$$\longrightarrow d\varepsilon^{pl} = \sum_i d\varepsilon_i^{pl}$$

Elasticity and joint opening/closing

When all joints at a point are closed, the elastic behavior of the material is assumed to be isotropic and linear. The material cannot be elastically incompressible (Poisson's ratio must be less than 0.5).

We use a stress-based joint opening criterion whereas joint closing is monitored based on strain. Joint system a opens when the estimated pressure stress across the joint (normal to the joint surface) is no longer positive:

$$p_a \leq 0.$$





Elasticity and joint opening/closing (cont.)

In this case the material is assumed to have no elastic stiffness with respect to direct strain across the joint system. Open joints, thus, create anisotropic elastic response at a point. The joint system remains open as long as:

$$\varepsilon_{an(ps)}^{el} \leq \varepsilon_{an}^{el}$$

$$\varepsilon_{an(ps)}^{el} = -\frac{\nu}{E}(\sigma_{a1} + \sigma_{a2}),$$

$$\sigma_{a\alpha} = \mathbf{t}_{a\alpha} \cdot \boldsymbol{\sigma} \cdot \mathbf{t}_{a\alpha},$$



Direct stresses in the plane of the joint

With: ε_{an}^{el} → component of direct elastic strain across the joint

$\varepsilon_{an}^{el}(ps)$ → component of direct elastic strain across the joint

Component of direct elastic strain across the joint calculated in plane stress .

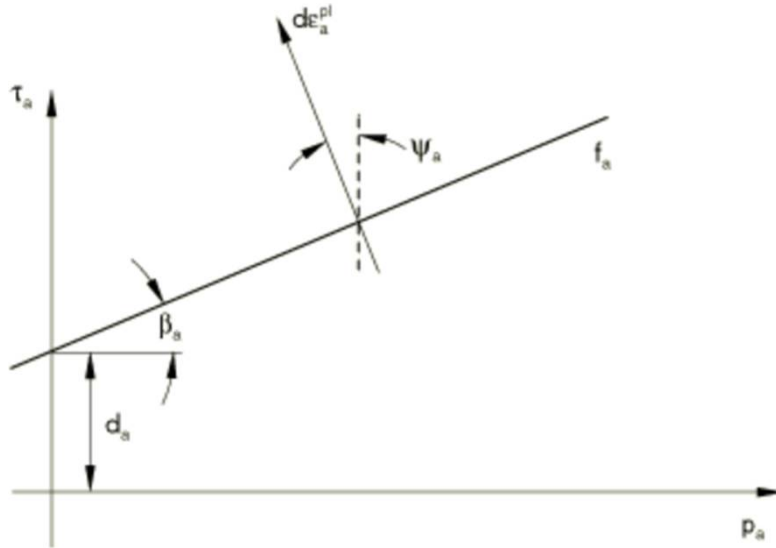
With: E → young's modulus of the material
 ν → Poisson's ratio

The shear response of open joints is governed by the shear retention parameter, f_{sr} , which represents the fraction of the elastic shear modulus retained when the joints are open ($f_{sr} = 0$ means no shear stiffness associated with open joints, while $f_{sr} = 1$ corresponds to elastic shear stiffness in open joints; any value between these two extremes can be used).





Plastic behavior of joint systems



$d\gamma_{a\alpha}^{pl}$ → Rate of inelastic shear strain in direction α on the joint surface

$d\bar{\epsilon}_a^{pl}$ → Magnitude of the inelastic strain rate

$$f_a = \tau_a - p_a \tan \beta_a - d_a = 0.$$

With: β_a → Friction angle for system a

d_a → Cohesion for system a

- $f_a < 0$ → Joint system a does not slip
- $f_a = 0$ → Joint system a slips

$$\left\{ \begin{aligned} d\gamma_{a\alpha}^{pl} &= d\bar{\epsilon}_a^{pl} \frac{\tau_{a\alpha}}{\tau_a} \cos \psi_a \\ d\epsilon_{an}^{pl} &= d\bar{\epsilon}_a^{pl} \sin \psi_a \end{aligned} \right. \rightarrow \text{Inelastic ("plastic") strain on the system}$$

ψ_a → Dilation angle for this joint system

$d\epsilon_{an}^{pl}$ → Inelastic strain normal to the joint surface

In order to add the plastic flow contributions from different systems we write the tensorial plastic strain rate for joint a as

$$d\epsilon_a^{pl} = d\epsilon_{an}^{pl} \mathbf{n}_a \mathbf{n}_a + d\gamma_{a\alpha}^{pl} (\mathbf{n}_a \mathbf{t}_{a\alpha} + \mathbf{t}_{a\alpha} \mathbf{n}_a).$$

PS: The sliding of the different joint systems at a point is independent, in the sense that sliding on one system does not change the failure criterion or the dilation angle for any other joint system at the same point. The model provides for up to three joint systems at a point.



Plastic behavior of bulk material

In addition to the joint systems, the model includes a bulk material failure mechanism. This is based on the Drucker-Prager failure criterion:

$$q - p \tan \beta_b - d_b = 0,$$

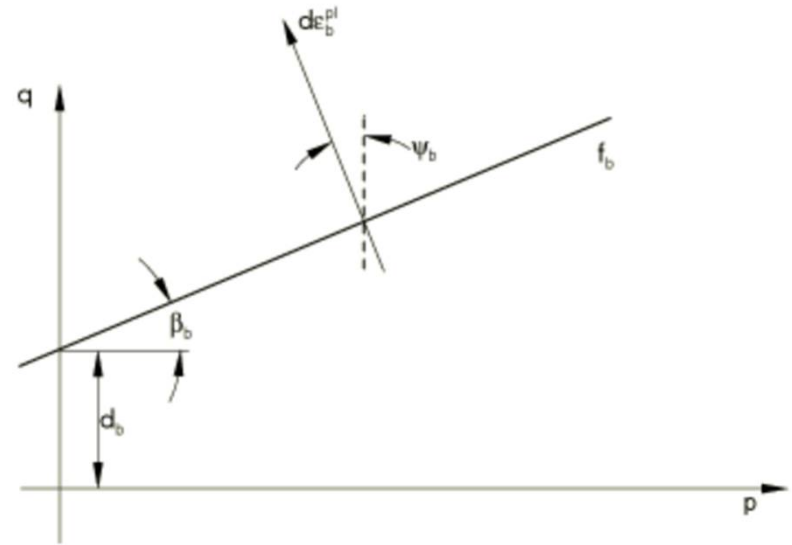
$$q \stackrel{\text{def}}{=} \sqrt{\frac{3}{2} \mathbf{S} : \mathbf{S}} \longrightarrow \text{Mises equivalent deviatoric stress}$$

$$\mathbf{S} \stackrel{\text{def}}{=} \boldsymbol{\sigma} + p \mathbf{I} \longrightarrow \text{Deviatoric stress}$$

$$p \stackrel{\text{def}}{=} -\frac{1}{3} \mathbf{I} : \boldsymbol{\sigma} \longrightarrow \text{Equivalent pressure stress}$$

$$\beta_b \longrightarrow \text{Friction angle for the bulk material}$$

$$d_b \longrightarrow \text{Cohesion for the bulk material}$$



If this failure criterion is reached, the bulk inelastic flow is defined by

$$d\boldsymbol{\varepsilon}_b^{pl} = d\bar{\boldsymbol{\varepsilon}}_b^{pl} \frac{1}{1 - \frac{1}{3} \tan \psi_b} \frac{\partial g_b}{\partial \boldsymbol{\sigma}},$$

$$g_b = q - p \tan \psi_b \longrightarrow \text{Flow potential}$$

$$d\bar{\boldsymbol{\varepsilon}}_b^{pl} \longrightarrow \text{Magnitude of the inelastic flow rate}$$

$$\psi_b \longrightarrow \text{Dilation angle for the bulk material}$$





Commercial software used for Naturally and Hydraulically Fractured Reservoir Modeling



□ References:

- Abaqus Theory Manual. “Constitutive Model for Jointed Materials”, Section 4.5.4.

Available in: жбк.рф:2080/v6.12/books/stm/default.htm?startat=ch04s05ath122.html

- Zienkiewicz, O. C., and G. N. Pande, “Time Dependent Multilaminate Model of Rocks—A Numerical Study of Deformation and Failure of Rock Masses,” International Journal for Numerical and Analytical Methods in Geomechanics, vol. 1, pp. 219–247, 1977.

